OAK RIDGE NATIONAL LABORATORY LIBRARY
3 4456 0034273 3

CD

ornl

ORNL/TM-9215

OAK RIDGE NATIONAL LABORATORY

MARTIN MARIETTA

A One-Dimensional Modeling of Radial Heat Removal During Depressurized Heatup Transients in Modular Pebble-Bed and Prismatic High Temperature Gas-Cooled Reactors

M. G. Savage

OAK RIDGE NATIONAL LABORATORY
CENTRAL RESEARCH LIBRARY
CIRCULATION SECTION
4500N ROOM 175
LIBRARY LOAN COPY
DO NOT TRANSFER TO ANOTHER PERSON
If you wish someone else to see this report, send in name with report and the library will arrange a loan.
UCN-7969 (3 9-77)

OPERATED BY
MARTIN MARIETTA ENERGY SYSTEMS, INC.
FOR THE UNITED STATES
DEPARTMENT OF ENERGY

Printed in the United States of America. Available from
National Technical Information Service
U.S. Department of Commerce
5285 Port Royal Road, Springfield, Virginia 22161
NTIS price codes—Printed Copy: A11 Microfiche A01

This report was prepared as an account of work sponsored by an agency of the United States Government. Neither the United States Government nor any agency thereof, nor any of their employees, makes any warranty, express or implied, or assumes any legal liability or responsibility for the accuracy, completeness, or usefulness of any information, apparatus, product, or process disclosed, or represents that its use would not infringe privately owned rights. Reference herein to any specific commercial product, process, or service by trade name, trademark, manufacturer, or otherwise, does not necessarily constitute or imply its endorsement, recommendation, or favoring by the United States Government or any agency thereof. The views and opinions of authors expressed herein do not necessarily state or reflect those of the United States Government or any agency thereof.

ORNL/TM-9215
Distribution Category UC-77

Engineering Physics and Mathematics Division

A One-Dimensional Modeling of Radial Heat Removal During Depressurized Heatup Transients in Modular Pebble-Bed and Prismatic High Temperature Gas-Cooled Reactors*

M. G. Savage

Manuscript Completed: May 1984
Date Published: July 1984

This Work Performed For
U.S. Department of Energy
Office of Converter Reactor Deployment

*Also published as a thesis for the Master of Science Degree in Nuclear Engineering at Pennsylvania State University

Prepared by the
Oak Ridge National Laboratory
Oak Ridge, Tennessee 37831
operated by
Martin Marietta Energy Systems, Inc.
for the
U.S. DEPARTMENT OF ENERGY
under Contract No. DE-AC05-840R21400

OAK RIDGE NATIONAL LABORATORY LIBRARY
3 4456 0034273 3

TABLE OF CONTENTS

Page

ABSTRACT vii

LIST OF TABLES ix

LIST OF FIGURES. xi

ACKNOWLEDGMENTS. xv

CHAPTERS

1 INTRODUCTION 1

1.1 Background. 3

1.1.1 Application of Modular HTGRs 3

1.1.2 Summary of Preliminary Designs 4

1.2 Purpose of This Study 10

2 CODE DEVELOPMENT 13

2.1 Heat Transfer Coefficients at Void Interfaces and Outermost Boundary 14

2.2 Steady-State Finite-Difference Equations. 17

2.2.1 Rectangular Coordinates. 17

2.2.2 Cylindrical Coordinates. 20

2.3 Transient Finite-Difference Equations 21

2.3.1 The One-dimensional, Transient Conduction Equation in Rectangular Coordinates. 21

2.3.2 Temperature Dependent Thermal Properties 26

2.3.3 Cylindrical Coordinates. 26

2.3.4 Summary of Transient Finite Difference Equations 29

2.4 Thermal Conductivity of Graphite. 35

2.5 Effective Thermal Conductivity in a Pebble Bed. 37

3 PROGRAMMING CONSIDERATIONS 43

3.1 Numerical Techniques. 44

3.1.1 Steady-state Solution Methods. 44

TABLE OF CONTENTS (Continued)

CHAPTERS Page

3.1.2 Transient Solution Methods 46

3.2 Determination of Properties and Heat Generation Rates 48

3.2.1 Thermal Conductivity 48

3.2.2 Density and Specific Heat. 48

3.2.3 Volumetric Heat Generation Rates 50

3.3 Flow of Problem Solution. 52

4 MODELING OF PRISMATIC-CORE AND PEBBLE-BED HTGRs FOR DEPRESSURIZED HEATUP ACCIDENT ANALYSIS 60

4.1 Prismatic Modular HTGR Model. 60

4.2 Pebble-Bed Modular HTGR Model 65

4.3 Materials Properties. 74

4.3.1 Graphite 74

4.3.2 304 Stainless Steel. 79

4.3.3 2-1/4 Cr : 1 Mo Steel. 79

4.3.4 Helium 79

5 RESULTS AND CONCLUSIONS. 88

5.1 Solid Graphite and Pebble-Bed Thermal Conductivities. 88

5.2 Prismatic Modular HTGR. 90

5.3 Pebble-Bed Modular HTGR 96

6 SUMMARY AND RECOMMENDATIONS FOR FURTHER STUDY. 102

6.1 Summary 102

6.2 Recommendations for Further Study 104

REFERENCES. 107

APPENDIX A: Derivation of the Steady-State Finite Difference Heat Transfer Equations 109

A.1 Rectangular Coordinates. 111

A.2 Cylindrical Coordinates. 118

TABLE OF CONTENTS (Continued)

Page

APPENDIX B: Derivation of the Time-Dependent Finite Difference Heat Transfer Equations 125

B.1 Rectangular Coordinates 128

B.2 Cylindrical Coordinates 139

APPENDIX C: User's Guide to SHERLOC 155

APPENDIX D: Listing of SHERLOC 191

ABSTRACT

A one-dimensional computational model was developed to evaluate the heat removal capabilities of both prismatic-core and pebble-bed modular HTGRs during depressurized heatup transients. A correlation was incorporated to calculate the temperature- and neutron-fluence-dependent thermal conductivity of graphite. The modified Zehner-Schlünder model was used to determine the effective thermal conductivity of a pebble bed, accounting for both conduction and radiation.

Studies were performed for prismatic-core and pebble-bed modular HTGRs, and the results were compared to analyses performed by GA and GE, respectively. For the particular modular reactor designs studied, the prismatic HTGR peak temperature was 2152.2 °C at 38 hours following the transient initiation, and the pebble-bed peak temperature was 1647.8 °C at 26 hours. These results compared favorably with those of GA and GE, with only slight differences caused by neglecting axial heat transfer in a one-dimensional radial model.

This study found that the magnitude of the initial power density had a greater effect on the temperature excursion than did the initial temperature. Neglecting the neutron fluence in the prismatic HTGR caused a 10% decrease in the peak temperature, and modeling gas gaps between prismatic fuel assemblies produced a 5% increase in the peak temperature. Replacing the prismatic core with a pebble bed resulted in a 1% increase in peak temperature.

LIST OF TABLES

Table		Page
2.1	Coefficients for Transient Finite Difference Equations in Rectangular and Cylindrical Geometries	31
2.2	Data Strings for Graphite Thermal Conductivity Correlation	38
4.1	Summary of Prismatic Modular HTGR Cases Analyzed Using SHERLOC	66
4.2	Steady-State Radial Power Density Distributions at Various Axial Locations in the Prismatic Modular HTGR	67
4.3	Steady-State Radial Temperature Distributions at Various Axial Locations in the Prismatic Modular HTGR	68
4.4	Radial Neutron Fluence Distribution Assumed for the Prismatic Modular HTGR	69
4.5	Summary of Pebble-bed Modular HTGR Cases Analyzed Using SHERLOC	75
4.6	Steady-State Radial Power Density Distributions at Various Axial Positions in the Pebble-bed Modular HTGR	76
4.7	Steady-State Radial Temperature Distributions at Various Axial Positions in the Pebble-bed Modular HTGR	77
4.8	Radial Neutron Fluence Distribution Assumed for the Pebble-bed Modular HTGR.	78
5.1	Summary of Results of Depressurized Heatup Accident Analyses for the Prismatic HTGR	91
5.2	Summary of Results of Depressurized Heatup Accident Analyses for the Pebble-Bed HTGR.	97

LIST OF FIGURES

Figure		Page
1.1	Prismatic-Core Modular HTGR Vessel Configuration Source: General Electric Company	6
1.2	Prismatic-Core Modular HTGR Normal Flow Path Source: General Electric Company	7
1.3	Prismatic-Core Modular HTGR Bypass Flow Path Source: General Electric Company	8
1.4	GHT Modular-Pabble-Bed Reactor Concept Source: Gosellschaft fuar Hochtemperatur-reactor - Technik mbH (GHT)	11
2.1	(a) Internal Mesh Point - Rectangular Geometry (b) Internal Mesh Point - Cylindrical Geometry.	18
2.2	Temperature- and Neutron-Fluence-Dependent Graphite Thermal Conductivity	39
2.3	Unit Cell for the Zehner-Schlünder Model.	40
3.1	General Flowchart for SHERLOC	53
3.2	Flowchart for Steady-State Problem.	54
3.3	Flowchart for Transient Problem	55
3.4	Flowchart for Subroutine CONDUC	56
3.5	Flowchart for Subroutine GRPHTE	57
3.6	Flowchart for Subroutine PEBBLE	58
4.1	Prismatic Core Modular HTGR Model for SHERLOC	61
4.2	Time-Dependent Decay Heat Fraction for the Prismatic HTGR.	64
4.3	Pebble-Bed Modular HTGR Model for SHERLOC	70
4.4	Time-Dependent Decay Heat Fraction for the Pebble-Bed HTGR	73

LIST OF FIGURES (Continued)

Figure		Page
4.5	Temperature-Dependent Graphite Specific Heat	80
4.6	304 Stainless Steel Thermal Conductivity	81
4.7	304 Stainless Steel Specific Heat.	82
4.8	2¼ Cr: 1 Mo Steel Thermal Conductivity	83
4.9	2¼ Cr: 1 Mo Steel Specific Heat.	84
4.10	Helium Thermal Conductivity at 1 Atmosphere.	86
4.11	Helium Density at 1 Atmosphere	87
5.1	Solid Graphite and Effective Pebble-Bed Thermal Conductivities	89
5.2	Response of the Center-line Temperature to the Depressurized Heatup Accident for the Prismatic HTGR	92
5.3	Radial Temperature Distribution at Axial Region 4 at Various Times in the Prismatic HTGR	94
5.4	Response of the Center-line Temperature to the Depressurized Heatup Accident for the Pebble-Bed HTGR.	98
5.5	Radial Temperature Distribution at 26 Hours at z/H = 0.2 in the Pebble-Bed HTGR.	100
5.6	SHERLOC Pebble-Bed Conductivity Correlation and GE Pebble-Bed Conductivity Correlation	101
A.1	Mesh Interval at the Origin - Rectangular Coordinates.	112
A.2	Mesh Interval Within a Material - Rectangular Coordinates.	113
A.3	Interface of Two Material Regions - Rectangular Coordinates	114

LIST OF FIGURES (Continued)

Figure		Page
A.4	Inner Boundary of a Void Region - Rectangular Coordinates	115
A.5	Outer Boundary of a Void Region - Rectangular Coordinates	116
A.6	Mesh Interval at the Outermost Boundary Rectangular Coordinates	117
A.7	Mesh Interval at the Origin Cylindrical Coordinates	118
A.8	Mesh Interval Within a Material - Cylindrical Coordinates	119
A.9	Interface of Two Material Regions - Cylindrical Coordinates	120
A.10	Inner Boundary of a Void Region - Cylindrical Coordinates	121
A.11	Outer Boundary of a Void Region - Cylindrical Coordinates	122
A.12	Mesh Interval at the Outermost Boundary - Cylindrical Coordinates	123
C.1	Model for Sample Problem	166
C.2	Input for SHERLOC Sample Problem - Steady-State	167
C.3	Output of SHERLOC Sample Problem - Steady-State	169
C.4	Input for SHERLOC Sample Problem - Transient	175
C.5	Output of SHERLOC Sample Problem - Transient	176

ACKNOWLEDGMENTS

The author would like to thank thesis co-advisers Dr. Gordon E. Robinson, The Pennsylvania State University Nuclear Engineering Department, and Dr. Brian A. Worley, Oak Ridge National Laboratory, for their support and guidance in the performance of this study. Appreciation is extended to Dr. Warren F. Witzig, Head of the Nuclear Engineering Department, and Dr. Anthony J. Baratta, graduate faculty reader, The Pennsylvania State University, and Dr. David L. Moses, Oak Ridge National Laboratory, for their reviews of this thesis.

This research was performed at the Oak Ridge National Laboratory under appointment to the Nuclear Science and Engineering and Health Physics Fellowship Program administered by Oak Ridge Associated Universities for the United States Department of Energy. The author is grateful for the cooperation of the personnel at the Oak Ridge National Laboratory, especially that of Dr. D. E. Bartine, Head of the Reactor Analysis and Shielding Section.

Finally, the author expresses gratitude to her husband, Chris R. Savage, for his constant support during this study.

1. INTRODUCTION

Development of High Temperature Gas-Cooled Reactor (HTGR) Technology has been underway in the United States and other countries since the 1950's, primarily for use in electric power generation. A major goal of this development was to achieve high coolant temperatures, which would lead to high plant efficiencies and possibly a closed-cycle using gas turbines. This goal led to the choice in the United States of helium for the coolant, and graphite, with its high heat capacity and good neutron slowing-down characteristics, for the moderator and structural material. More recently, a potential has been identified for the use of HTGRs in the industrial heat market. In the past, the emphasis has been on the development of large, monolithic nuclear reactors; however, presently under consideration is a small or "modular" HTGR concept.

One of the major advantages of a small HTGR design is that, when properly designed, a core auxiliary cooling system need not be included. Following a loss of forced convection accident, if the system remains pressurized, natural circulation of the helium will sufficiently cool the reactor core and internal components. In the "worst case" accident scenario, the system would depressurize and the gas would become stagnant. In this case, decay heat removal by passive conduction through the core and radiation from the vessel will prevent core damage. The inherent safety of the modular HTGR design makes it particularly attractive.

Few computer codes are openly available which may be used to analyze the depressurized heatup transient in both pebble-bed and prismatic HTGRs.

In their analysis of the prismatic HTGR, General Atomic Technologies (GA) used a proprietary computer code entitled CORCON. Two-dimensional calculations may be performed using CORCON; however, it is limited to the analysis of prismatic HTGRs. General Electric Company (GE) used the THERMIX-2 computer code, a proprietary code developed by Kernforschungasanlage Julich GmbH (KFA) in the Federal Republic of Germany, to analyze the pebble-bed HTGR. The effective pebble-bed thermal conductivity is input to THERMIX-2 as a function of temperature only. It would be more precise to allow the pebble-bed effective conductivity to be determined internally as a function of not only temperature, but also neutron fluence, pebble diameter, and pebble-bed porosity. Simple conduction heat transfer codes such as HEATING6 [1] abound. They, however, are not easily adapted to calculate heat transfer through graphite or through pebble beds. A computer code which is openly available and which uses non-proprietary correlations for graphite and pebble-bed thermal conductivities was deemed useful for independent evaluation of both pebble-bed and prismatic modular HTGR designs.

Described herein is a FORTRAN computer code (SHERLOC - Small HTGR Thermal Response to Loss of Circulation) which has been developed to calculate fuel temperature distributions in modular HTGR concepts during a loss of forced convection and depressurization accident. Several studies have been performed and are presented here. A primary concern in performing decay heat removal calculations for modular HTGRs is the thermal conductivity of graphite, which is dependent upon both temperature and neutron irradiation. A correlation modeling this behavior of graphite conductivity has been incorporated into SHERLOC.

Also, in pebble-bed cores, thermal radiation through the voids between pebbles must be accounted for as well as conduction. SHERLOC calculates an effective thermal conductivity for heat transfer by conduction and radiation in a randomly packed pebble bed.

1.1 Background

1.1.1 Application of Modular HTGRs

Interest in the development of small nuclear reactors for potential applications in the industrial heat market has been expressed in the United States, Federal Republic of Germany, Japan, and the Soviet Union. In the United States, industrial energy comsumption accounts for 40 percent of the total energy consumption [2]. Of the industrial energy used, 57 percent is used as process steam, and 43 percent as direct heat. Methods considered for serving the industrial heat market include the thermochemical pipeline, steam transmission, and sensible energy transport. The thermochemical pipeline may be used for district heating over long distances. Reactor heat is used to convert water and methane into hydroben and carbon monoxide, which are then transported through separate pipes. Where heat is needed the reverse reaction takes place, liberating energy. Steam transmission through pipelines can provide heat over short distances (less than 10 to 20 miles); while sensible energy transport, in which molten salt is used as the working fluid, can provide heat at somewhat greater distances than steam transmission.

The HTGR may also have applications in hydrogen production via several mechanisms: 1) steam reforming of a light hydrocarbon, 2) carbon-steam reaction using a heavy hydrocarbon, 3) thermochemical water splitting, and 4) electrolyses of water [3]. The HTGR has been

considered for use in steel production by the American Iron and Steel Institute and the General Atomic Technologies in the United States [3], and by Japan [4]. West Germany has investigated using a small HTGR for the following applications: generation of synthetic gas from coal and natural gas; process steam; generation of synthetic natural gas; process heat for conversion of fossil-energy raw materials, especially coal to liquid and gaseous secondary energy carriers; and production of hydrogen or methanol [5]. In addition, the HTGR could be used for cogeneration of process steam and electrical power. In such a mode, a small HTGR could provide the energy needs of an industrial community, a military complex, or an urban area. The Soviet Union is pursuing applications of HTGRs for cogeneration, hydrogen production, gasification of coal, reduction of iron ore, and district heating [6].

1.1.2 Summary of Preliminary Designs

It is evident that the HTGR, due to its capability of producing high temperature gas, has potential in the industrial heat market. Several preliminary designs for small HTGRs have been proposed. Designs proposed by General Electric Company, General Atomic Technologies, and Gesellschaft für Hochtemperaturreaktor - Technik are summarized here.

General Electric Company [2] and General Atomic Technologies [7]

The industrial heat market requires a higher availability of its heat source than does the electric power industry, where electricity is being channeled into an already existing grid. In the past, HTGR design has emphasized the large, monolithic HTGR which has a projected availability of 70 to 80 percent at best. For use as a source of

industrial heat, an availability of close to 100 percent is required. In response to this requirement, it has been suggested that several small reactors, or "modules," be used in parallel to support process heat or a thermochemical pipeline and a normal steam-electric plant. In the modular concept, one reactor may be shut down for refueling or maintenance without causing the entire plant to shut down; thus an availability of at least a portion of the full capacity of greater than 95 percent may be achieved.

The modular HTGR proposed by GE and GA consists of a prismatic core with internal, bottom entry control rods in a steel reactor vessel. The thermal rating of the core is 250 MWt, with a power density of 4.1 Wcc and outlet coolant temperature of 950°C. The core diameter is approximately 3.5 m. With a net electrical power of 11.5 MWe available for export and 147 MWt of thermochemical energy produced, the overall efficiency of each modular system is 63.4 percent. The reactor design employs an upflow, vertical in-line configuration with the heat exchanger located directly above the core. This configuration is designed to allow decay heat to be dissipated by natural circulation, radiation, and conduction; therefore, no core auxiliary cooling system is present. This design facilitates natural circulation through the core when forced circulation is lost. Figure 1.1 shows the vessel configuration; and Figures 1.2 and 1.3 show the coolant natural circulation paths with an active and inactive steam generator, respectively. Given a depressurized situation with no circulation whatsoever, heat would be conducted and radiated from the vessel to the surrounding environment.

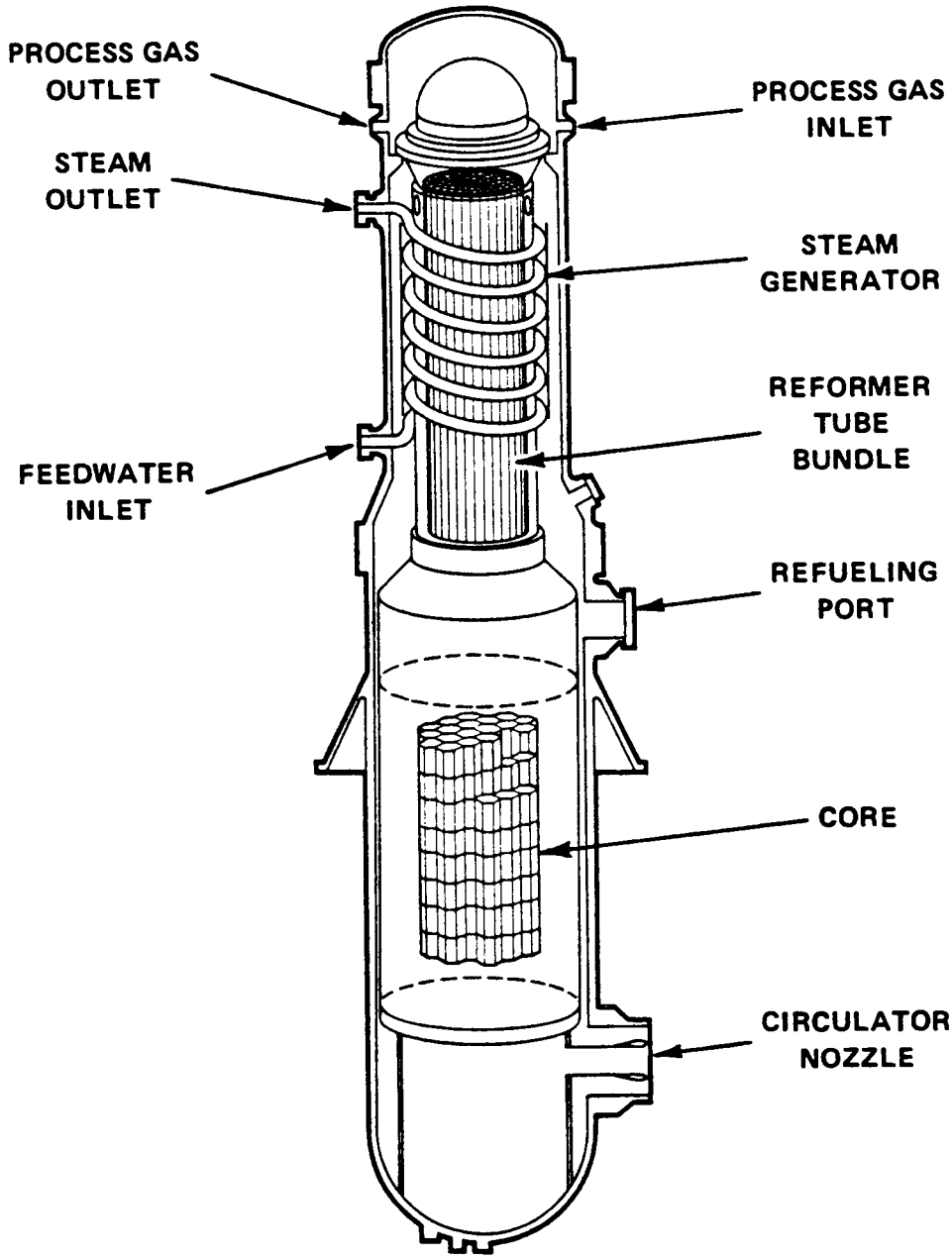

Figure 1.1 Prismatic-Core Modular HTGR Vessel Configuration
Source: General Electric Company

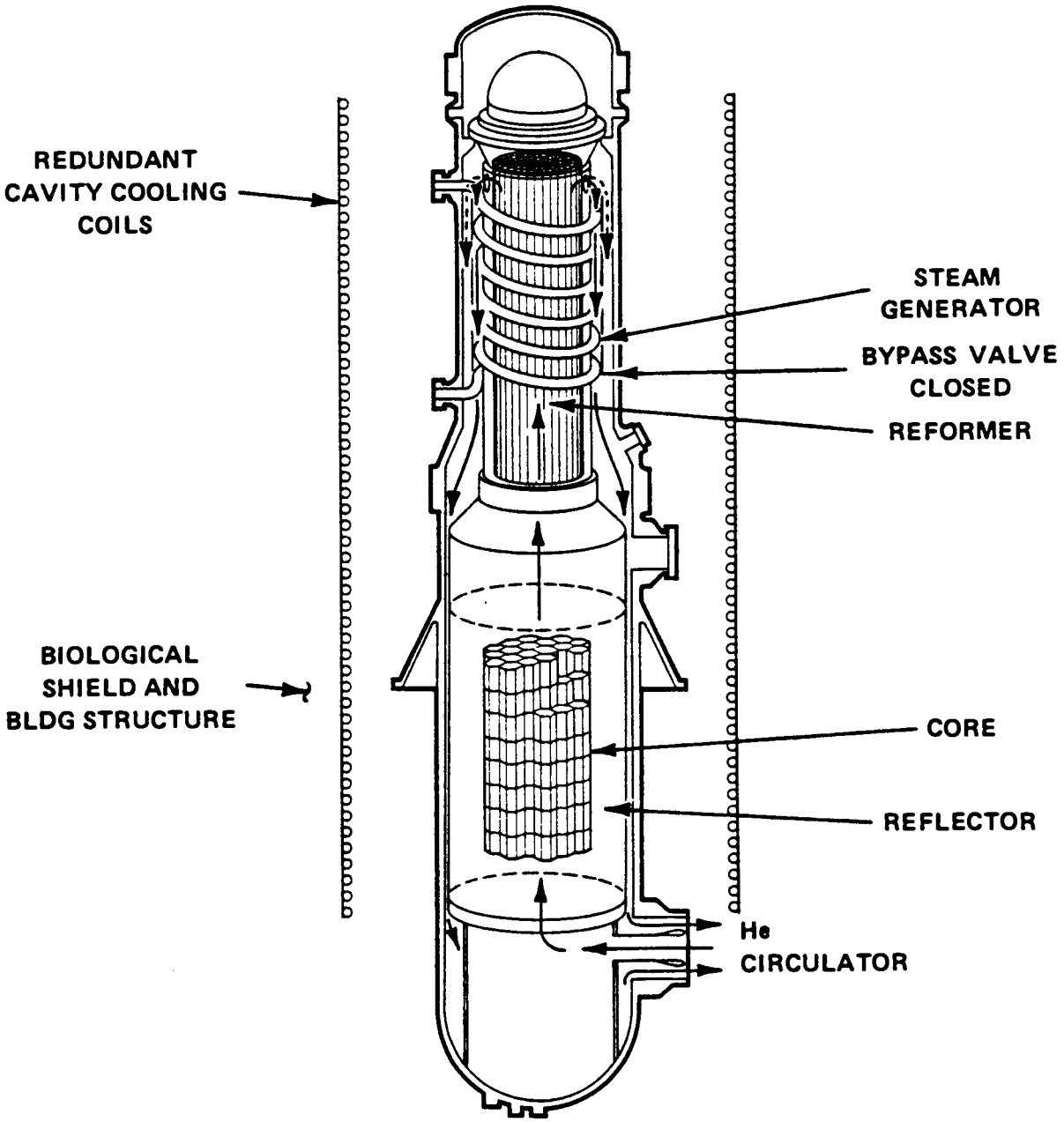

Figure 1.2 Prismatic-Core Modular HTGR Normal Flow Path
Source: General Electric Company

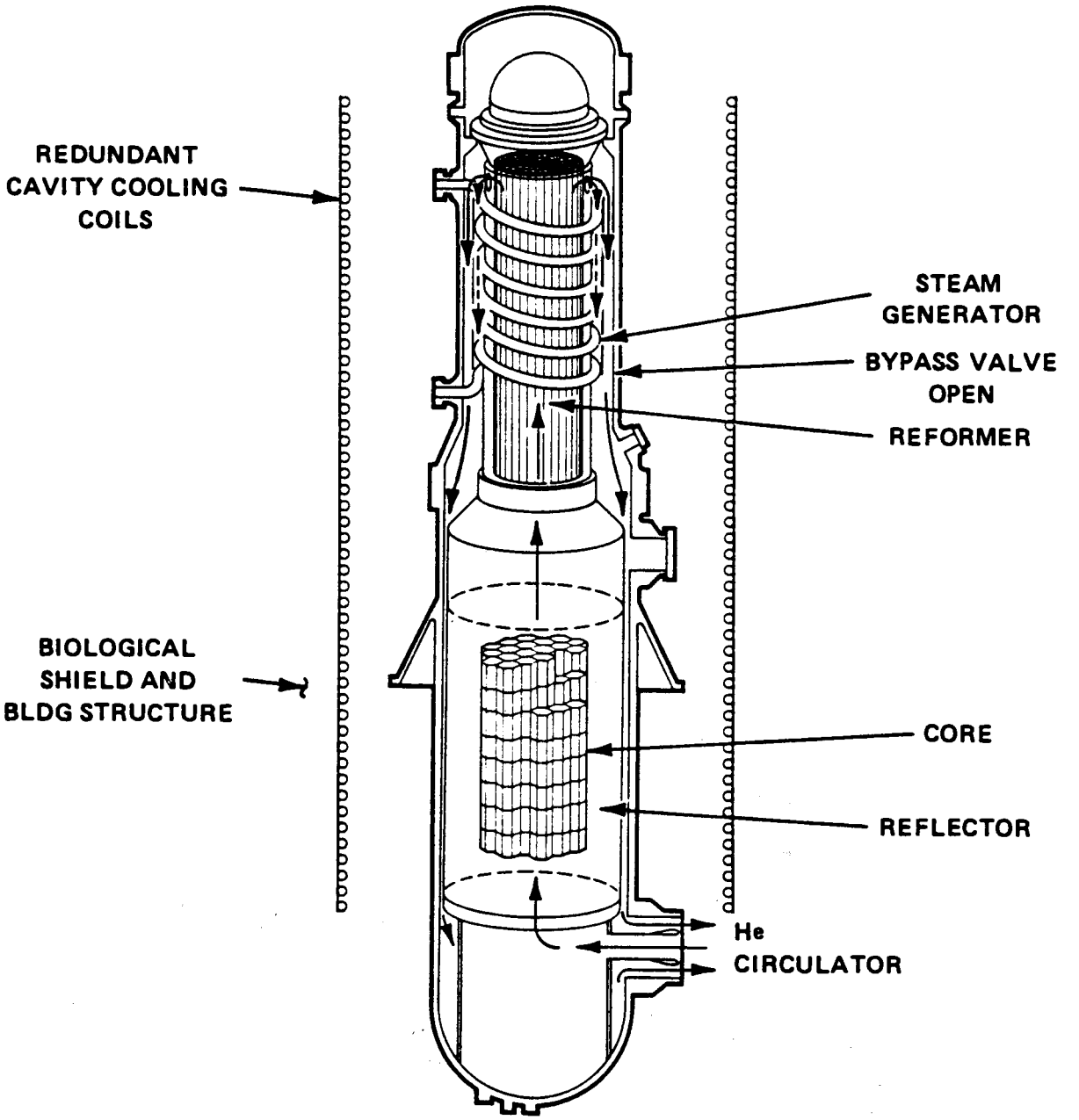

Figure 1.3 Prismatic-Core Modular HTGR Bypass Flow Path
Source: General Electric Company

The modular concept involves locating eight modules at a site to provide a total thermal rating of 2000 MWt and to achieve the desired high availability. A high degree of standardization among reactors and of factory pre-fabrication are expected to yield a site construction time of less than four years. The high availability and short construction time will offset the typically high direct costs of an HTGR system. Also, with replaceable modular units, the site life is expected to be one hundred years or more.

Gesellschaft für Hochtemperaturreaktor - Technik (GHT) [5]

The West German proposed modular reactor design stems from the design of the 15 MWe Arbeitsgemeinschaft Versuchs-reaktor (AVR), a steam cycle demonstration plant which has been in successful operation since 1967. The core of the AVR consists of approximately 100,000 graphite pebbles (6 cm in diameter) containing coated fuel particles. One of the advantages of the AVR is that on-line refueling is possible. The fuel pebbles are passed continuously through the core from top to bottom. After being withdrawn from the core, a pebble is either discarded or cycled through the core again, depending on its burnup.

The GHT modular reactor design uses a pebble-bed core with a thermal rating of 170 MWt, a power density of 2.5 W/cc, and a helium coolant outlet temperature of 950°C. The pebbles are circulated continuously, allowing on-line refueling - a pebble will pass through the core about 15 times during its life. Shutdown and control are accomplished with 6 short absorber rods located in the reflector region only. No control rods are inserted into the core itself. This control design limits the core diameter to 3 m and the power density to 2.5 W/cc.

A side-by-side configuration is used for the steel reactor vessel and heat exchanger, and is shown in Figure 1.4. Helium coolant flows down through the core in this design. Because the fuel at the top of the core has a lower burnup than the fuel at the bottom, the reactivity is higher at the top of the core. Temperatures would therefore tend to peak at the top of the core, and downflow allows maximum cooling of the high reactivity fuel. The side-by-side concept allows greater ease in maintenance and in-service inspection than does the vertical in-line configuration. Also, in the event of a scram, components such as the steam generator, circulator, and reformer are isolated and will not be exposed to a heat-up transient. Because the vessels are shorter in the side-by-side design, the reactor building height will also be considerably shorter.

1.2 Purpose of This Study

The objective of this study was to develop and apply a computational model to calculate fuel temperature distributions in modular, graphite-moderated HTGRs in a "worst case" accident situation - loss of forced convection and loss of pressure. In this accident scenario, the gas coolant is stagnant and heat is removed from the core by conduction and radiation only. The responses of several core configurations to the depressurized heatup accident have been investigated and compared.

The study consisted of two parts. The first part involved the development of the computer code SHERLOC, which analyzes the Small HTGR Thermal Response to Loss of Circulation. SHERLOC is a one-dimensional, finite-difference heat transfer code which has the capability of solving steady-state or transient problems in

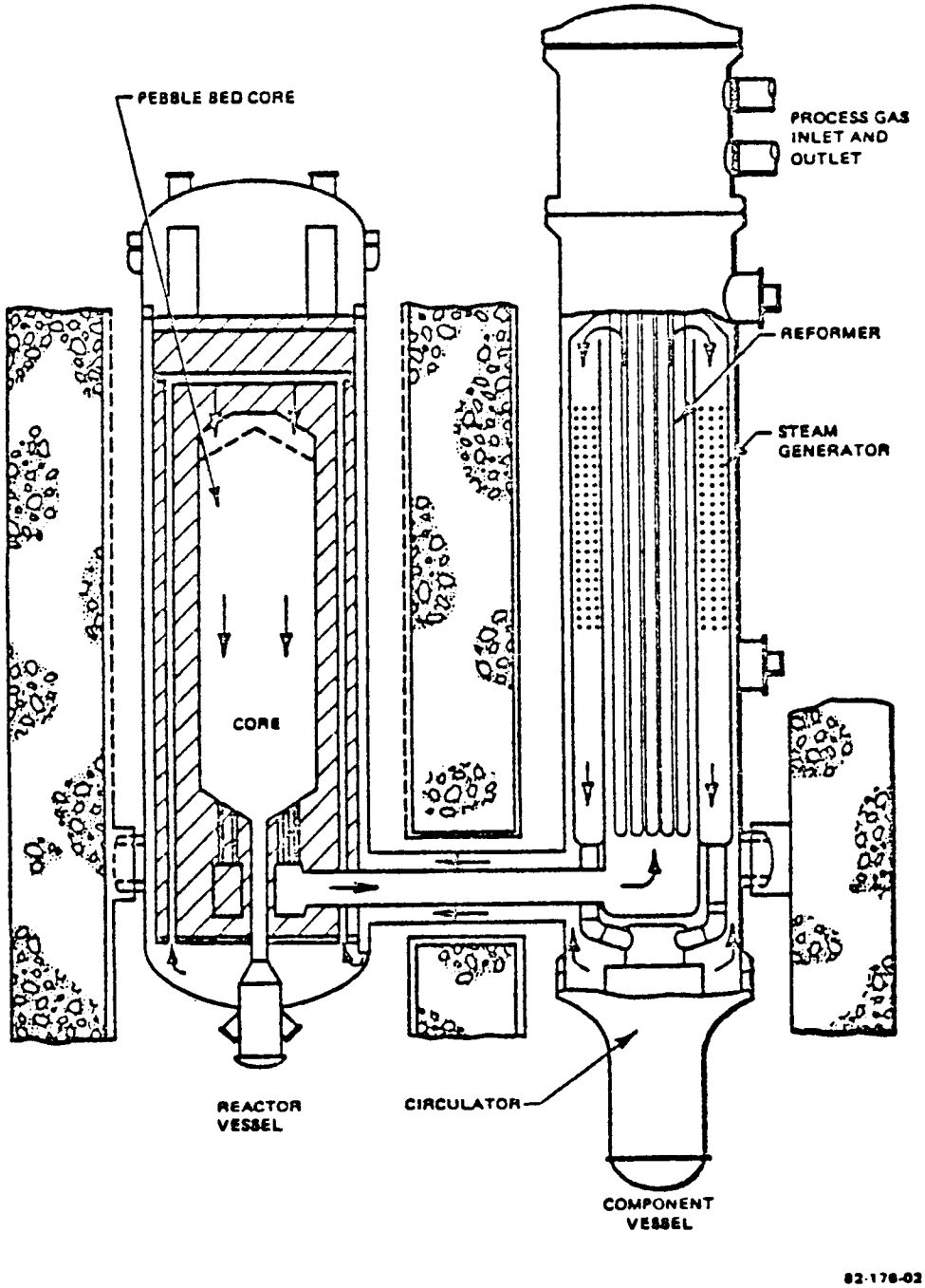

Figure 1.4 GHT Modular-Pebble-Bed Reactor Concept
Source: Gosellschaft fuar Hochtemperatur-reactor - Technik mbH (GHT)

rectangular or cylindrical coordinates and with convective and/or radiative boundary conditions. A multi-region, multi-material problem with temperature dependent thermal properties and space and time dependent internal heat generation may be modeled using SHERLOC. Considering heat transfer in only one dimension will produce a conservative analysis of the depressurized heatup accident.

Since the core of an HTGR consists primarily of graphite, the thermal conductivity of graphite is important in determining heat transfer from the core. Graphite thermal conductivity is a function not only of temperature, but also neutron irradiation, and this is accounted for by SHERLOC in regions specified as graphite. Also, when a pebble-bed core is considered, conduction is not the only means of heat transfer in the core - radiation occurs through the voids between pebbles. The modified Zehner-Schlünder model proposed by Breitbach and Barthels [8] is used to calculate an effective thermal conductivity for the pebble-bed which takes radiative heat transfer into account.

The second phase of this study involved the modeling of both pebble-bed and prismatic modular HTGRs and the calculation of the temperature distributions during the depressurized heatup transient. The effects of power density, initial temperature, neutron fluence, and vessel boundary conditions were investigated. Also the effects of modeling small, helium-filled gaps between prismatic fuel assemblies and of replacing the prismatic core with a bed of pebbles were studied.

2. CODE DEVELOPMENT

The development of the SHERLOC computer code consisted basically of four different sections: 1) the steady-state finite difference equations, 2) the transient finite difference equations, 3) the method of calculating fluence and temperature dependent graphite thermal conductivity, and 4) the modified Zehner-Schlünder model for effective conductivity in a pebble bed.

The steady-state and transient finite difference equations were derived in rectangular and cylindrical coordinates at the following unique locations: 1) the origin - an adiabatic boundary condition was assumed, 2) a mesh point within a material region, 3) the interface between two material regions, 4) the left-hand interface between a material region and a void region, 5) the right-hand interface between a void region and a material region, and 6) the outermost boundary - convective and/or radiative boundary conditions were assumed. At void interfaces and the outermost boundary, effective heat transfer coefficients are calculated to account for radiation and/or convection. The heat transfer equations may be non-homogeneous and non-linear; that is, heat generation may be a function of position and time, and thermal properties may be functions of temperature (and fluence for graphite). The mesh spacing within a given region is uniform; however, the mesh spacing may vary from region-to-region. The development of the finite difference equations and the methods of solution were patterned after those used by the HEATING6 computer code [1], a heat transfer code developed at the Oak Ridge National Laboratory.

2.1 Heat Transfer Coefficients at Void Interfaces and Outermost Boundary

Radiation occurs through void regions such as between a core barrel and reactor vessel, and radiation and/or convection occurs at the outermost boundary. In calculating heat transfer across the boundaries of a void region or the outer boundary, an effective heat transfer coefficient is determined. Radiative heat transfer between two surfaces is given by:

$$q'' = \sigma\varepsilon_{12}(T_1^{\,4}-T_2^{\,4}) = h_r(T_1-T_2) \tag{2.1}$$

where

q'' = heat flux

σ = Stefan-Boltzmann constant = $5.669\text{x}10^{-8}$ W/m^2K^4

ε_{12} = effective emittance from surface 1 to 2

h_r = effective radiation heat transfer coefficient

T_1 = temperature on surface 1

T_2 = temperature on surface 2

Solving equation (2.1) for h_r:

$$h_r = \sigma\varepsilon_{12}\frac{(T_1^{\,4}-T_2^{\,4})}{(T_1-T_2)}$$

$$= \sigma\varepsilon_{12}\frac{(T_1^{\,2}+T_2^{\,2})(T_1^{\,2}-T_2^{\,2})}{(T_1-T_2)}$$

$$= \sigma\varepsilon_{12}\frac{(T_1^{\,2}+T_2^{\,2})(T_1+T_2)(T_1-T_2)}{(T_1-T_2)}$$

$$h_r = \sigma\varepsilon_{12}(T_1^{\,2}+T_2^{\,2})(T_1+T_2) \tag{2.2}$$

The effective emittance ε_{12} (Ref. 9) is given by:

$$\varepsilon_{12} = \frac{1}{\left(\frac{1-\varepsilon_1}{\varepsilon_1}\right) + F_{12} + \frac{A_1}{A_2}\left(\frac{1-\varepsilon_2}{\varepsilon_2}\right)} \tag{2.3}$$

where

ε_1 = emissivity of surface 1

ε_2 = emissivity of surface 2

A_1 = surface area of surface 1

A_2 = surface area of surface 2

F_{12} = shape factor = fraction of radiation leaving surface 1 which reaches surface 2

For infinite concentric cylinders or infinite slabs, $F_{12} = 1.0$. Therefore, manipulating equation (2.2) yields:

$$\varepsilon_{12} = \frac{1}{\frac{1}{\varepsilon_1} + \frac{A_1}{A_2}\left(\frac{1}{\varepsilon_2} - 1\right)} \tag{2.4}$$

In rectangular coordinates, $A_1/A_2 = 1$; in cylindrical coordinates, $A_1/A_2 = r_1/r_2$, where r_1 and r_2 are the radii of surfaces 1 and 2, respectively.

The radiation heat transfer coefficient h_r must be calculated at both boundaries of a void region. On the inner surface, equation (2.2) applies; on the outer void surface, the effective emittance ε_{21} must be used in equation (2.2) rather than ε_{12} · ε_{21} is given by:

$$\varepsilon_{21} = \frac{1}{\left(\frac{1-\varepsilon_2}{\varepsilon_2}\right) + F_{21} + \frac{A_2}{A_1}\left(\frac{1-\varepsilon_1}{\varepsilon_1}\right)} \tag{2.5}$$

where

F_{21} = the fraction of energy leaving surface 2 reaching surface 1

We have the reciprocity relation (Ref. 9):

$$A_1F_{12} = A_2F_{21}$$

or

$$F_{21} = \frac{A_1}{A_2} F_{12}$$

Since $F_{12} = 1.0$,

$$F_{21} = \frac{A_1}{A_2} \tag{2.6}$$

By substituting equation (2.6) into equation (2.5), and with some minor algebraic manipulation and comparison with equation (2.4) we obtain:

$$\varepsilon_{21} = \frac{A_1}{A_2} \varepsilon_{12} \tag{2.7}$$

On the outermost boundary, it is assumed that the surrounding area is much greater than the outer surface area; thus A_1/A_2 goes to 0 in equation (2.3). Therefore, on the outer boundary, the radiation heat transfer coefficient reduces to:

$$h_r = \sigma\varepsilon_s(T_s^{\,2} + T_\infty^{\,2})(T_s + T_\infty) \tag{2.8}$$

where

ε_s = emissivity of the surface material

T_s = surface temperature

T_∞ = ambient temperature

To obtain the effective heat transfer coefficient at the surface, the convective heat transfer coefficient h_c (which is assumed to be given) and the radiative heat transfer coefficient are combined in series:

$$h_r = h_r + h_c$$

where

h_r = effective heat transfer coefficient

2.2 Steady-State Finite-Difference Equations

In the steady-state, no heat is stored in a volume, and the heat balance on a control volume V may be represented as

$$\begin{bmatrix}\text{Net rate of heat}\\ \text{entering V through}\\ \text{its boundaries}\end{bmatrix} + \begin{bmatrix}\text{Rate of heat}\\ \text{generation}\\ \text{in V}\end{bmatrix} = 0$$

2.2.1 Rectangular Coordinates

The one-dimensional, steady-state conduction equation in rectangular coordinates is:

$$k(T)\,\frac{d^2T(x)}{dx^2} + g(x) = 0 \qquad (2.9)$$

where

$k(T)$ = temperature dependent thermal conductivity

$g(x)$ = position dependent volumetric heat generation rate

Consider a mesh point within a given region, as shown in Figure 2.1a. The finite difference heat balance on mesh point i is:

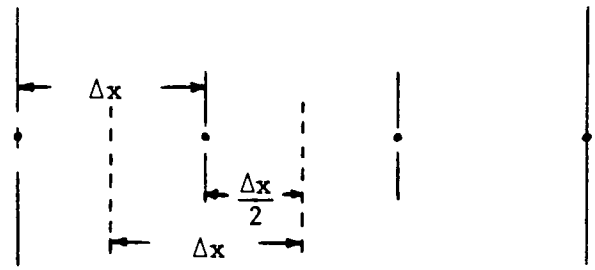

(a)

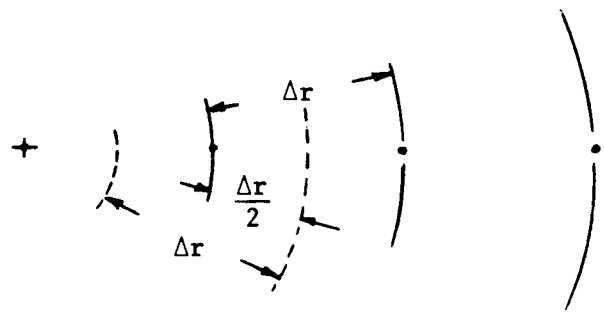

(b)

Figure 2.1

(a) Internal Mesh Point - Rectangular Geometry

(b) Internal Mesh Point - Cylindrical Geometry

$$ {}_iK_{i-1} \frac{(T_{i-1}-T_i)}{\Delta x} + {}_kK_{i+1} \frac{(T_{i+1}-T_i)}{\Delta x} = -g_i \, \Delta x \qquad (2.10) $$

where

${}_iK_{i-1}$ = thermal conductivity between mesh points i and i-1

${}_iK_{i+1}$ = thermal conductivity between mesh points i and i+1

T_i = temperature at mesh point i

g_i = volumetric heat generation of mesh interval i

Manipulating equation (2.10) yields:

$$ {}_iK_{i-1}T_{i-1} - ({}_iK_{i-1}+K_{i+1})T_i + {}_iK_{i+1}T_{i+1} = -g_i(\Delta x)^2 \qquad (2.11) $$

The steady-state, rectangular, finite difference equations for each unique type of mesh point (listed in Chapter 2) are derived in detail in Appendix A. It is easily seen that a problem containing n mesh points will produce n equations in n unknowns, which may be solved simultaneously. The equations may be represented in the matrix form

$$ A\hat{T} = \hat{b} \qquad (2.12) $$

where

A = matrix of coefficients

$\hat{T}$ = vector of temperatures

$\hat{b}$ = vector of forcing functions

Since only three terms appear on the left-hand side of the equations, the coefficient matrix A will be tridiagonal. The equations may be solved using any one of a number of techinques for solving a linear system of equations in matrix form.

2.2.2 Cylindrical Coordinates

The one-dimensional, steady-state conduction equation in cylindrical coordinates is:

$$k(T)\,\frac{d^2T(r)}{dr^2} + k(T)\,\frac{1}{r}\,\frac{dT(r)}{dr} + g(r) = 0 \qquad (2.13)$$

Again we shall consider here a mesh point within a given region, as shown in Figure 2.1b. The finite-difference form of the heat balance equation is:

$$2\pi r_a\ {}_iK_{i-1}\,\frac{(T_{i-1}-T_i)}{\Delta r} + 2\pi r_b\ {}_iK_{i+1}\,\frac{(T_{i+1}-T_i)}{\Delta r} = -g_i\pi(r_b{}^2-r_a{}^2) \qquad (2.14)$$

It is assumed that the mesh spacing within a region will be constant. Therefore,

$$r_a = r_i - \Delta r/2 \qquad (2.15a)$$

$$r_b = r_i + \Delta r/2 \qquad (2.15b)$$

Substituting equations (2.15a) and (2.15b) into equation (2.14) and rearranging:

$$\frac{(r_i+\Delta r/2)}{\Delta r}\ {}_iK_{i+1}T_{i+1} + \frac{(r_i-\Delta r/2)}{\Delta r}\ {}_iK_{i-1}T_{i-1}$$

$$-\left[\frac{(r_i+\Delta r/2)}{\Delta r} + \frac{(r_i-\Delta r/2)}{\Delta r}\ {}_iK_{i-1}\right] T_i = -g_i\,\frac{(r_a + r_b)(r_a - r_b)}{2}$$

or

$$\frac{(r_i-\Delta r/2)}{\Delta r}\,{}_iK_{i-1}T_{i-1} - \left[\frac{(r_i-\Delta r/2)}{\Delta r}\,{}_iK_{i-1} + \frac{(r_i+\Delta r/2)}{\Delta r}\,{}_iK_{i+1}\right]$$

$$+\frac{(r_i+\Delta r/2)}{\Delta r}\,{}_iK_{i+1}T_{i+1} = -g_i r_i \Delta r \qquad (2.16)$$

The steady-state, cylindrical, finite-difference equations for each unique type of point are derived in detail in Appendix A. Again, a tridiagonal matrix may be constructed to represent the equations and may be solved for the temperature distribution.

2.3 Transient Finite-Difference Equations

The heat balance on a control volume V in a transient case may be represented by

$$\begin{bmatrix}\text{Net rate of heat}\\ \text{entering V through}\\ \text{its boundaries}\end{bmatrix} + \begin{bmatrix}\text{Rate of heat}\\ \text{generation}\\ \text{in V}\end{bmatrix} = \begin{bmatrix}\text{Energy}\\ \text{stored}\\ \text{in V}\end{bmatrix}$$

2.3.1 The One-dimensional, Transient Conduction Equation in Rectangular Coordinates

$$K(T)\,\frac{\partial^2 T(x,t)}{\partial x^2} + g(x,t) = \rho(T)C_p(T)\,\frac{\partial T(x,t)}{\partial t}$$

where

$g(x,t)$ = space and time dependent volumetric heat generation

$C_p(T)$ = temperature dependent specific heat

$\rho(T)$ = temperature dependent density

For a mesh point within a given region (see Figure 2.1a), the transient finite difference equation is

$$\rho_i C_{pi} \frac{(T_i^{n+1} - T_i^{\,n})}{\Delta t} \Delta x = g_i^n \Delta x + {}_iK_{i-1} \frac{(T_{i-1}^n - T_i^n)}{\Delta x} + {}_iK_{i+1} \frac{(T_{i+1}^n - T_i^n)}{\Delta x} \tag{2.18}$$

where

T_i^n = temperature at node i at time t_n

T_i^{n+1} = temperature at node i at time t_{n+1}

The transient, rectangular, finite difference equations at each unique type of point are derived in detail in Appendix B. Equation (2.18) is a forward difference equation; the temperature at time t_{n+1} is given in terms of the temperature at time t_n. However, the forward differencing scheme, or Classical Explicit Method, may be unstable for some time steps [10]. If the right-hand side of equation (2.18) is evaluated at t_{n+1} rather than at t_n, the algorithm is the backwards Euler, or Classical Implicit Procedure (CIP), and is stable for any time step [10]. If the right-hand side of equation (2.18) is evaluated at $t_{n+\frac{1}{2}}$, the procedure is known as central differencing, or the Crank-Nicholson (CN) procedure. The CN procedure is also stable for any time step [10]. For stability reasons, a θ-differencing scheme is employed in SHERLOC. In this procedure, equation (2.18) is given as

$$(\rho_i C_{pi})^{n+\theta} \frac{(T_i^{n+1}-T_i^n)}{\Delta t} (\Delta x)^2 = g_i^n(\Delta x)^2 + \theta\left\{{}_iK_{i-1}^{n+\theta}(T_{i-1}^{n+1}-T_i^{n+1}) + {}_iK_{i+1}^{n+\theta}(T_{i+1}^{n+1}-T_i^{n+1})\right\} + (1-\theta)\left\{{}_iK_{i-1}^{n+\theta}(T_{i-1}^{n}-T_i^{n}) + {}_iK_{i+1}^{n+\theta}(T_{i+1}^{n}-T_i^{n})\right\} \quad (2.19)$$

If θ=0.0, equation (2.19) reduces to equation (2.18). If θ=0.5, the method is the CN method; if θ=1.0, equation (2.19) becomes the CIP. We shall choose to limit the value of θ to $0.5 < \theta < 1.0$ so that the solution will be stable for all time steps.

Rewriting equation (2.19) with all the terms evaluated at t_{n+1} on the left-hand side:

$$-\theta\left\{{}_iK_{i-1}^{n+\theta}(T_{i-1}^{n+1}-T_i^{n+1}) + {}_iK_{i+1}^{n+\theta}(T_{i+1}^{n+1}-T_i^{n+1})\right\} + (\rho_i C_{pi})^{n+\theta}(\Delta x)^2 \frac{T_i^{n+1}}{\Delta t} = H_i \quad (2.20)$$

where

$$H_i = (\rho_i C_{pi})^{n+\theta}(\Delta x)^2 \frac{T_i^n}{\Delta t} + g_i^n(\Delta x)^2 + (1-\theta) \times \left\{{}_iK_{i-1}^{n+\theta}(T_{i-1}^{n}-T_i^{n}) + {}_iK_{i+1}^{n+\theta}(T_{i+1}^{n}-T_i^{n})\right\} \quad (2.21)$$

Collecting the T_i^{n+1} terms in equation (2.20):

$$-\theta\left\{{}_iK_{i-1}^{n+\theta}\, T_{i-1}^{n+1} + {}_iK_{i+1}^{n+\theta}\, T_{i+1}^{n+1}\right\} + \left\{\theta({}_iK_{i-1}^{n+\theta} + {}_iK_{i+1}^{n+\theta}) + (\rho_i C_{pi})^{n+\theta}\frac{(\Delta x)^2}{\Delta t}\right\} T_i^{n+1} = H_i \quad (2.22)$$

Let

$$D_i = \left[\theta({}_iK_{i-1}^{n+\theta} + {}_iK_{i+1}^{n+\theta}) + (\rho_i C_{pi})^{n+\theta} \frac{(\Delta x)^2}{\Delta t}\right] \tag{2.23}$$

Then

$$-\theta\left[{}_iK_{i-}^{n+\theta} T_{i-1}^{n+1} + {}_iK_{i+1}^{n+\theta} T_{i+1}^{n+1}\right] + D_i T_i^{n+1} = H_i$$

Solving for T_i^{n+1}:

$$T_i^{n+1} = \frac{1}{D_i}\left\{H_i + \theta\left[{}_iK_{i-1}^{n+\theta} T_{i-1}^{n+1} + {}_iK_{i+1}^{n+\theta} T_{i+1}^{n+1}\right]\right\} \tag{2.24}$$

Note that D_i and H_i are known; they are dependent on temperatures at time t_n, properties, and geometry. Therefore the superscript n+1 is dropped from equation (2.24) and it is understood that the temperatures appearing in that equation are evaluated at t_{n+1}. Thus,

$$T_i = \frac{1}{D_i}\left\{H_i + \theta\left[{}_iK_{i-1}^{n+\theta} T_{i-1}^{n+1} + {}_iK_{i+1}^{n+\theta} T_{i+1}^{n+1}\right]\right\} \tag{2.25}$$

The temperature distribution at t_{n+1} is solved for one mesh point at a time, beginning with the first mesh point. Therefore, in equation (2.25), T_{i-1} is known, but T_{i+1} is not. An estimate must be made for T_{i+1}, and an iterative process used to solve for the temperature distribution at t_{n+1}. For the first estimation, T_{i+1}^n will be used rather than $T_{i+1}^{(n+1)}$. An estimate of the temperature at each node i is solved for, and used for the new estimate at T_{i+1}. Thus we have

$$T_i^{\ell+1} = \frac{1}{D_i}\left\{H_i + \theta\left[{}_iK_{i-1}^{n+\theta} T_{i-1}^{\ell+1} + {}_iK_{i+}^{n+\theta} T_{i+1}^{\ell}\right]\right\} \tag{2.26}$$

where the superscript $\ell+1$ refers to the $(\ell+1)$st iteration on the temperature distribution at time t_{n+1}. Iterations are continued until convergence is reached (convergence will be discussed in Chapter 3).

The iterative process can be further refined by taking $T_i^{\ell+1}$ in equation (2.26) to be an estimate of the temperature at the $(\ell+1)$st iteration. Let

$$\hat{T}_i^{\ell+1} = \frac{1}{D_1}\left\{H_i + \theta\left[{}_iK_{i-1}^{n+\theta}\, T_{i-1}^{\ell+1} + {}_iK_{i+1}^{n+\theta}\, T_{i+1}^{\ell}\right]\right\} \tag{2.27}$$

Then, let the temperature at the $(\ell+1)$st iteration be defined as

$$T_i^{\ell+1} = T_i^{\ell} + \omega\,(\hat{T}_i^{\ell+1} - T_i^{\ell}) \tag{2.28}$$

or

$$T_i^{\ell+1} = (1-\omega)T_i^{\ell} + \hat{T}_i^{\ell+1} \tag{2.29}$$

where ω is referred to as the acceleration factor. The range of ω is $0.0 < \omega < 2.0$, and the solution generally converges faster if $\omega \neq 1$ [1]. If $\omega < 1$, the solution is underrelaxed; if $\omega > 1$, the solution is overrelaxed. This process is referred to as point successive overrelaxation [1]. Combining equations (2.29) and (2.26) yields the following for the temperature at the $(\ell+1)$st iteration on the time t_{n+1}

$$T_i^{\ell+1} = (1-\omega)T_i^{\ell} + \frac{\omega}{D_i}\left\{H_i + \theta\left[{}_iK_{i-1}^{n+\theta}\, T_{i-1}^{\ell+1} + {}_iK_{i+1}^{n+\theta}\, T_{i+1}^{\ell}\right]\right\} \tag{2.30}$$

2.3.2 Temperature Dependent Thermal Properties

Thermal properties which vary with temperature are treated in the following manner. Initially the properties are calculated using the initial temperature distribution, which is given. Then the iterative procedure given by equation (2.30) is used to calculate the temperature distribution at the time step t_{n+1}. However, in this iterative procedure the thermal properties are not updated, so the converged solution given by equation (2.30) is only an estimate of the actual temperature distribution. The thermal properties are updated, and the procedure repeated. Thus the problem solution consists of two levels of iteration: the inner loop iterates on the temperature distribution using equation (2.30), while the outer loop iterates on the thermal properties. The thermal properties are updated as follows: T_i^n is the final, converged temperature distribution at time t_n. $\hat{T}_i^{n,m}$ is the estimate of the temperature distribution at time t_{n+1} after the mth iteration on properties. The thermal properties will be reevaluated at the temperature:

$$T_i^{n+\theta} = (1-\theta)T_i^n + \theta\hat{T}_i^{n+1,m} \tag{2.31}$$

2.3.3 Cylindrical Coordinates

The one-dimensional, transient conduction equation in cylindrical coordinates is

$$k(T)\frac{\partial^2 T(r,t)}{\partial r^2} + k(T)\frac{1}{r}\frac{\partial T(r,t)}{\partial r} + g(r,t) = \rho(T)C_p(T)\frac{\partial T(r,t)}{\partial t} \tag{2.32}$$

For a mesh point within a given region (see Figure 2.1b) the transient finite difference equation is

$$(\rho_i C_{pi}) \frac{(T_i^{n+1}-T_i^n)}{\Delta t} \pi(r_b^2 - r_a^2) = g_i \pi(r_b^2 - r_a^2) + 2\pi r_a \, {}_iK_{i-1} \frac{(T_{i-1}^n - T_i^n)}{\Delta r}$$

$$+ \; 2\pi r_b \, {}_iK_{i+1} \frac{(T_{i+1}^n - T_i^n)}{\Delta r} \tag{2.33}$$

We have the following:

$$r_a = r_i - \Delta r/2 \tag{2.34a}$$

$$r_b = r_i + \Delta r/2 \tag{2.34b}$$

$$r_b^2 - r_a^2 = 2r_i \Delta r \tag{2.34c}$$

Substituting equations (2.34a-c) into equation (2.33) and applying the θ-differencing scheme described in section 2.3.1 yields the following

$$(\rho_i C_{pi})^{n+\theta} \frac{(T_i^{n+1}-T_i^n)}{\Delta t} (2r_i \Delta r) = g_i^n (2r_i \Delta r) + \theta \left[{}_iK_{i-1}^{n+\theta} (T_{i-1}^{n+1} - T_i^{n+1}) \frac{(2r_i - \Delta r)}{\Delta r} \right.$$

$$\left. + \; {}_iK_{i+1}^{n+\theta} (T_{i+1}^{n+1} - T_i^{n+1}) \frac{(2r_i + \Delta r)}{\Delta r} \right] + (1-\theta) \left[{}_iK_{i-1}^{n+\theta} (T_{i-1}^n - T_i^n) \frac{(2r_i - \Delta r)}{\Delta r} \right.$$

$$\left. + \; {}_iK_{i+1}^{n+\theta} (T_{i+1}^n - T_i^n) \frac{(2r_i + \Delta r)}{\Delta r} \right] \tag{2.35}$$

Rewriting equation (2.35) with all the terms evaluated at t_{n+1} on the left-hand side

$$- \theta\left[{}_iK_{i-1}^{n+\theta}(T_{i-1}^{n+1}-T_i^{n+1}) \frac{(2r_i-\Delta r)}{\Delta r} + {}_iK_{i+1}^{n+\theta}(T_{i+1}^{n+1}-T_i^{n+1}) \frac{(2r_i+\Delta r)}{\Delta r}\right] +$$

$$(\rho_i C_{pi})^{n+\theta}(2r_i\Delta r) \frac{T_i^{n+1}}{\Delta t} = H_i \qquad (2.36)$$

where

$$H_i = (\rho_i C_{pi})^{n+\theta}(2r_i\Delta r) \frac{T_i^n}{\Delta t} + g_i^n(2r_i\Delta r) + (1-\theta)$$

$$\left[{}_iK_{i-1}^{n+\theta} (T_{i-1}^n-T_i^n) \frac{(2r_i-\Delta r)}{\Delta r} + {}_iK_{i+1}^{n+\theta} (T_{i+1}^n-T_i^n) \frac{(2r_i+\Delta r)}{\Delta r}\right] \qquad (2.37)$$

Collecting the T_i^{n+1} terms in equation (2.36)

$$-\theta\left[{}_iK_{i-1}^{n+\theta} T_{i-1}^{n+1} \frac{(2r_i-\Delta r)}{\Delta r} + {}_iK_{i+1}^{n+\theta} T_{i+1}^{n+1} \frac{(2r_i+\Delta r)}{\Delta r}\right] +$$

$$\left\{\theta\left[{}_iK_{i-1}^{n+\theta} \frac{(2r_i+\Delta r)}{\Delta r} + {}_iK_{i+1}^{n+\theta} \frac{(2r_i+\Delta r)}{\Delta r}\right] + (\rho_i C_{pi})^{n+\theta}\frac{(2r_i\Delta r)}{\Delta r}\right\} T_i^{n+1} = H_i$$

(2.38)

Let

$$D_i = \left\{\theta\left[{}_iK_{i-1}^{n+\theta} \frac{(2r_i-\Delta r)}{\Delta r} + {}_iK_{i+1}^{n+\theta} \frac{(2r_i+\Delta r)}{\Delta r}\right] + (\rho_i C_{pi})^{n+\theta}\frac{(2r_i\Delta r)}{\Delta t}\right\}$$

(2.39)

Substituting equation (2.39) into equation (2.38) and solving for T_i^{n+1}

$$T_i^{n+1} = \frac{1}{D_i}\left\{H_i + \theta\left[{}_iK_{i-1}^{n+\theta}\, T_{i-1}^{n+1}\, \frac{(2r_i-\Delta r)}{\Delta r} + {}_iK_{i+1}^{n+\theta}\, T_{i+1}^{n+1}\, \frac{(2r_i+\Delta r)}{\Delta r}\right]\right\} \tag{2.40}$$

Since T_{i+1}^{n+1} is unknown, the iterative procedure described in section 2.3.1 is used. Combining the notation for the iterative procedure and the point successive overrelaxation method described in section 2.3.1, we obtain

$$T_i^{\ell+1} = (1-\omega)T_i^{\ell} + \frac{\omega}{D_i}\left\{H_i + \theta\left[{}_iK_{i-1}^{n+\theta}\, T_{i-1}^{\ell+1}\, \frac{(2r_i-\Delta r)}{\Delta r} + {}_iK_{i+1}^{n+\theta}\, T_i^{\ell}\, \frac{(2r_i+\Delta r)}{\Delta r}\right]\right\} \tag{2.41}$$

Again, the inner loop on equation (2.41) must be performed, and then the outer loop on the thermal properties, until convergence is reached for both loops.

2.3.4 Summary of Transient Finite Difference Equations

The transient finite difference equations for each unique type of mesh point are summarized here for both rectangular and cylindrical coordinates. (These equations are derived in Appendix B.) The equations have the same form for both types of geometries, but

with different geometric coefficients. The coefficients are given in Table 2.1.

Origin:

$$T_i^{\ell+1} = (1-\omega)T_i^{\ell} + \frac{}{D_i}\left[H_i + \theta(s_1\ {}_iK_{i+1}^{n+\theta}\ T_{i+1}^{\ell})\right] \tag{2.42a}$$

where

$$D_i = \theta\ s_1\ {}_iK_{i+}^{n+\theta} + (\rho_i C_{pi})^{n+\theta}\frac{s_2}{\Delta t} \tag{2.42b}$$

$$H_i = \frac{s_2}{\Delta t}(\rho_i C_{pi})^{n+\theta}T_i^n + g_i^n\ s_2 + (1-\theta)\left[s_1\ {}_iK_{i+1}^{n+\theta}(T_{i+1}^n - T_i^n)\right] \tag{2.42c}$$

Internal Node:

$$T_i^{\ell+1} = (1-\omega)T_i^{\ell} + \frac{\omega}{D_i}\left[H_i + \theta(a_1\ {}_iK_{i-1}^{n+\theta}\ T_{i-1}^{\ell+1} + a_2\ {}_iK_{i+1}^{n+\theta}\ T_{i+1}^{\ell})\right] \tag{2.43a}$$

where

$$D_i = \theta\left[a_1\ {}_iK_{i-1}^{n+\theta} + a_2\ {}_iK_{i+1}^{n+\theta}\right] + \frac{a_3}{\Delta t}(\rho_i C_{pi})^{n+\theta} \tag{2.43b}$$

$$H_i = \frac{a_3}{\Delta t}(\rho_i C_{pi})^{n+\theta}T_i^n + g_i^n\ a_3 + (1-\theta)\left[a_1\ {}_iK_{i-1}^{n+\theta}\ (T_{i-1}^n - T_i^n) + a_2\ {}_iK_{i+1}^{n+\theta}\ (T_{i+1}^n - T_i^n)\right] \tag{2.43c}$$

Material Region Interface: Same as equations (2.43a-c), but with different coefficients as shown in Table 2.1.

Table 2.1

Coefficients for Transient Finite Difference Equations in Rectangular and Cylindrical Geometries

Mesh Point Type	Coefficient	Rectangular	Cylindrical
ORIGIN	s_1	1.0	2.0
	s_2	$\frac{(\Delta x)^2}{2}$	$\frac{(\Delta r)^2}{2}$
INTERNAL NODE	a_1	1.0	$\frac{(2r_i-\Delta r)}{\Delta r}$
	a_2	1.0	$\frac{(2r_i+\Delta r)}{\Delta r}$
	a_3	$(\Delta x)^2$	$2r_i\Delta r$
MATERIAL REGION INTERFACE	a_1	$\Delta_2/(\Delta_1+\Delta_2)$	$\frac{(2r_i-\Delta_1)}{\Delta_1}$
	a_2	$\Delta_1/(\Delta_1+\Delta_2)$	$\frac{(2r_i+\Delta_2)}{\Delta_2}$
	a_3	$\Delta_1\Delta_2/2$	$\frac{(\Delta_1+\Delta_2)(r_i+\Delta_2-\Delta_1)}{4}$

Table 2.1 (Continued)

Mesh Point Type	Coefficient	Rectangular	Cylindrical
LEFT VOID BOUNDARY	a_1	1.0	$\frac{(r_i-\Delta_1/2)}{\Delta_1}$
	a_2	Δ_1	r_i
	a_3	$(\Delta_1)^2$	$\Delta_1(r_i-\frac{\Delta 1}{4})$
RIGHT VOID BOUNDARY	a_1	Δ_1	r_i
	a_2	1.0	$\frac{(r_i+\Delta_2/2)}{\Delta_2}$
	a_3	$(\Delta_1)^2$	$\Delta_2(r_i+\frac{\Delta_2}{4})$
OUTERMOST BOUNDARY	b_1	1.0	$\frac{(R-\Delta r/2)}{\Delta r}$
	b_2	Δx	R
	b_3	$(\Delta x)^2$	$\Delta r(R-\frac{\Delta r}{4})$

NOTE: At interfaces - Δ_1 refers to mesh spacing to the left of the interface
Δ_2 refers to mesh spacing to the right of the interface

Left Void Boundary:

$$T_i^{\ell+1} = (1-\omega)T_i^{\ell} + \frac{\omega}{D_i}\left[H_i + 2\theta(a_1\ {}_iK_{i-1}^{n+\theta}\ T_{i-1}^{\ell+1} + a_2\ h_{r_{12}}^{n+\theta}\ T_{i+1}^{\ell})\right] \tag{2.44a}$$

where

$$D_i = 2\theta\left[a_1\ {}_iK_{i-1}^{n+\theta} + a_2\ h_{r_{12}}^{n+\theta}\right] + \frac{a_3}{\Delta t}\ (\rho_i C_{pi})^{n+\theta} \tag{2.44b}$$

$$H_i = \frac{a_3}{\Delta t}(\rho_i C_{pi})^{n+\theta} T_i^n + g_i^n\ a_3 + 2(1-\theta)\left[a_1\ {}_iK_{i-1}^{n+\theta}\ (T_{i-1}^n - T_i^n) + a_2\ h_{r_{12}}^{n+\theta}\ (T_{i+1}^n - T_i^n)\right] \tag{2.44c}$$

Right Void Boundary:

$$T_i^{\ell+1} = (1-\omega)T_i^{\ell} + \frac{\omega}{D_i}\left[H_i + 2\theta(a_1\ h_{r_{21}}^{n+\theta}\ T_{i-1}^{\ell+1} + a_2\ {}_iK_{i+1}^{n+\theta}\ T_{i+1}^{\ell})\right] \tag{2.45a}$$

where

$$D_i = 2\theta\left[a_1\ h_{r_{21}}^{n+\theta} + a_2\ {}_iK_{i+1}^{n+\theta}\right] + (\rho_i C_{pi})^{n+\theta}\ \frac{a_3}{\Delta t} \tag{2.45b}$$

$$H_i = \frac{a_3}{\Delta t} (\rho_i C_{pi})^{n+\theta} T_i^n + g_i^n a_3 + 2(1-\theta)\left[a_1 h_{r_{21}}^{n+\theta}(T_{i-1}^n - T_i^n) + a_2 {}_iK_{i+\theta}^{n+\theta}(T_{i+1}^n - T_i^n)\right] \tag{2.45c}$$

Outermost Boundary:

$$T_i^{\ell+1} = (1-\omega)T_i^{\ell} + \frac{\omega}{D_i}\left[H_i + 2\theta(b_1 {}_iK_{i-1}^{n+\theta} T_{i-1}^{\ell+1} + b_2 h_T^{n+\theta} T_\infty)\right] \tag{2.46a}$$

where

$$D_i = 2\theta\left[b_1 {}_iK_{i-1}^{n+\theta} + b_2 h_T^{n+\theta}\right] + (\rho_i C_{pi})^{n+\theta} \frac{b_3}{\Delta t} \tag{2.46b}$$

$$H_i = \frac{b_3}{\Delta t} (\rho_i C_{pi})^{n+\theta} T_i^n + g_i^n b_3 + 2(1-\theta)\left[b_1 {}_iK_{i-1}^{n+\theta} (T_{i-1}^n - T_i^n) + b_2 h_T^{n+\theta}(T_\infty - T_i^n)\right] \tag{2.46c}$$

where

$h_T^{n+\theta}$ = effective heat transfer coefficient at boundary

T_∞ = ambient temperature

2.4 Thermal Conductivity of Graphite

The transport of heat in graphite occurs primarily by lattice vibrations (phonons) rather than by electrons or holes. One example of the evidence supporting this theory is the Weidemann-Franz ratio R_{WF} in graphite

$$R_{WF} = \frac{k\rho}{T}$$

where

k = thermal conductivity

ρ = electrical resistivity

T = absolute temperature

The value of the Weidemann-Franz ratio is 10 to 100 times higher for graphite than it is for most metals [11] in which heat conduction occurs primarily by electron transport. The thermal conductivity of graphite is approximately proportional to the lattice wave mean free path, which is essentially the size of the crystal. Lattice waves are scattered at crystal boundaries and at radiation-induced scattering centers. Radiation damage in a material may be caused by 1) displacement of atoms from the lattice by transfer of energy from neutrons, 2) excitation of electrons, and 3) transmutation of the atoms in the solid [12]. In graphite, a significant number of free electrons are present, and thus cannot be permanently displaced. Also, very few transmutations of atoms by neutron capture will occur relative to the number of atoms which will be permanently displaced; therefore the primary cause of radiation damage in graphite is due to displacement [11]. When a neutron collides with a carbon atom and displaces it, if

enough energy is imparted by the neutron, the carbon atom may in turn displace other atoms as it slows down. A good discussion of the displacement of carbon atoms due to irradiation may be found in Ref. [11].

The radiation damage caused, and thus the thermal conductivity, is dependent not only on the fluence, but also the temperature at which the irradiation occurs. In general, the thermal conductivity will decrease with increasing neutron fluence, and will increase with decreasing temperature. (The conductivity of unirradiated graphite is a maximum near room temperature [11].)

The method used to determine the thermal conductivity of graphite has been used in other codes at the Oak Ridge National Laboratory [13]. The method uses the following correlations which were developed from experimental data obtained in West Germany and the United States:

$$\alpha(T_t) = 1.055 - 0.00057\ T_r \qquad \alpha \geq 0 \tag{2.48}$$

$$H(T) = [1-8.45 \times 10^{-8}\ T(420+1.65T)]\alpha \tag{2.49}$$

$$\beta(T) = 1.116 - 0.000269T_r \qquad \beta \geq 0 \tag{2.50}$$

$$F = 8.8\ H(T) \left\{1-\exp\left[-\beta(T_r) \times 10^{-21}S\right]\right\} \tag{2.51}$$

$$R = (1.0)/ \left\{1 + F\ K(T)[C(T_r)\delta(T) + (1-C(T_r))A(T)]\right\} \tag{2.52}$$

$$K_g(S,T) = R\ K(T) \tag{2.53}$$

where

T_r = temperature at which radiation occurs (K)

T = temperature at which conductivity is to be calculated (present temp.) (K)

S = neutron fluence (n/cm^2)

K_g = graphite thermal conductivity (W/cmK)

The values of $\delta(T)$, $A(T)$, $K(T)$, and $C(T_r)$ are obtained by interpolation and normalization of data strings. These data strings are given in Table 2.2 and each parameter is normalized to the second term in its respective data string. For simplicity, it is assumed that the irradiation temperature T_r is equal to the initial temperature of the problem. Figure 2.2 displays the behavior of the thermal conductivity of graphite as a function of temperature and fluence as calculated using the algorithm described. The temperature range for the data strings of Table 2.2 is 300 K to 1600 K. However, the correlation is such that reasonable values for the graphite conductivity are still obtained for temperatures greater than 1600 K (see Figure 2.2).

2.5 Effective Thermal Conductivity in a Pebble Bed

In the "worst case" loss of forced convection and depressurization accident, it is assumed that the gas remaining in the voids in a pebble bed is stagnant and does not contribute to heat removal. Therefore, heat removal will occur via conduction through the pebbles and radiation through the voids. The cell model of Zehner and Schlünder was developed to determine an effective thermal conductivity in a packed bed of spheres, taking conduction and radiation into account. Breitbach and Barthels developed a modified Zehner-Schlünder model which agrees well with experimental data [8].

The pebble bed is modeled as an arrangement of unit cells by Zehner and Schlünder; a unit cell is shown in Figure 2.3. A unit cell contains two halves of the pebbles which are in contact. The bounding surfaces which contain the sections of pebbles are termed "base areas." Zehner and Schlünder assume that the open portions of the base areas

Table 2.2

Data Strings for Graphite Thermal Conductivity Correlation

Temperature (K)	$\delta(T)$	A(T)	C(T)	K(T)
300	74.2	1.12	1.0	1.10
350	71.0	0.905	1.0	1.05
400	68.2	0.766	1.0	1.00
500	63.5	0.605	1.0	0.90
600	60.5	0.518	1.0	0.84
700	58.4	0.467	0.7	0.78
800	56.4	0.431	0.7	0.72
900	55.5	0.410	0.7	0.67
1000	55.0	0.394	0.7	0.62
1100	54.9	0.384	0.7	0.58
1200	54.3	0.375	0.7	0.54
1300	54.1	0.368	0.2	0.50
1600	54.3	0.355	0.2	0.46

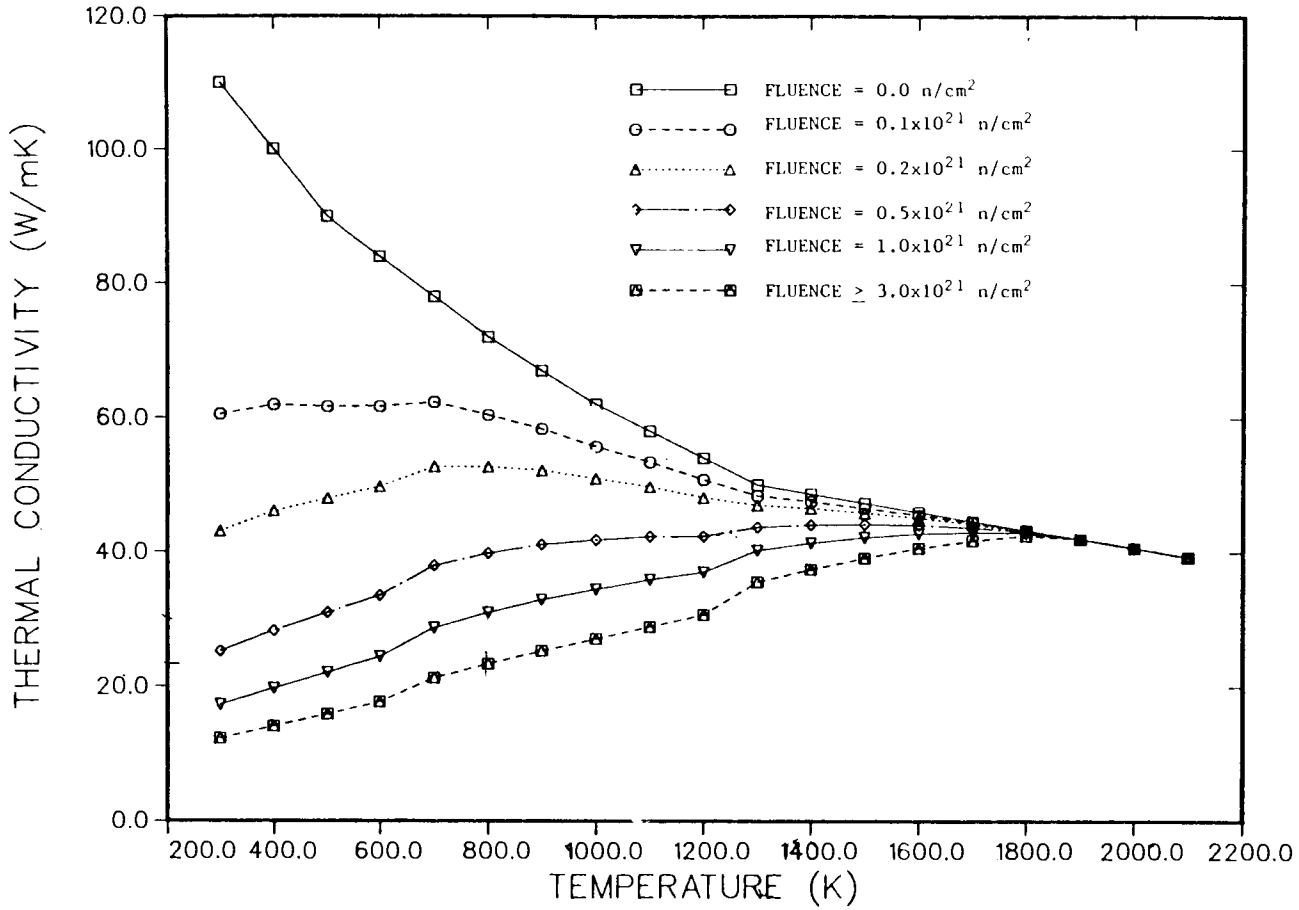

Figure 2.2 Temperature- and Neutron-Fluence-Dependent Graphite Thermal Conductivity

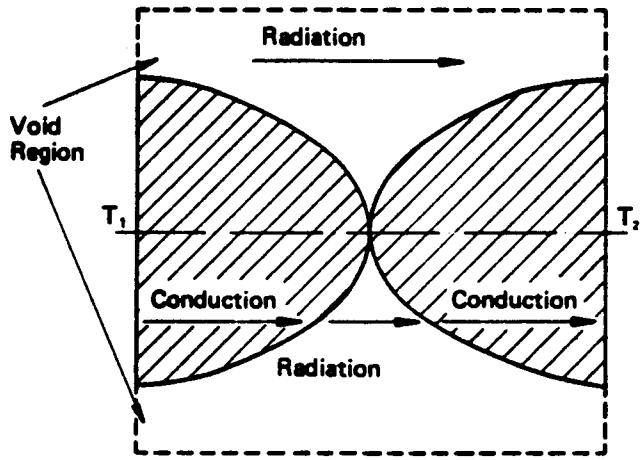

Figure 2.3 Unit Cell for the Zehner-Schlünder Model (Ref. 8)

have the same emittance as the pebbles, and the other boundaries are considered to be specular reflecting surfaces. Zehner and Schlünder derive the following expression for the effective thermal conductivity in a pebble bed:

$$\lambda_{eff}^{2S} = \left\{ \frac{[1-(1-\phi)^{1/2}]\phi}{(\frac{2}{\varepsilon} - 1)} + \frac{(1-\phi)^{1/2}}{(\frac{2}{\varepsilon} - 1)} \frac{(B_z+1)}{B_z} \cdot \left[\frac{1}{1 + \frac{1}{(\frac{2}{\varepsilon} - 1)\Lambda_f}} \right] \right\} 4\sigma T^3 d \tag{2.54}$$

where

ϕ = porosity of the pebble bed

ε = emissivity of pebble

d = diameter of pebble

σ = Stefan-Boltzmann constant

$$B_z = 1.25 \left(\frac{1-\phi}{\phi}\right)^{10/9} \tag{2.55}$$

$$\Lambda_f = \frac{\lambda_f}{4\sigma T^3 d} \tag{2.56}$$

λ_f = thermal conductivity of pebbles

The first term in the brackets represents the radiation between the base areas, which dominates at high temperatures.

Breitbach and Barthels modify the Zehner-Schlünder model given by equation (2.50) by assuming that the open portions of the base areas are assumed to be black surfaces rather than surfaces with the same emittance as the pebbles. The modified Zehner-Schlünder equation is then:

$$\lambda_{eff} = \left\{ [1 - (1-\phi)^{\frac{1}{2}}]\ \phi + \frac{(1-\phi)^{\frac{1}{2}}}{(\frac{2}{\varepsilon} - 1)} \ \frac{(B_z+1)}{B_z} \left[\frac{1}{1 + \frac{1}{(\frac{2}{\varepsilon} - 1)\Lambda_f}} \right] \right\} 4\sigma T^3 d \tag{2.57}$$

where B_z is known from equation (2.55) and Λ_f is known from equation (2.56). Breitbach and Barthels assume that λ_f in equation (2.56), the conductivity of the pebble material (in this case graphite), is a constant. However, we desire to use a thermal conductivity of graphite which is dependent on temperature and fluence. Therefore, the method described in section 2.4 is used to calculate graphite conductivity, which is then used as λ_f in equation (2.56) and subsequently in equation (2.57) to obtain the pebble-bed effective thermal conductivity.

3. PROGRAMMING CONSIDERATIONS

In this chapter, some of the mechanics of the code SHERLOC and the solution methods used are discussed.

The initial temperature, fluence, and volumetric heat generation distributions, as well as the thermal properties (density, thermal conductivity, and specific heat) as functions of temperature, are input as tabular functions. Tables of the position-dependent parameters are input for each region, and tables of the temperature-dependent parameters are input for each material. The input to SHERLOC is discussed further in Appendix C.

Characteristics of heat transport problems which may be modeled using SHERLOC include the following:

1) transient or steady-state;
2) rectangular or cylindrical coordinates;
3) one-dimensional;
4) adiabatic boundary conditions at the origin;
5) convective and/or radiative conditions at the outermost boundary
6) up to 20 different regions - some of which may be void regions;
7) up to 20 different materials (the total number of materials must be less than or equal to the total number of regions);
8) void regions not containing material;
9) temperature dependent thermal conductivity, density, and/or specific heat;

10) temperature and neutron fluence dependent graphite thermal conductivity;

11) time and space dependent internal heat generation;

12) radiation and conduction within a pebble-bed region;

13) up to a total of 200 mesh points; and

14) up to 20 ordered pairs in each tabular function (density, initial temperature, heat generation, thermal conductivity, etc.).

3.1 Numerical Techniques

3.1.1 Steady-state Solution Methods

The steady-state finite difference equations are constructed and placed into the matrix form given by equation (2.12). The system of n equations in n unknowns is solved using the system subroutines DGBFA and DGBSL [14], which are in use at the Oak Ridge National Laboratory. DGBFA factors a banded matrix by elimination, and DGBSL solves the system using the factors generated by DGBFA. This method is efficient for narrowly banded matrices (1-or 2-dimensional problems). Since the equations are solved simultaneously, the method is a direct solution technique (as opposed to an iterative technique). If a problem is linear, i.e., constant thermal properties, the solution to the matrix equation is the final, converged solution. If however, the thermal properties are not constant, an initial guess at the steady-state temperature distribution must be supplied in order to estimate the properties. The properties are evaluated at the initial guess for the temperature, and the equations solved. However, since the properties were evaluated at the initial estimate of the temperature, the solution

is only an estimate of the actual steady-state temperature distribution. The properties are reevaluated and the equations solved again.

The procedure continues in this fashion until convergence is reached. Two methods are used to monitor convergence; however, only the first method is used to determine when the problem is actually solved. The first method monitors the average relative change in the temperature distribution from one iteration to the next, and the second method monitors the heat balance at each mesh point. The relative change in the temperature distribution converges more slowly than does the heat balance. Therefore, the convergence criterion for a steady-state problem is that the average relative change in the temperature distribution be less than the value input by the user.

The average relative change in the temperature distribution is calculated by

$$\varepsilon_1 = \frac{1}{I} \sum_{i=1}^{I} \left| \frac{T_i^n - T_i^{n-1}}{T_i^n} \right| \tag{3.1}$$

where

I = total number of mesh points

T_i^n = temperature of mesh point i at the present iteration

T_i^{n-1} = temperature of mesh point i at the previous iteration

The value of ε_1 must be less than the criterion input by the user for the problem to be considered converged. In general, values of ε_1 of 10^{-6} or 10^{-7} should indicate a converged temperature distribution.

The second check for convergence involves performing a heat balance on each mesh point i. Using the point represented in equation (2.11), a "heat residual" is calculated at each mesh point i:

$$\varepsilon_{2i} = {}_iK_{i-1}T_{i-1} - ({}_iK_{i+1})T_i + {}_iK_{i+1}T_{i+1} + g_i(\Delta x)^2 \qquad (3.2)$$

where

ε_{2i} = heat residual at mesh point i

A heat residual of zero at each mesh point occurs when the exact temperature distribution is reached. Since the temperature distribution does not converge until after the heat balance converges, the heat balance is monitored for informational purposes only. In general, when the temperature distribution is converged ($\varepsilon_1 \approx 10^{-6}$) the value of the heat residual will be on the order of 10^{-10} to 10^{-12}. A steady-state problem should converge in approximately 20 to 30 iterations.

3.1.2 Transient Solution Methods

The θ-differencing, implicit technique described in section 2.3.1 is used for transient problems to describe the finite-difference equations; and the point successive overrelaxation technique, also presented in section 2.3.1, is used to solve the equations iteratively. The procedure for solving non-linear problems is as follows:

1) Thermal properties are calculated at the initial temperature distribution.
2) The temperature distribution is solved using successive overrelaxation. Iterations are performed until convergence is reached.
3) The thermal properties are updated.

4) Step 2 is repeated.

5) Convergence of the outer iteration (on properties) is checked.

6) If converged, the next time step is begun. If not converged, steps 3 through 5 are repeated.

To determine when the iterative process of the inner loop is converged, a heat residual is calculated at each mesh point. Consider the point represented by equation (2.26) as an example. When the (ℓ+1)st iteration is complete, the entire temperature distribution is known. Therefore, T_{i+1} is substituted for T_{i+1}, and the heat residual is

$$e_i = H_i + \theta\left[{}_iK_{i-1}^{n+\theta}\, T_{i+1}^{\ell+1} + {}_iK_{i+1}^{n+\theta}\, T_{i+1}^{\ell+1}\right] + D_i T_i^{\ell+1} \tag{3.3}$$

The heat residual is normalized by dividing equation (3.3) by H_i:

$$\varepsilon_{3i} = \frac{1}{H_i}\left\{H_i + \theta\left[{}_iK_{i-1}^{n+\theta}\, T_{i-1}^{\ell+1} + {}_iK_{i+1}^{n+\theta}\, T_{i+1}^{\ell+1}\right] + D_i T_i^{\ell+1}\right\} \tag{3.4}$$

The convergence criteria is supplied by the user, and iterations are performed until convergence is reached at all mesh points (unless the number of iterations exceeds the maximum allowed by the user).

To determine when the iterations on the thermal properties are converged, the norm of the relative temperature difference between the present property iteration and the previous property iteration is calculated. If $T_i^{n,m}$ is the temperature of mesh point i at time T_n after the mth iteration on properties, the norm of the relative

temperature difference is: $$\varepsilon_4 = \frac{1}{I} \sum_{i=1}^{I} \left| \frac{T_i^{n,m} - T_i^{n,m-1}}{T_i^{n,m}} \right| \qquad (3.5)$$

where

I = total number of mesh points

The iterative process is repeated until ε_4 is less than the criteria input by the user (or the number of iterations exceeds that allowed).

3.2 Determination of Properties and Heat Generation Rates

3.2.1 Thermal Conductivity

The temperature dependent thermal conductivity between mesh points i and i+1 (${}_iK_{i+1}$) is calculated by interpolation of a given tabular function at the average temperature of the two nodes.

$$\hat{T} = \frac{(T_i + T_{i+1})}{2} \qquad (3.6)$$

3.2.2 Density and Specific Heat

The density and specific heat at each mesh point determine the amount of energy which may be stored in a given interval over time, and thus are required only for transient problems. It should be noted that using a temperature-dependent density will not satisfy conservation of mass. In general, the temperature dependent density and specific heat for a given mesh point in a given material are determined at the temperature of the mesh point under consideration. However, at material interfaces (not void/material interfaces) the properties of the differing regions must be volume averaged. Since the mesh spacing may vary from region-to-region, let Δ_1 be the mesh spacing for region 1 (left of the

interface) and let Δ_2 be the mesh spacing for region 2 (right of the interface). Let p_1 be the property (density or specific heat) of the material in region 1 at the temperature of the interface, and p_2 the property of the material in region 2 at the interface temperature. Then, in rectangular coordinates, the volume-averaged property at the interface is

$$\hat{p} = \frac{\frac{\Delta_1}{2} p_1 + \frac{\Delta_2}{2} p_2}{(\frac{\Delta_1}{2} + \frac{\Delta_2}{2})}$$

or

$$\hat{p} = \frac{(\Delta_1 p_1 + \Delta_2 p_2)}{(\Delta_1 + \Delta_2)} \tag{3.7}$$

In cylindrical coordinates, volume averaging occurs as follows:

$$\hat{p} = \frac{[r_i^2 - (r_i-\Delta_1/2)^2]p_1 + [(r_i+\Delta_2/2)^2 - r_i^2]p_2}{[(r_i+\Delta_2/2)^2 - (r_i-\Delta_1/2)^2]} \tag{3.8}$$

where

r_i = radius at mesh point i (interface)

Equation (3.8) reduces to:

$$\hat{p} = \frac{\Delta_1(4r_i-\Delta_1)p_1 + \Delta_2(4r_i+\Delta_2)p_2}{(\Delta_1+\Delta_2)[4r_i+(\Delta_2-\Delta_1)]} \tag{3.9}$$

At material/void interfaces, the properties are calculated at the temperature of the interface for the material involved. Since heat will be stored only in the material, not in the void, the properties are not volume-averaged over the entire mesh interval. The heat storage term

in the transient equation will then be multiplied by the volume of the material portion of the interval, not the volume of the entire interval (see Appendix B, equations B.25, B.33, B75, and B.83).

3.2.3 Volumetric Heat Generation Rates

Since the volumetric heat generation of a mesh interval will be multiplied by the volume of the mesh interval, the value of g_i must be the average volumetric heat generation of the interval. The heat generation distribution is supplied to the code as a tabular function of power density versus position. Linear interpolation is used between the user-supplied data points to obtain the heat generation at each mesh point i.

For a mesh point within a given material region (see Figures 2.1a and 2.1b), it is assumed that the linearly-interpolated value of the heat generation function is indeed the average heat generation for the mesh interval. This assumption is reasonable if the given tabular heat generation function is fairly linear between the data points input by the user.

We now consider a mesh point i at the origin or at the right-hand boundary of a void region. No heat is generated in a void region. Therefore, the average power density for the mesh interval i is

$$g_i = \frac{1}{2}\left[f_i + \frac{1}{2}(f_i + f_{i+1})\right] \qquad (3.10)$$

where

f_i = linearly interpolated value of the volumetric heat generation function at mesh point i

f_{i+1} = linearly interpolated value of the volumetric heat generation function at mesh point i+1

Reducing equation (3.10) yields

$$g_i = \frac{3}{4} f_i + \frac{1}{4} f_{i+1} \tag{3.11}$$

Consider mesh point i at the outermost boundary or at the left-hand boundary of a void region. The average power density for the mesh interval i becomes

$$g_i = \frac{1}{4} f_{i-1} + \frac{3}{4} f_i \tag{3.12}$$

where

f_{i-1} = linearly interpolated value of the volumetric heat generation function at mesh point i-1

At a material region interface, values for the heat generation must first be calculated from the functions given for each region, and then volume-averaged together. Let g_L be the average heat generation in the portion of the mesh interval to the left of the interface, and g_R be the average heat generation in the portion of the mesh interval to the right of the interface. We have

$$g_L = \frac{1}{4} f_{i-1} + \frac{3}{4} f_i \tag{3.13}$$

and

$$g_R = \frac{3}{4} f_i + \frac{1}{4} f_{i+1} \tag{3.14}$$

Then, volume averaging g_L and g_R in rectangular coordinates:

$$g_i = \frac{\Delta_1 g_L + \Delta_2 g_R}{(\Delta_1 + \Delta_2)} \tag{3.15}$$

where

Δ_1 = mesh spacing in region left of interface

Δ_2 = mesh spacing in region right of interface

Similarly, in cylindrical coordinates:

$$g_i = \frac{\Delta_1(4r_i-\Delta_1)g_L + \Delta_2(4r_i+\Delta_2)g_R}{(\Delta_1+\Delta_2)[4r_i + (\Delta_2-\Delta_1)]} \tag{3.16}$$

3.3 Flow of Problem Solution

Several flowcharts are presented here to depict the progression of SHERLOC in the solution of a problem. Figure 3.1 contains a very general flowchart of the entire code, showing the major sections of the code and how they are reached. Figures 3.2 and 3.3 show more detailed flowcharts of the steady-state and transient solutions, respectively. The progression of the subroutine CONDUC, which calculates the thermal conductivity between each mesh point, is shown in Figure 3.4. The subroutine GRPHTE, which uses the correlations of section 2.4 to determine the neutron fluence and temperature dependent graphite thermal conductivity, is called from CONDUC. A flow diagram of GRPHTE is shown in Figure 3.5. The effective thermal conductivity for mesh points in a pebble-bed is calculated in subroutine PEBBLE, which is also called from CONDUC. Figure 3.6 contains a flowchart of PEBBLE.

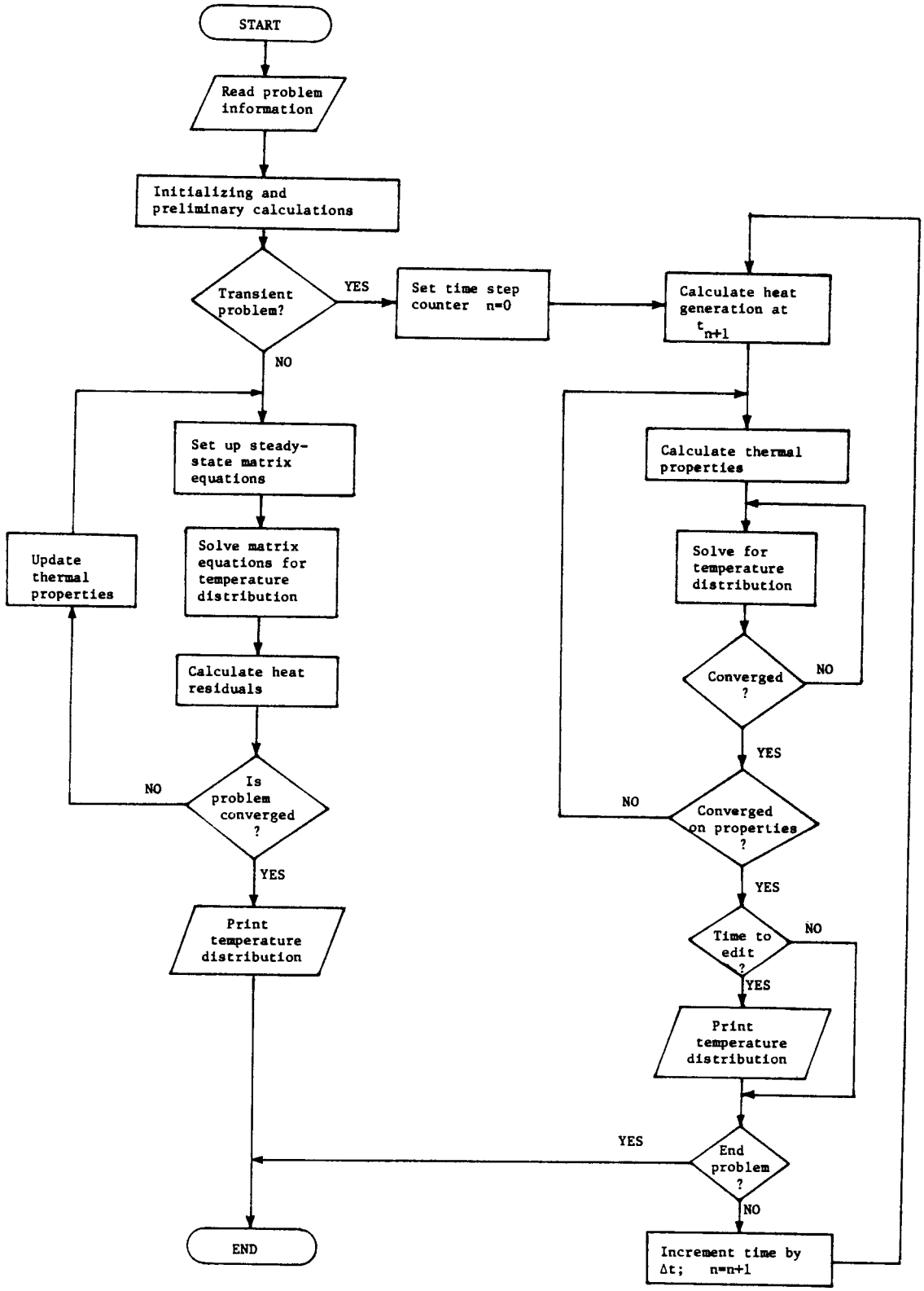

Figure 3.1 General Flowchart for SHERLOC

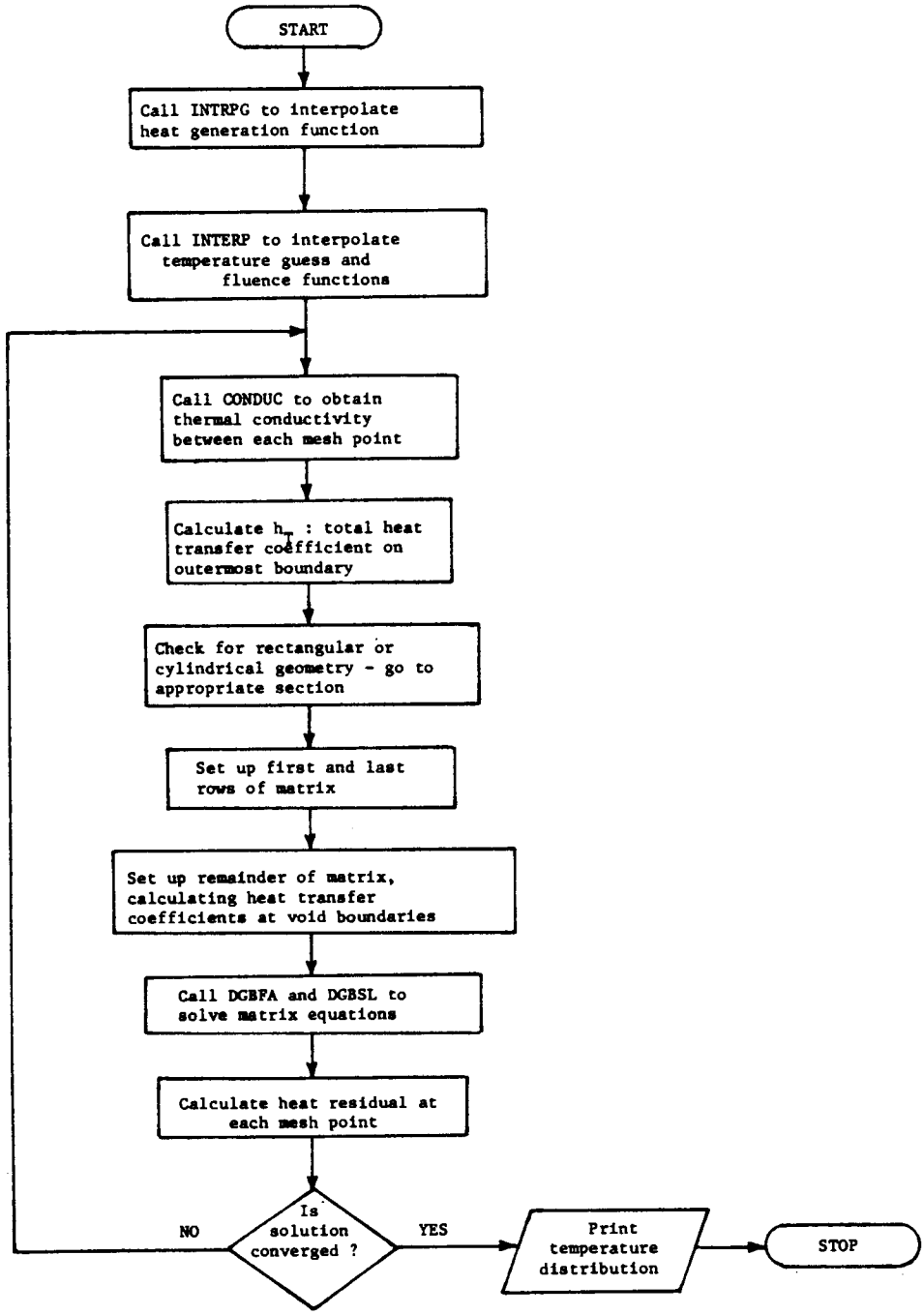

Figure 3.2 Flowchart for Steady-State Problem

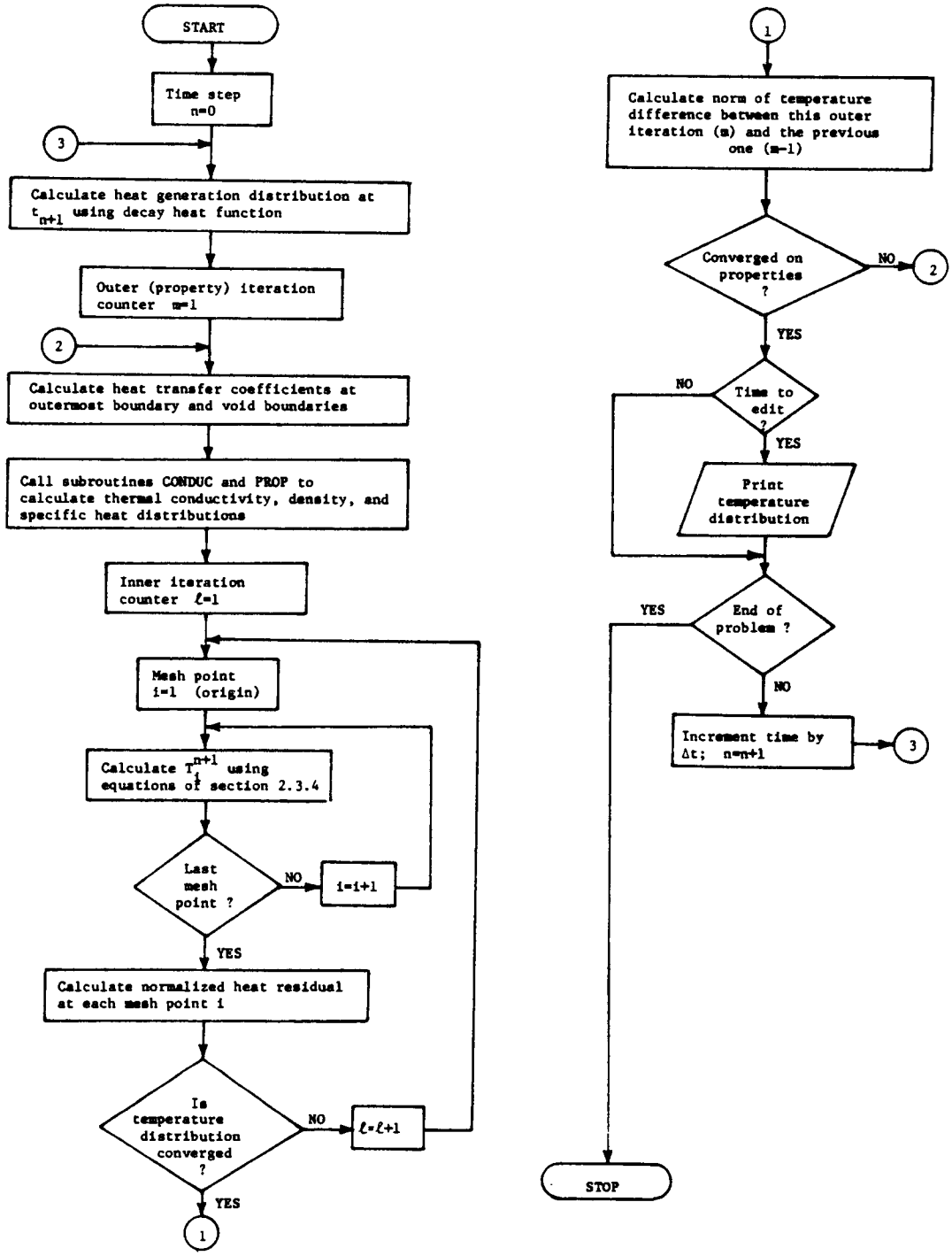

Figure 3.3 Flowchart for Transient Problem

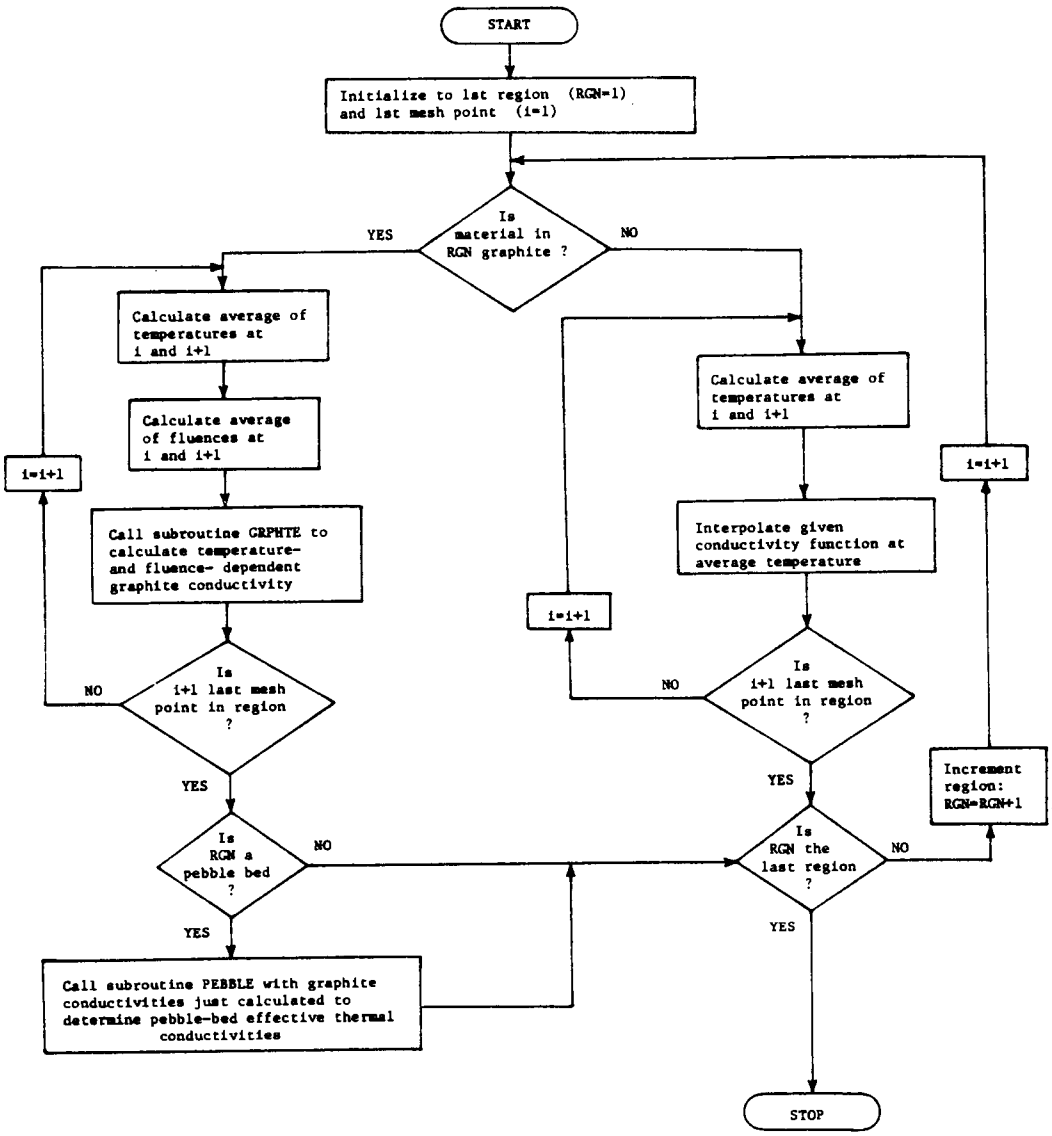

Figure 3.4 Flowchart for Subroutine CONDUC

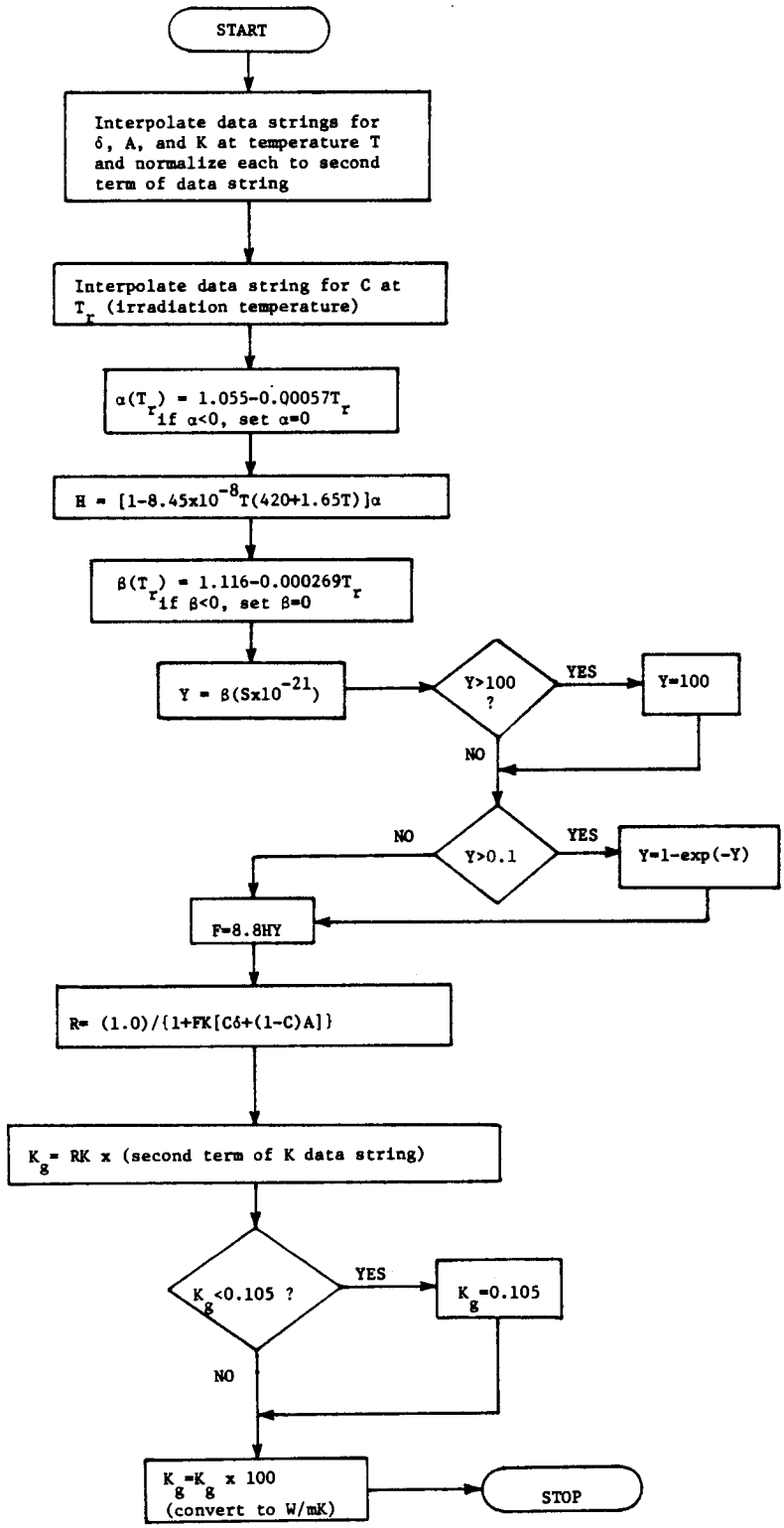

Figure 3.5 Flowchart for Subroutine GRPHTE

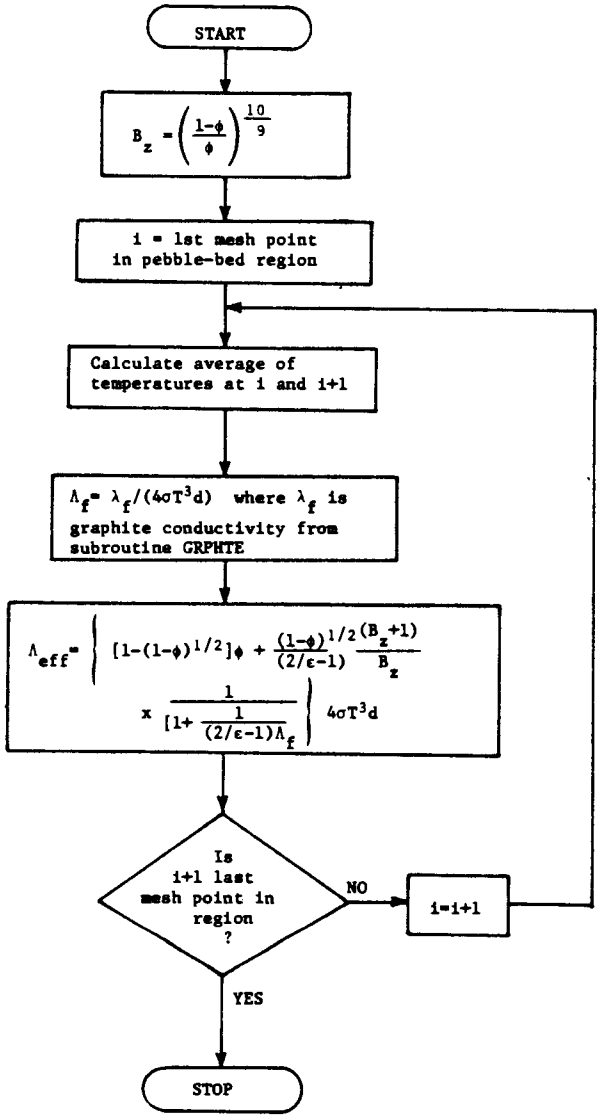

Figure 3.6 Flowchart for Subroutine PEBBLE

The subroutine INTRPG, INTERP, and PROP are used to interpolate user-supplied functions. INTRPG determines the volumetric heat generation of each mesh interval; INTERP calculates the neutron fluence and initial temperature at each mesh point; and PROP determines the values of the density and specific heat of each mesh point, volume averaging where necessary. The progression of each of these subroutines is fairly straightforward.

A complete listing of SHERLOC is found in Appendix D; and an input guide, a sample input, and a sample output is found in Appendix C.

4. MODELING OF PRISMATIC-CORE AND PEBBLE-BED HTGRs FOR DEPRESSURIZED HEATUP ACCIDENT ANALYSIS

The responses of both prismatic-core and pebble-bed modular HTGRs to the "worst case" depressurized heatup accident were analyzed using SHERLOC, and the results compared to studies performed by General Atomic Technologies (GA) and the General Electric Company (GE). Several sensitivity studies were performed for both types of modular reactors.

4.1 Prismatic Modular HTGR Model

The one-dimensional SHERLOC model of the GA-designed prismatic modular (described in Section 1.1.2) is shown in Figure 4.1. The core is divided radially into six regions. The reflector is modeled as a single region, as are the core barrel, side plenum (void region between the core barrel and reactor vessel), and the reactor vessel. A convective heat transfer coefficient is specified on the outer surface of the reactor vessel, and the temperature of the surrounding environment is given as 150°F (338.7 K) following a depressurized loss of forced convection accident.

The following assumptions were made in modeling the system:

1) the density of each material is constant;
2) the core is treated as a homogeneous region of graphite - the graphite density in the matrix is smeared over the entire core volume;

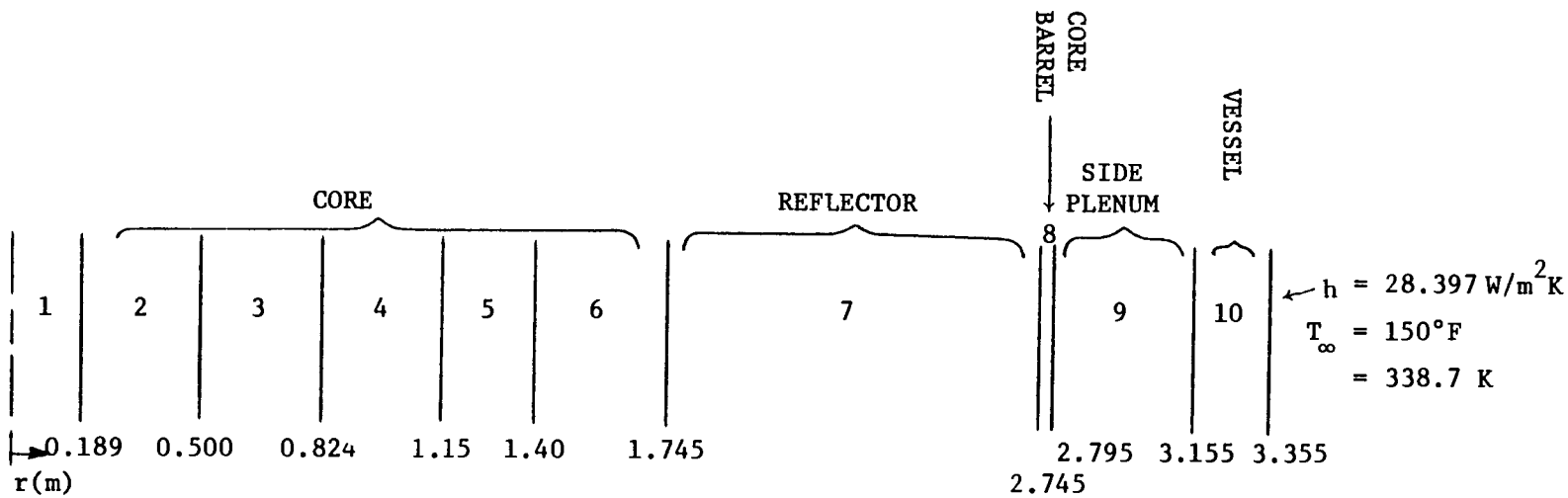

Figure 4.1 Prismatic Core Modular HTGR Model for SHERLOC

3) the emittances of the core barrel and reactor vessel (on inner surface) are assumed to be 0.8;
4) the core barrel is 304 stainless steel, and the reactor vessel is 2-1/4 Cr : 1 Mo steel;
5) heat transfer through the side plenum is by radiation alone;
6) the fast neutron fluence in the reflector is negligible;
7) heat is transferred from the vessel to the environment by natural convection and radiation only; and
8) no heat is generated outside of the active core.

Although the active core and the reflector are both graphite, they have different densities and are thus treated as different materials by SHERLOC. The volume-averaged core density is 1195.5 kg/m^3, and the density of the reflector is 1394.8 kg/m^3. These densities were obtained from values of carbon number densities in the core and reflector supplied by GA. The material properties which were used are given in Section 4.3.

The volumetric heat generation in the core is given by:

$$P(r,t) = P_o(r)f(t) \tag{4.1}$$

where

$P_o(r)$ = initial power density at radius $r(W/m^3)$

$f(t)$ = decay heat fraction at time t

The decay heat fraction was determined as follows [15]:

$$f(t) = 0.128(t + 3.796\text{x}10^{-4})^{-0.261} \tag{4.2}$$

where

t = time after accident initiation (seconds)

The decay heat fraction as a function of time is shown in Figure 4.2

Of primary interest is the peak temperature reached in the core during the transient. Also of interest are the effects of varying the power density and initial temperature distributions. To investigate these effects, the core was divided axially into eight regions, each with a height of 79.25 cm, and calculations were performed at axial regions 1 (bottom of core), 3, 4 (just below core mid-plane), and 5 (just above core mid-plane). One would expect the peak transient temperature to occur where the power density is greatest. The power density peaks in axial region 4; therefore axial region 4 was chosen as the reference case.

In addition to the power density and initial temperature effects, the impact of using a fluence-dependent graphite thermal conductivity was investigated. This was done by simply neglecting the fluence in axial region 4 and comparing the results to the reference case (with fluence). In the cases discussed above, heat transfer from the vessel occurred via convection and radiation only, with a combined heat transfer coefficient of 5.0 Btu/hr ft^2 °F (28.4 W/m^2-K). To determine the effect on the transient of an active vessel cooling system, a case was run in which the heat transfer coefficient on the surface of the vessel was 150 Btu/hr ft^2 °F (851.7 W/m^2K) [16].

The effect of small gaps between the prismatic fuel assemblies was studied by placing 0.1-cm-wide gaps every 36 cm radially in the core. (The prismatic fuel assemblies are 36 cm across flats.) These

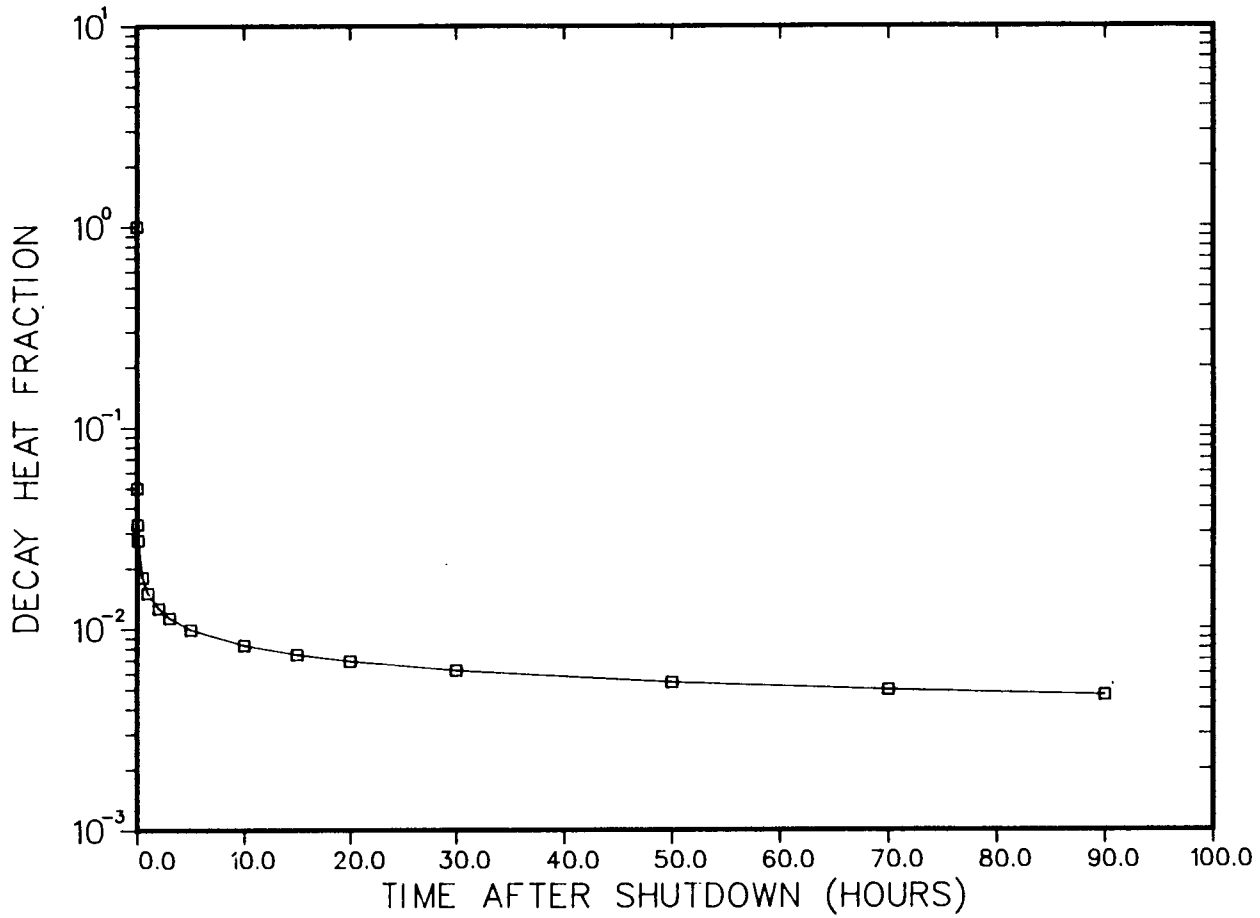

Figure 4.2 Time-Dependent Decay Heat Fraction for the Prismatic HTGR

calculations were performed at axial region 4. Heat was assumed to be transferred by conduction through the helium in these gaps, and no heat was generated in the gaps.

In order to compare the behavior of a prismatic core and a pebble-bed core under the same initial conditions and configuration, the prismatic core was replaced by a pebble-bed core and calculations were performed using the conditions of the reference case. The pebbles were assumed to be 6 cm in diameter, have an emittance of 0.8, and a graphite density of 1.70 gm/cm^3. The volume fraction of pebbles to the entire core was 0.61; thus the volume-averaged core density was 1037 kg/m^3.

A summary of the reference case and the sensitivity studies performed is given in Table 4.1. The steady-state radial power density (P_o in equation 4.1) and temperature distributions for the various axial locations of interest are given in Table 4.2 and 4.3, respectively. The radial neutron fluence distribution which was assumed for all axial locations is given in Table 4.4

4.2 Pebble-Bed Modular HTGR Model

The modular pebble-bed reactor which was studied is similar to the one proposed by GHT (see Section 1.1.2). The model used was adapted from a study of the depressurized heatup accident in the pebble-bed reactor performed by General Electric [17]. The model used is shown in Figure 4.3, and consists of 11 radial regions; 6 in the core, 2 in the reflector, and 1 each for the core barrel, side plenum, and reactor vessel. Heat is removed from the surface of the vessel by radiation alone to the cooling coils located on the inner surface of

Table 4.1

Summary of Prismatic Modular HTGR Cases Analyzed Using SHERLOC

Case	Description
1 - Reference Case	Axial region 4 - just below core midplane location of peak axial power density
2	Axial region 5 - just above core midplane
3	Axial region 3
4	Axial region 1 - bottom of core
5	Axial region 4 - neutron fluence neglected
6	Axial region 4 - active vessel cooling $h = 150$ Btu/hr ft^2 °F = 851.7 W/m^2K
7	Axial region 4 - 0.1 cm, helium filled gaps between fuel assemblies in core
8	Axial region 4 - replacing prismatic fuel with 6 cm DIA fuel pebbles

Table 4.2

Steady-State Radial Power Density Distributions at Various Axial Locations in the Prismatic Modular HTGR

Axial Region	1	3	4	5
Radial Region				
1	6.82 W/cc	7.76 Wcc	7.82 W/cc	3.93 Wcc
2	6.71	7.64	7.69	3.87
3	6.07	6.91	6.95	3.50
4	6.17	7.03	7.08	3.56
5	5.42	6.17	6.22	3.13
6	4.46	5.07	5.11	2.57

Table 4.3

Steady-State Radial Temperature Distributions at Various Axial Locations in the Prismatic Modular HTGR

Axial Region	1	3	4	5
Radial Region				
1	732.24 °C	915.34 °C	1037.74 °C	1093.3 °C
2	732.24	915.34	1037.74	1093.3
3	732.24	915.34	1037.74	1093.3
4	693.34	839.84	937.74	954.44
5	693.34	839.84	937.74	954.44
6	693.34	839.84	937.74	954.44
7	482.24	542.94	586.44	586.44
8	482.24	482.24	482.24	482.24
9	420.0	420.0	420.0	420.0
10	260.0	260.0	260.0	260.0

Table 4.4

Radial Neutron Fluence Distribution Assumed for the Prismatic Modular HTGR

Radial Region	Fluence ($x10^{21}$ n/cm^2)
1	5.48
2	5.48
3	4.94
4	4.45
5	3.90
6	2.95

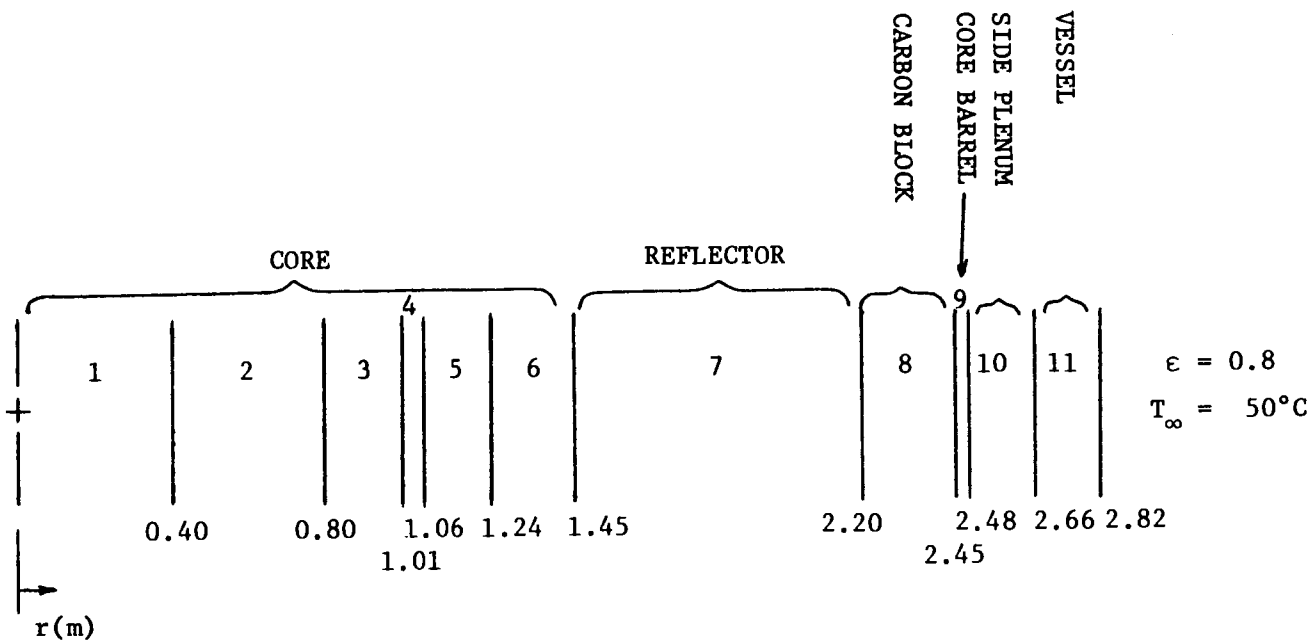

Figure 4.3 Pebble-Bed Modular HTGR Model for SHERLOC

the confinement building. The cooling coils are assumed to remain at a constant temperature of 50°C throughout the transient.

The following assumptions were made in modeling the system:

1) the density of each material is constant;
2) the density of the graphite in the pebbles was smeared over the entire core to obtain an effective core density;
3) the pebbles have diameters of 6 cm and emittances of 0.8;
4) the volume fraction of pebbles to the entire core is

$$\left(\frac{V_{pebbles}}{V_{core}}\right) = 0.61 \ ;$$

5) the emittances of the core barrel and reactor vessel are 0.8;
6) heat transfer is via radiation alone through the side plenum;
7) the core barrel is of 304 stainless steel, and the reactor vessel is 2-1/4 Cr : 1 Mo steel;
8) the fast neutron fluence in the reflector is negligible; and
9) no heat is generated outside of the core.

The volume-averaged density of the core is 1037.0 kg/m^3, assuming a pebble graphite density of 1.70 gm/cm^3 [17]. The density of the reflector was assumed to be the same as the density of the prismatic core reflector, namely, 1394.8 kg/m^3. The other material properties which were used are discussed in Section 4.3.

The time- and space-dependent volumetric heat generation in the core was determined using equation (4.1), where f(t) is given by [18]:

$$f(t) = 0.0622[t^{-0.2} - (t + e.184x10^{7})^{-0.2}] \qquad (4.3)$$

where

t = time after accident initiation (seconds)

The decay heat fraction f(t) for the pebble-bed core is shown graphically in Figure 4.4.

As with the prismatic HTGR, the reference case for the pebble-bed reactor was taken at the axial location of the peak power density - 185.2 cm below the ball fill (top of core). The height of the core is 926 cm, and if one takes the origin (z=0.0) at the top of the core, the peak axial power density occurs at z/H=0.2. In addition, cases were studied at z/H=-.3 and z/H=1.0 (bottom of the core). Since the pebbles and coolant are flowing downward through the core, the power is peaked towards the top and the steady-state temperature is greatest at the bottom of the core.

The functions used for graphite thermal conductivity and heat capacity by GE in their two-dimensional study were different than the functions used here. To examine the effects of performing a 1-D calculation versus a 2-D calculation, the GE conductivity and heat capacity were used in SHERLOC for z/H=0.2 and z/H=0.3. The GE graphite thermal conductivity function for the pebble-bed core is [18]:

$$k(T) = 1.1536x10^{-6}(T + 100)^{1.6622} \qquad (4.4)$$

where

k(T) = temperature dependent thermal conductivity (W/cm °C)

T = temperature (°C)

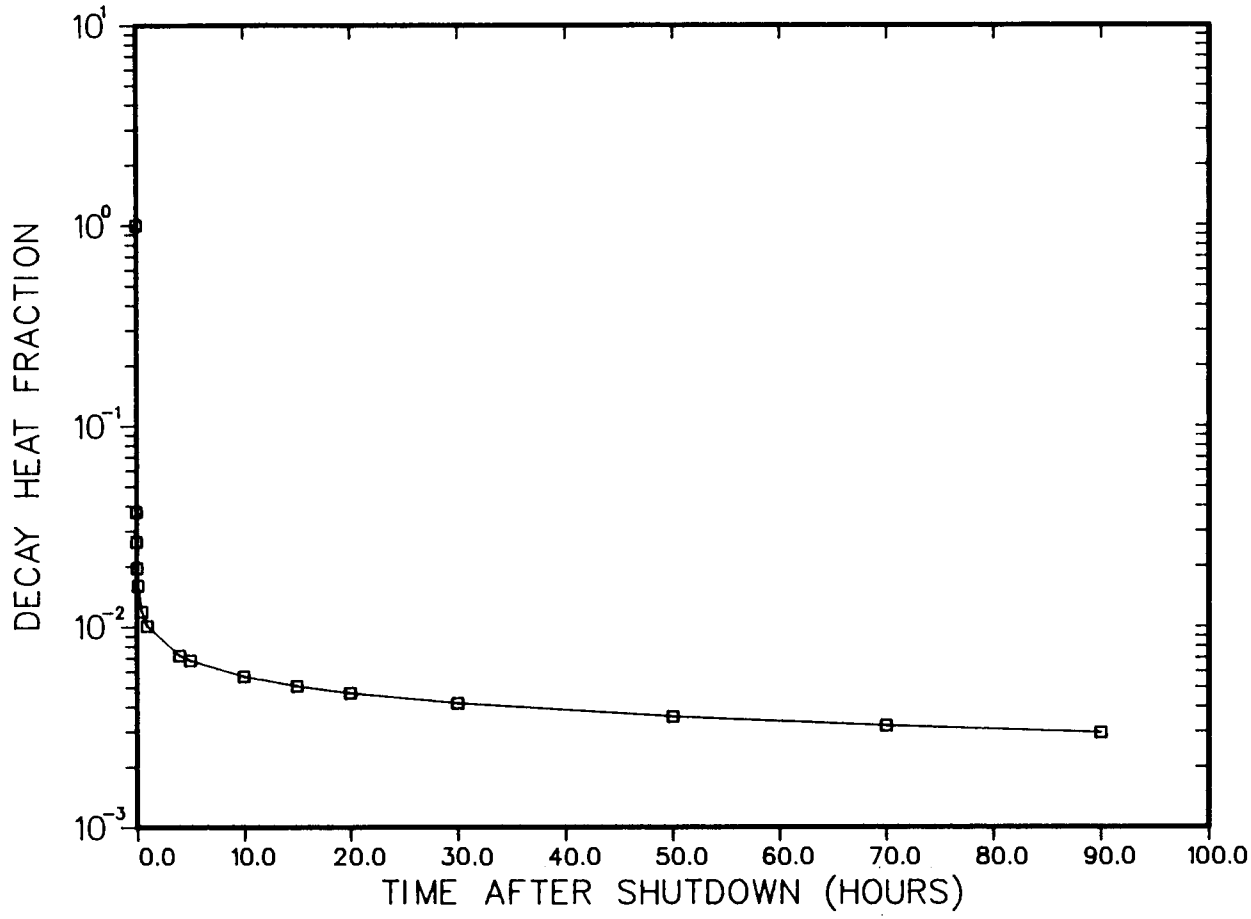

Figure 4.4 Time-Dependent Decay Heat Fraction for the Pebble-Bed HTGR

The heat capacity of the core is given as [18]:

$$\rho C_p(T) = \rho_o \, 1.75[0.645 + 3.14 \left(\frac{T}{1000}\right) - 2.809 \left(\frac{T}{1000}\right)^2 + 0.959 \left(\frac{T}{1000}\right)^3] \quad (4.5)$$

where

ρ_o = pebble volume fraction = 0.61

T = temperature (°C)

$\rho C_p(T)$ = heat capacity (J/cm °C)

The actual values of the properties used by GE for the core barrel and reactor vessel were unknown; therefore, the properties given in Section 4.3 were used. These may be somewhat different than the values used in the GE study.

A summary of the cases studied for the pebble-bed reactor is given in Table 4.5. The steady-state radial power density (P_o in equation 4.1) and temperature distributions for the axial locations investigated are given in Tables 4.6 and 4.7, respectively. The assumed radial neutron fluence distribution is given in Table 4.8.

4.3 Materials Properties

4.3.1 Graphite

The densities used for the graphite pebble-bed and prismatic cores and the reflector are given in the preceding section. The graphite thermal conductivity was calculated using the correlation described in Section 2.4, and the effective pebble-bed conductivity was determined using the modified Zehner-Schlünder equation of

Table 4.5

Summary of Pebble-bed Modular HTGR Cases Analyzed Using SHERLOC

Case	Description
1 - Reference Case	z/H = 0.2 - location of peak axial power density
2	z/H = 0.3
3	z/H = 1.0 - bottom of core maximum initial temperatures
4	z/H = 0.2 using GE core conductivity and heat capacity functions
5	z/H = 0.3 using GE core conductivity and heat capacity functions

Table 4.6

Steady-State Radial Power Density Distributions at Various Axial Positions in the Pebble-bed Modular HTGR

Distance Below Ball Fill (cm)	185.2($\frac{z}{H}$ = 0.2)	277.8($\frac{z}{H}$ = 0.3)	926.0($\frac{z}{H}$ = 1.0)
Radius (cm)			
0.0	8.21 W/cc	7.37 W/cc	0.76 W/cc
40.0	8.01	7.19	0.74
80.0	7.24	6.50	0.66
101.0	6.67	6.00	0.60
106.0	7.33	6.55	0.64
124.0	6.87	6.13	0.58
145.0	6.96	6.17	0.54

Table 4.7

Steady-State Radial Temperature Distributions at Various Axial Positions in the Pebble-bed Modular HTGR

Distance Below Ball Fill (cm)	185.2 ($\frac{z}{H}$ = 0.2)	277.8 ($\frac{z}{H}$ = 0.3)	($\frac{z}{H}$ = 1.0)
Radius (cm)			
0.0	582.0°C	699.0°C	1020.0°C
20.0	579.0	695.0	1010.0
40.0	572.0	684.0	995.0
60.0	560.0	668.0	974.0
80.0	544.0	647.0	950.0
101.0	539.3	639.5	935.9
106.0	538.5	638.1	933.6
124.0	536.0	634.0	927.0
145.0	531.0	628.0	917.0
170.0	466.0	545.0	772.0
194.0	399.0	463.0	644.0
220.0	319.0	372.0	518.0
245.0	310.6	359.3	487.5
248.0	309.0	357.0	482.0
266.0	241.5	279.5	384.5
270.0	220.0	255.0	354.0
282.0	213.0	246.0	334.0

Table 4.8

Radial Neutron Fluence Distribution Assumed for the Pebble-bed Modular HTGR

Radial Region	Fluence ($x10^{21}$ n/cm^2)
1	5.48
2	4.90
3	4.50
4	4.50
5	3.90
6	2.95

Section 2.5. The thermal conductivity of the graphite reflector was calculated assuming a neutron fluence of 0.0 n/cm^2. The specific heat (C_p) of graphite as a function of temperature [11,19] is shown in Figure 4.5.

4.3.2 304 Stainless Steel [20]

The core barrel was modeled as 304 stainless steel for both the pebble-bed and prismatic reactor designs. The density of 304 stainless steel was taken as a constant value of 7800 kg/m^3. The temperature-dependent thermal conductivity and specific heat functions are given in Figures 4.6 and 4.7, respectively.

4.3.3 2-1/4 Cr : 1 Mo Steel [20]

2-1/4 Cr : 1 Mo steel was used in the reactor vessel for both reactor types. A constant value of 7675 kg/m^3 was used for the density. The temperature-dependent thermal conductivity and specific heat functions are given in Figures 4.8 and 4.9, respectively.

4.3.4 Helium [21]

Properties of helium were required for Case 7 in the prismatic HTGR study, in which small gaps (filled with stagnant helium) between fuel assemblies were modeled. Since the reactor was assumed to be depressurized in this study, properties were taken at a pressure of 1 atm (1.01325 bar). The specific heat (C_p) was given as a constant value of 5195 J/kg K.

The thermal conductivity may be determined using the following correlation:

$$k(p,T) = 2.682\text{x}10^{-3}(1 + 1.123\text{x}10^{-3}\ p)T^{0.71(1-2\text{x}10^{-4}p)} \qquad (4.6)$$

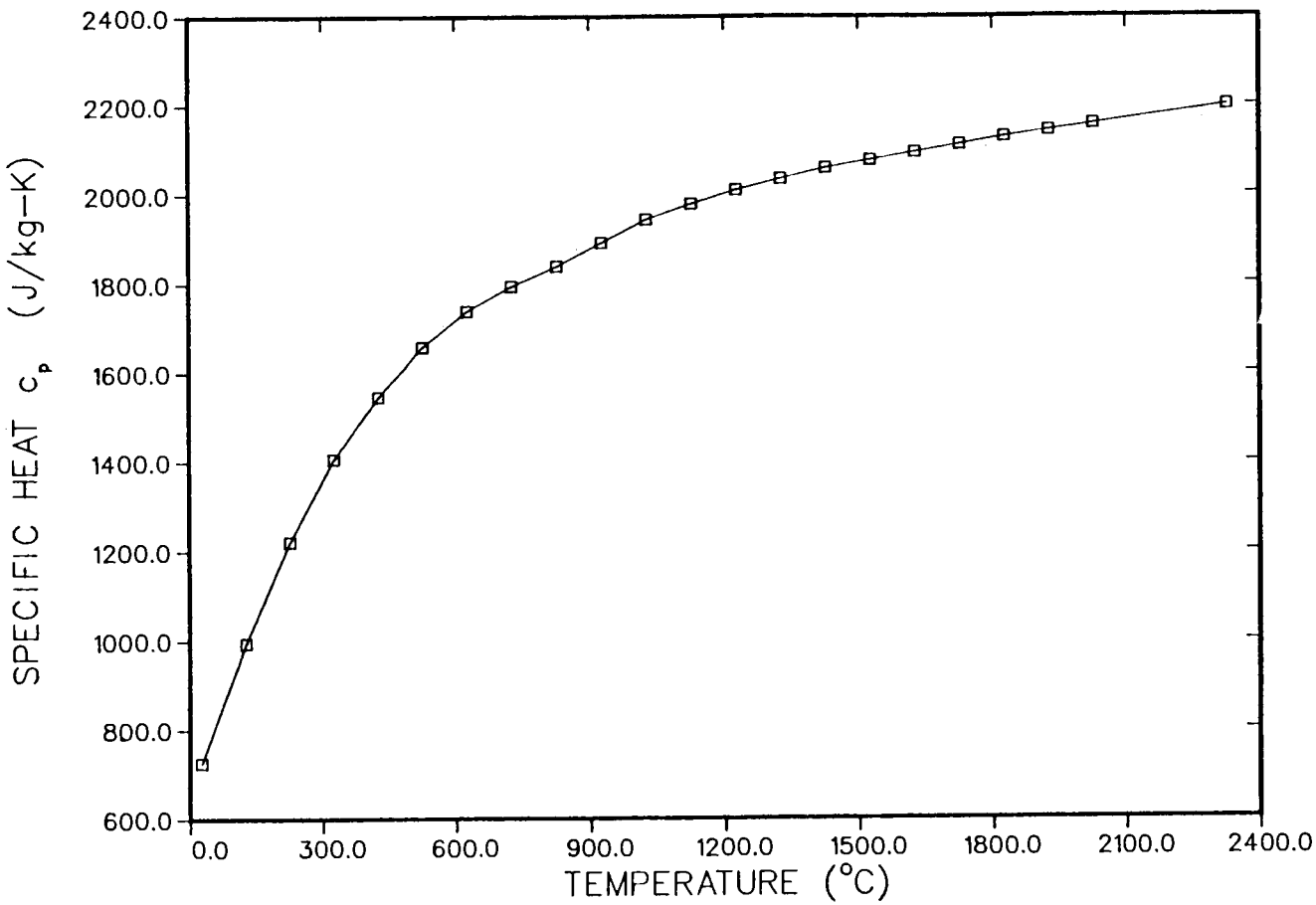

Figure 4.5 Temperature-Dependent Graphite Specific Heat

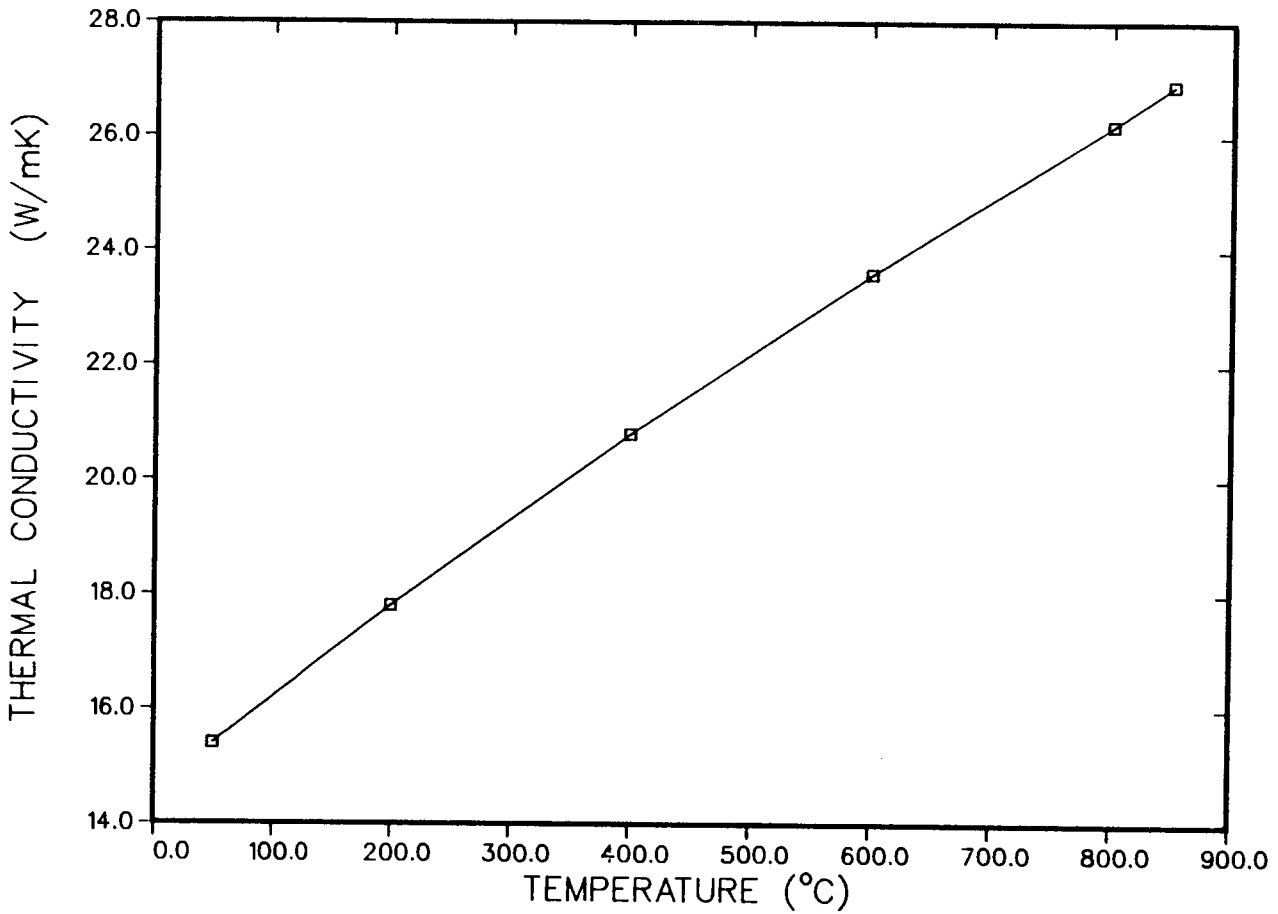

Figure 4.6 304 Stainless Steel Thermal Conductivity

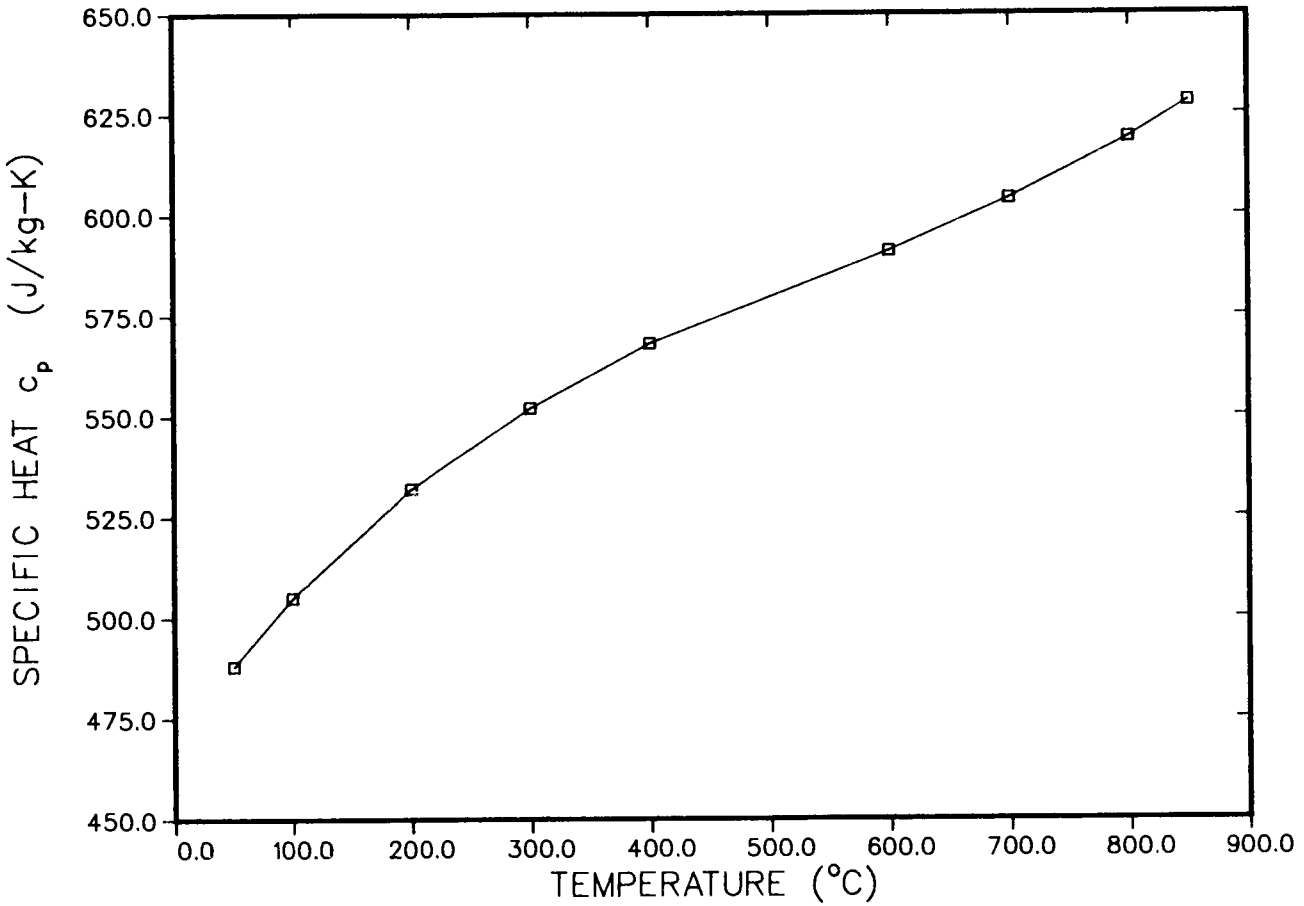

Figure 4.7 304 Stainless Steel Specific Heat

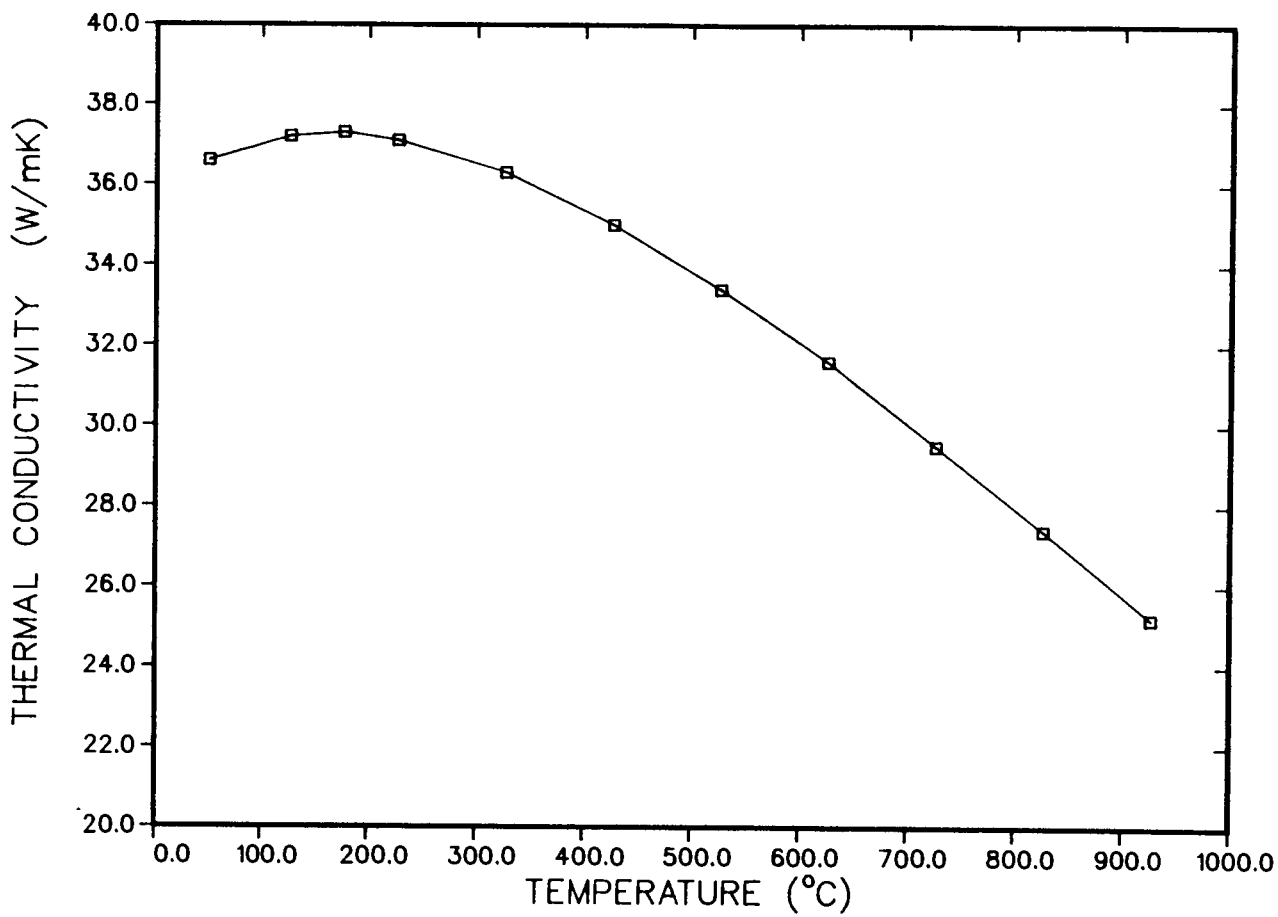

Figure 4.8 2¼ Cr: 1 Mo Steel Thermal Conductivity

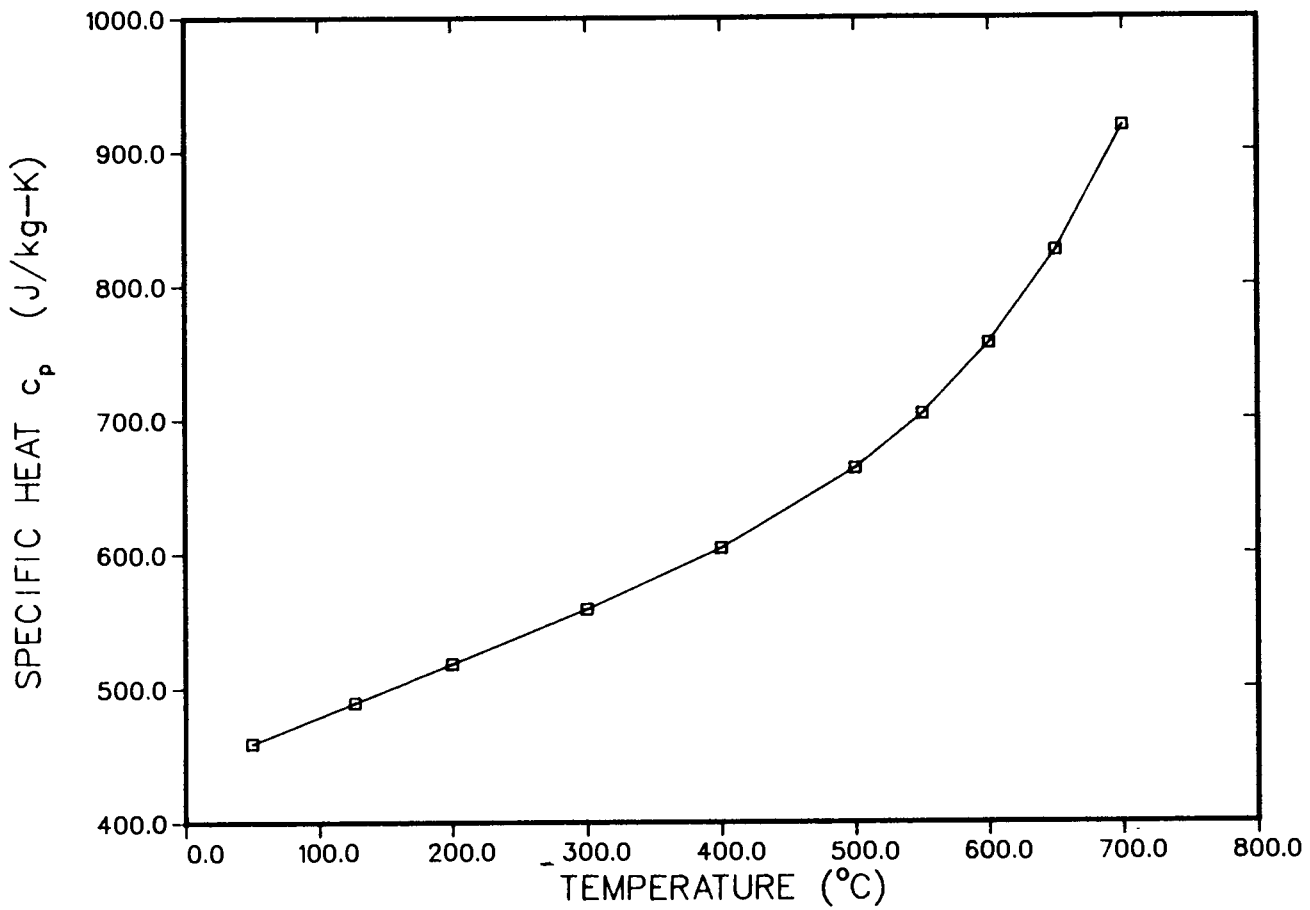

Figure 4.9 2¼ Cr: 1 Mo Steel Specific Heat

where

p = pressure (bar)

T = temperature (K)

$k(p,T)$ = thermal conductivity (W/m K)

The helium thermal conductivity as a function of temperature at 1.01325 bar is plotted in Figure 4.10.

The density of helium is calculated using the following correlation:

$$(p,T) = \frac{48.14(p/T)}{(1+\frac{0.446p}{T^{1.2}})} \tag{4.7}$$

where

p = pressure (bar)

T = temperature (K)

(p,T) = density (kg/m^3)

Helium density is plotted as a function of temperature at 1.01325 bar in Figure 4.11.

Equations (4.5) and (4.6) are valid in the range 1 bar < p < 100 bar and 20°C < T < 1500°C; however, they were assumed to be valid for temperatures up to ∿ 2200°C for the purposes of this study. The values of helium conductivity and density obtained from equations (4.5) and (4.6) at temperatures greater than 1500°C were within 3.7% of the corresponding values reported in Reference 22.

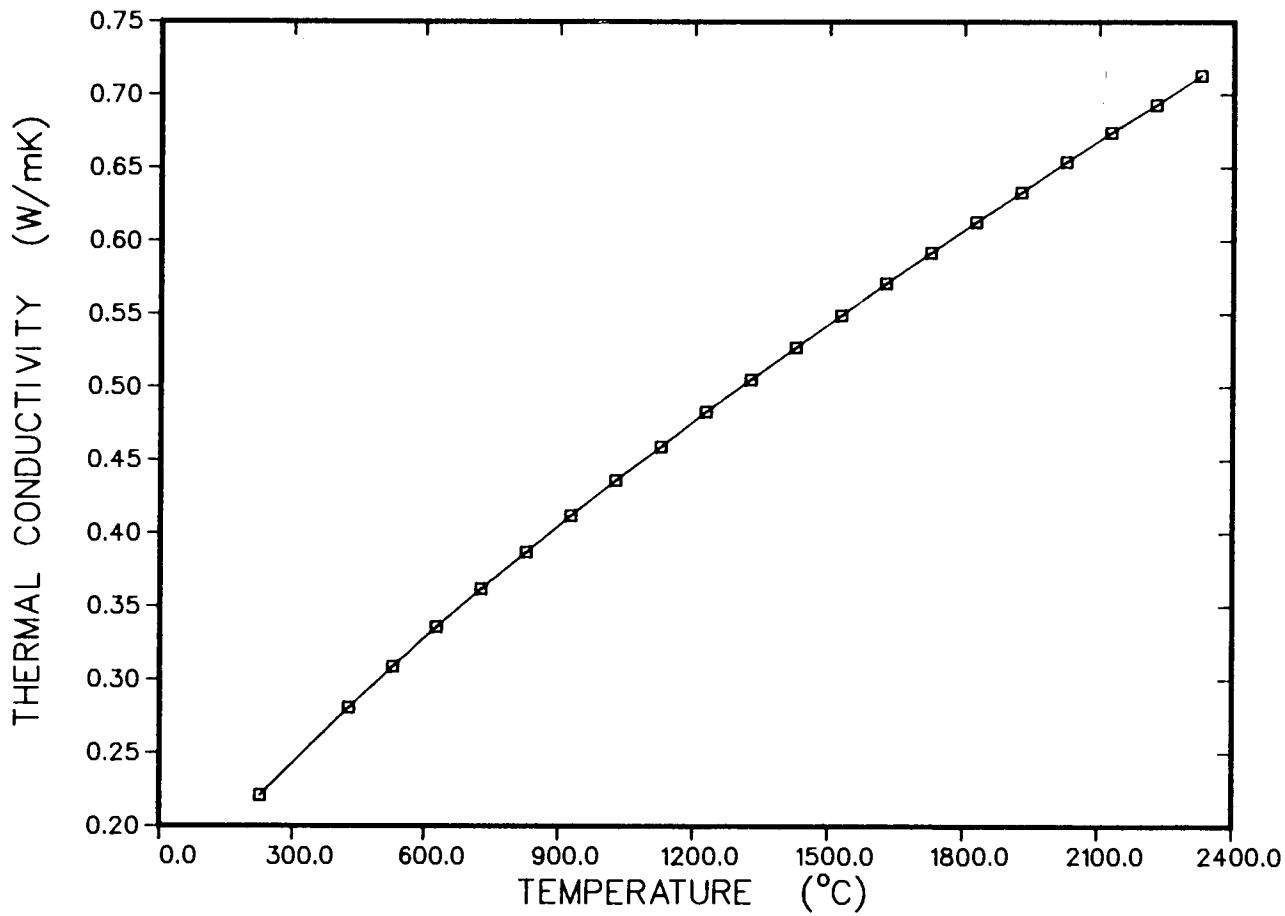

Figure 4.10 Helium Thermal Conductivity at 1 Atmosphere

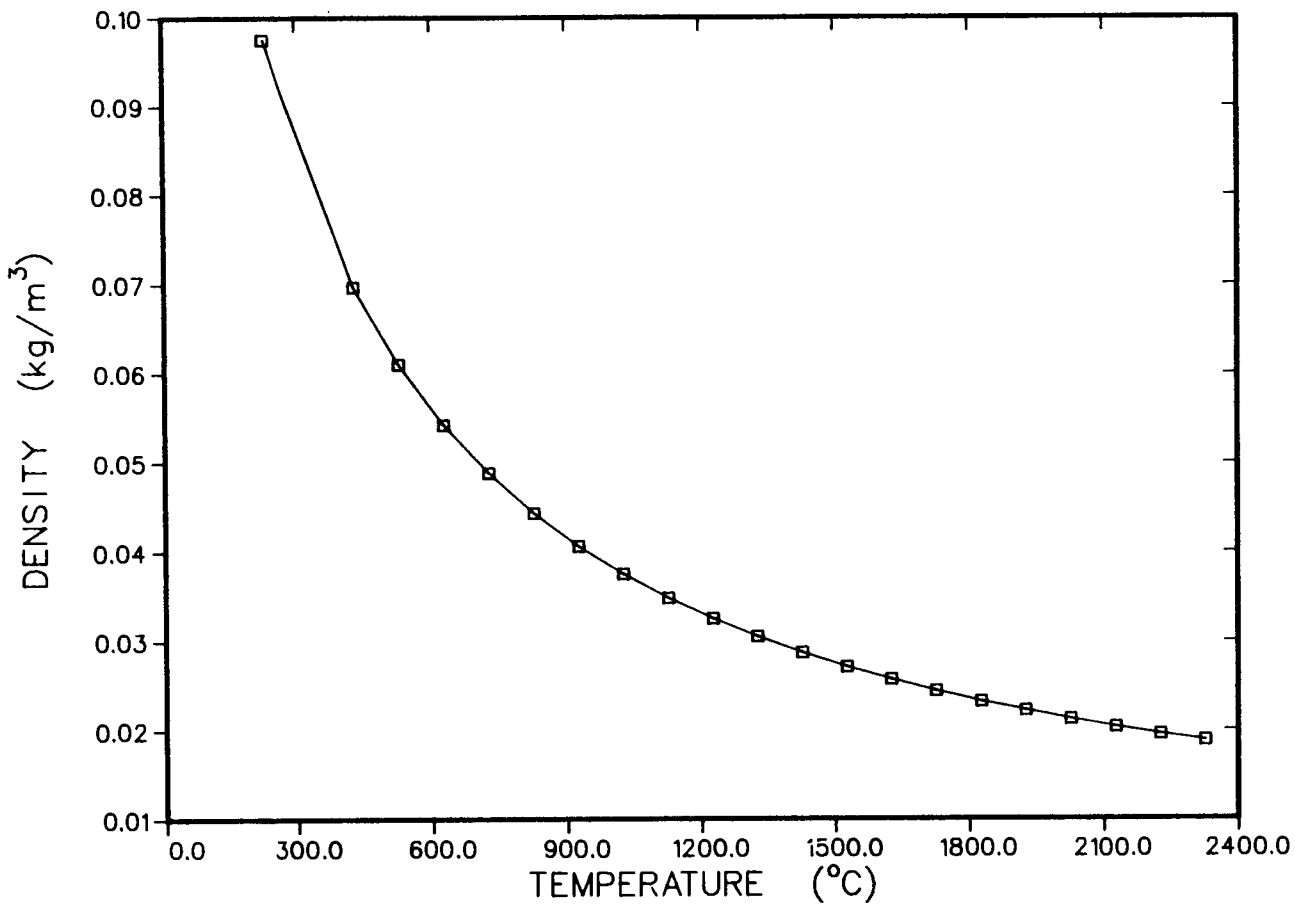

Figure 4.11 Helium Density at 1 Atmosphere

5. RESULTS AND CONCLUSIONS

5.1 Solid Graphite and Pebble-Bed Thermal Conductivities

As previously shown in Figure 2.2 (Temperature- and Neutron-Fluence-Dependent Graphite Thermal Conductivity), radiation damage to graphite causes a significant reduction in the thermal conductivity of graphite. It should be noted, however, that fluences greater than $3x10^{21}$ n/cm^2 result in little further reduction of the conductivity. At high temperatures (T > 1500°C), the graphite conductivity becomes independent of the fluence.

Because heat transfer via radiation is effective only at high temperatures, the effective thermal conductivity of a pebble-bed predicted by the modified Zehner-Schlünder model is lower than that of a prismatic core at temperatures below 1750°C. Figure 5.1 shows the thermal conductivity of a pebble-bed as a function of temperature (at a neutron fluence of 0.0 for illustrative purposes). The pebbles were assumed to be 6 cm in diameter, have an emissivity of 0.8, and the porosity (ϕ in equation 2.57) of the pebble-bed was 0.39. These are the same conditions used in the analysis of the pebble-bed reactor. At temperatures above 1750°C it is seen that radiation becomes the dominant mechanism of heat transfer, and the effective pebble-bed conductivity exceeds that of solid graphite. In addition, due to the more significant effect of thermal radiation (either as a resistance to or a mode of heat transfer) in a pebble-bed, the effect of neutron

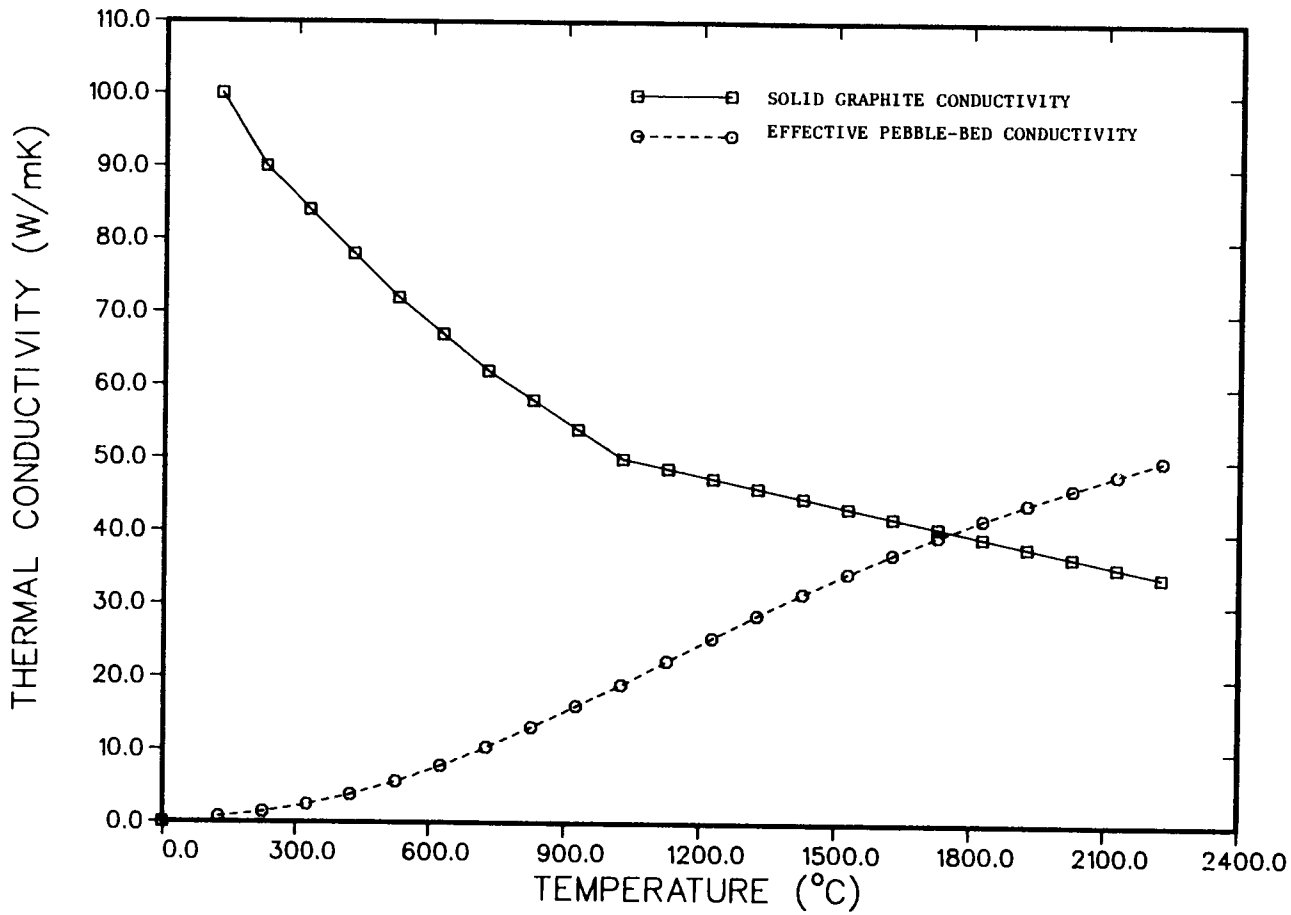

Figure 5.1 Solid Graphite and Effective Pebble-Bed Thermal Conductivities (Fluence = 0.0 n/cm^2)

radiation damage on the effective conductivity is much less pronounced (< 15%) than on the conductivity of solid graphite.

5.2 Prismatic Modular HTGR

The peak temperature reached and the time after depressurization until peaking for the prismatic HTGR cases outlined in Section 4.1 are summarized in Table 5.1. The GA study, using a two-dimensional model, calculated a peak temperature of 2093°C at axial region 3 occurring 26 hours after reactor trip [16]. Using a one-dimensional model at various axial planes, we found the peak temperature to be 2152.2°C in axial region 4 occurring 38 hours after reactor trip - a difference in peak temperature of 3%.

The reason for the differences in the axial location of the peak and the time until peaking between the GA analysis and this study is that SHERLOC neglects heat transfer in the axial direction. The axial peaking factors of axial regions 3, 4, and 5 are 1.48, 1.49, and 0.75, respectively. Therefore, one would expect considerable heat loss from axial region 4 to the region above it (5) even though axial region 5 is initially at a higher temperature. Figure 5.2 shows the response of the center-line temperature through the transient for the Reference Case (axial region 4), and axial regions 1, 3, and 5. Due to the low power density in axial region 5, it is seen that the temperatures during the transient are quite low; peaking at only 1430.8°C. Since the GA study was performed in two-dimensions, it accounted for this heat loss in the axial direction and produced the peak temperature in axial region 3. Thus the peak temperature predicted by SHERLOC in axial

Table 5.1

Summary of Results of Depressurized Heatup Accident Analyses for the Prismatic HTGR

Case	Description of Case	Peak Temp. (°C)	Time of Peak (hours after initiation)
GA	General Atomic (2-D)	2093	26
1	Reference case - Axial region 4	2152.2	38
2	Axial region 5	1430.8	14
3	Axial region 3	2144.4	42
4	Axial region 1 - bottom of core	1952.3	46
5	Axial region 4 - neutron fluence neglected	1947.9	40
6	Axial region 4 - active vessel cooling	2108.7	30
7	Axial region 4 - with He gaps	2252.9	40
8	Replacing prismatic core with pebble-bed	2172.4	24

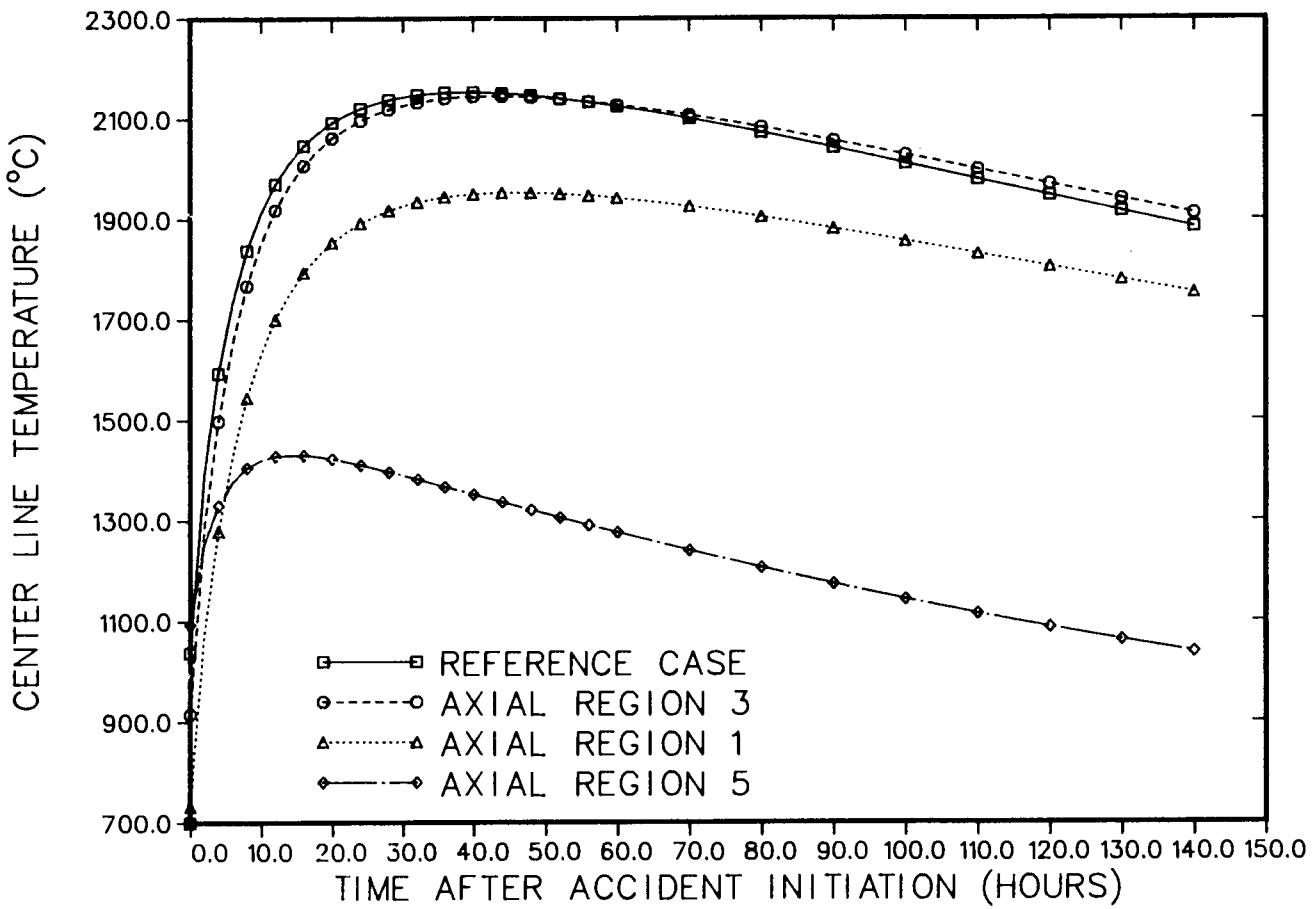

Figure 5.2 Response of the Center-line Temperature to the Depressurized Heatup Accident for the Prismatic HTGR

region 4 is probably somewhat high, and the peak temperature in region 5 is somewhat low.

The radial temperature distribution at axial position 4 at various times following the accident initiation is shown in Figure 5.3. The reflector temperature reached a maximum of 1185.7°C at 65 hours, and the reactor vessel peak temperature was 649.7°C at 80 hours.

The effects of the power densities and initial temperatures are of interest. Axial region 5 was at a 5% higher initial temperature and a 50% lower power density than was axial region 4. The resulting transient was much less severe at axial region 5 than for region 4. Conversely, axial region 1 (bottom of core) was at a 30% lower initial temperature and a 13% lower power density than was axial region 4. While the transient was less severe than for axial region 4, the peak temperature of 1952.3°C was 36% higher than the peak temperature in axial region 5. It is evident that the power density is a greater factor in the peak temperatures than is the initial temperature.

It is interesting to note the differences in the time until peaking for axial regions 1, 3, and 4. As seen in Table 4.3, the initial radial temperature distribution is flattest for axial region 1, and steepest for axial region 4. The flatter the radial temperature distribution, the slower the temperature will change with time. Referring to equation (2.33), as $\Delta T/\Delta r$ decreases, $\Delta T/\Delta t$ will also decrease. Thus for a flatter initial radial temperature distribution, the time until reaching the peak temperature will increase. This is seen in that the temperatures of axial regions 1, 3, and 4 peak at 46 hours, 42 hours, and 38 hours, respectively.

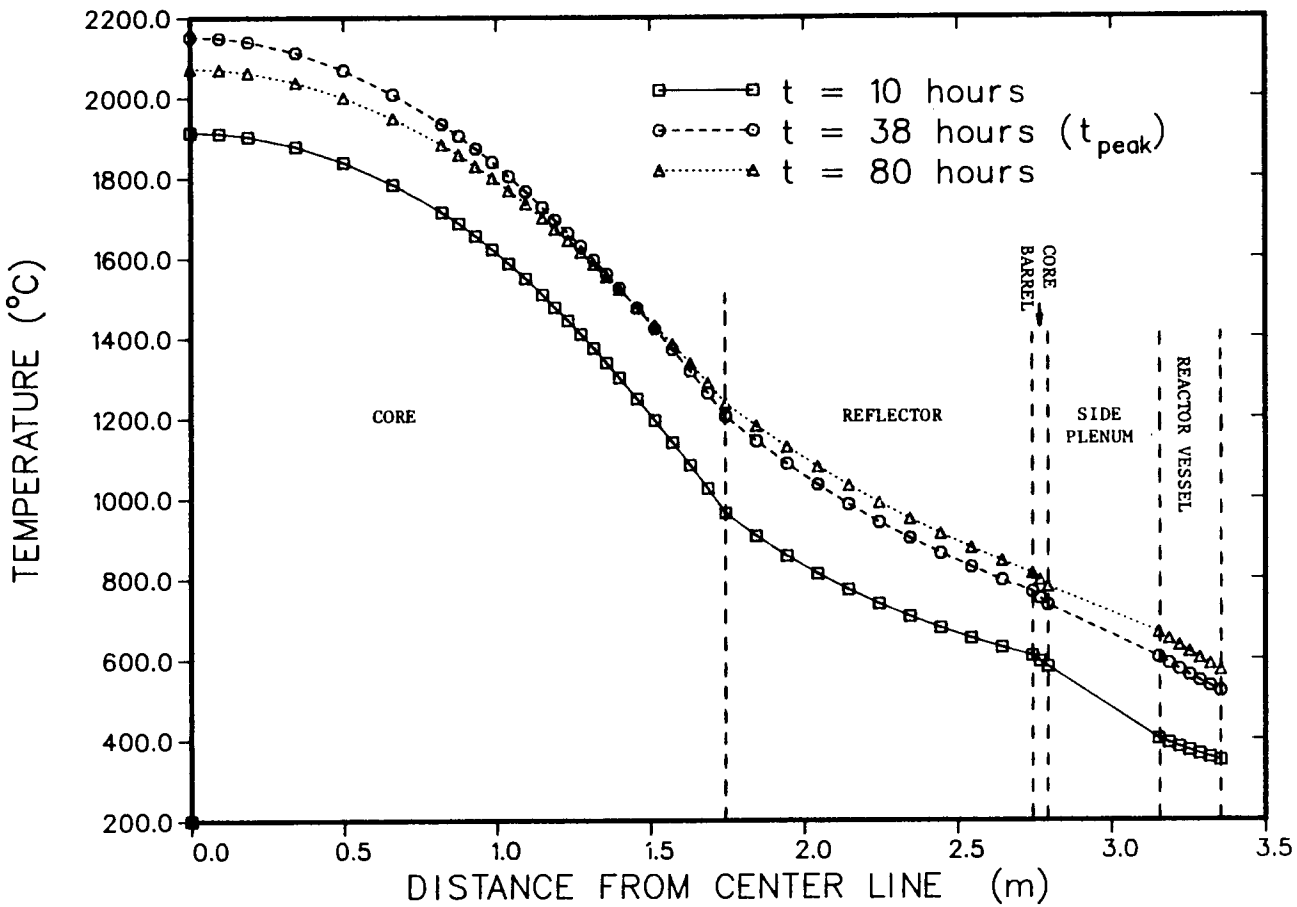

Figure 5.3 Radial Temperature Distribution at Axial Region 4 at Various Times in the Prismatic HTGR

The neutron fluence has a significant effect on the graphite thermal conductivity, as seen in Figure 2.2. Neglecting the effect of irradiation in determining the graphite conductivity causes the predicted peak temperature to decrease by 10%, and produce little effect on the time until peaking, as seen in Table 5.1. Since the graphite conductivity is fairly independent of fluence above 1500°C, the effect on the predicted temperatures would be greater for a transient which produces lower temperatures. Neglecting the effect of radiation damage on the graphite conductivity produces non-conservative results.

When active vessel cooling was considered (Case 5 - h_T = 851.7 W/m^2K), the maximum temperature was decreased by only 2%; however, the time until peaking was decreased by 8 hours. This indicates that the maximum core temperature is fairly insensitive to vessel cooling, but that steady-state will be reached sooner with an active vessel cooling system. These results are consistent with results reported in the GA study. Their analysis indicated a decrease in the maximum temperature of less than 1%, and that steady-state would be reached sooner with vessel cooling [16].

The result of modeling small helium-filled gaps between prismatic fuel assemblies was to increase the predicted peak temperature by 5%. Thus it is important to model the gaps if they are known to be present.

Finally, to examine the effect of the Zehner-Schlünder model for effective pebble-bed conductivity, the replacement of the prismatic fuel with pebbles 6 cm in diameter was simulated. The core graphite density was decreased from 1195.5 kg/m^3 to 1037 kg/m^3. All initial conditions and reactor dimensions were left the same as for the Reference Case. The peak temperature predicted increased by only

20.2°C (1%); however, the time until peaking decreased by 14 hours. Initially the effective pebble-bed conductivity is lower than the conductivity of solid graphite, but the depressurized transient produces temperatures which are high enough to cause heat transfer via radiation to become more effective than heat transfer by conduction. Therefore, the peak temperatures predicted are very similar. Because the pebble-bed conductivity increases rather than decreases with temperature (see Figure 5.1), the pebble-bed heat capacity is lower than the prismatic, and the temperatures themselves are higher than in the prismatic core, the change of temperature with time is greater for the pebble-bed case and the temperature peaks earlier.

5.3 Pebble-Bed Modular HTGR

The peak temperature reached and the time after depressurization until peaking for the pebble-bed HTGR cases outlined in Section 4.2 are summarized in Table 5.2. The GE study predicted a peak temperature of 1644°C at an axial position of z/H=0.3 (z=0.0 at top of core; H=926 cm) occurring 27 hours after reactor trip [17]. This study found the peak temperature to be 1647.8°C at z/H=0.2 occurring 26 hours after reactor trip - a difference in peak temperature of less than 1%.

As was the case for the prismatic HTGR comparison, the difference in the axial location of the peak temperature is due to two-dimensional effects, which are not considered by SHERLOC. Figure 5.4 shows the response of the center-line temperature throughout the transient at the following axial positions: z/H=0.2, 0.3, and 1.0. It should be noted that although the initial temperature is highest at the bottom of the core (z/H=1.0), the power density is low enough that the

Table 5.2

Summary of Results of Depressurized Heatup Accident Analyses for the Pebble-Bed HTGR

Case	Description of Case	Peak Temp. (°C)	Time of Peak (hours after initiation)
GE	General Electric (2-D)	1644	27
1	Reference case - z/H = 0.2	1647.8	26
2	z/H = 0.3	1583.8	24
3	z/H = 1.0 - bottom of core	1020	0.0
4	z/H = 0.2 - with GE k & ρC_p correlations	1653.1	24
5	z/H = 0.3 - with GE k & ρC_p correlations	1616.2	24

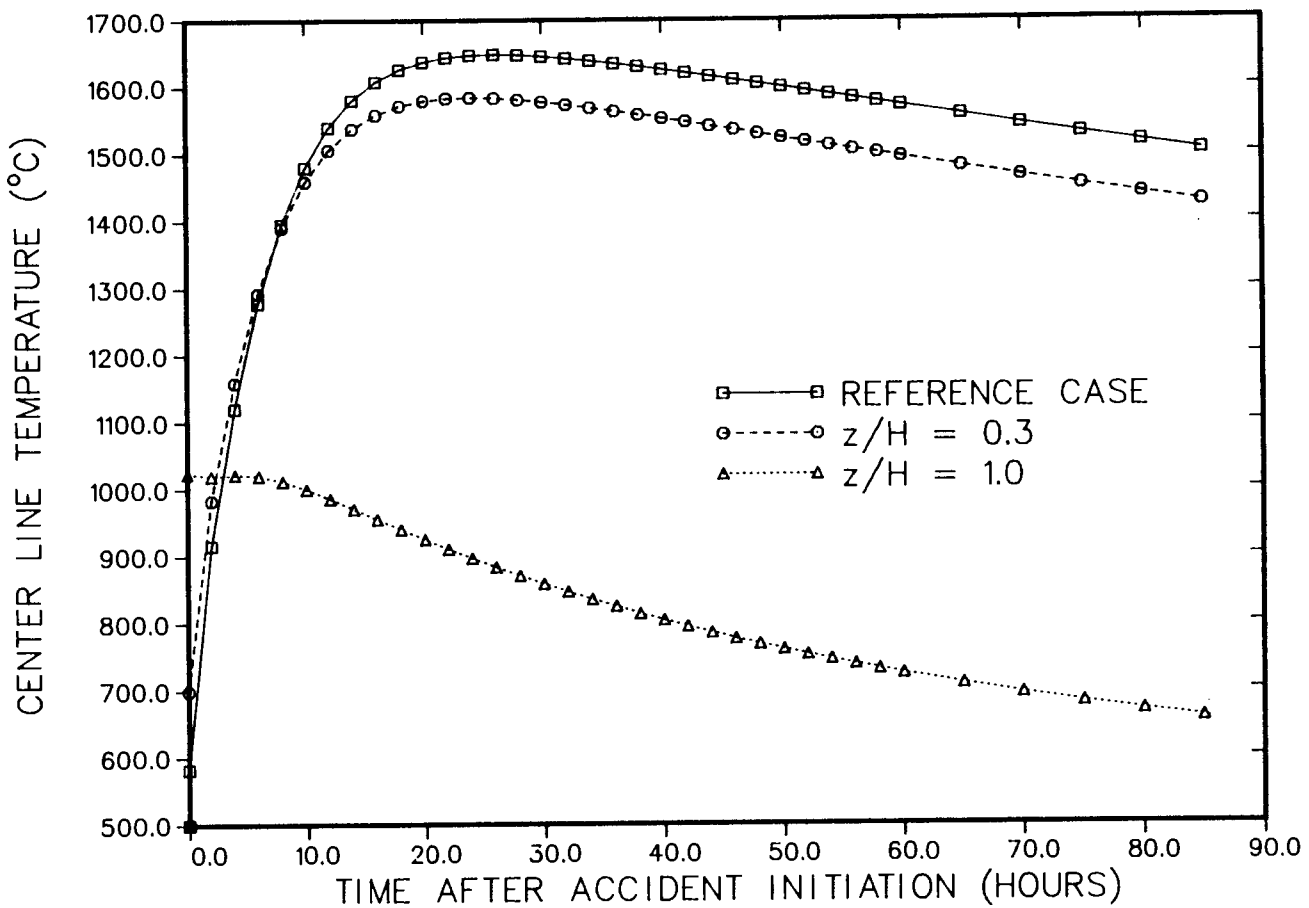

Figure 5.4 Response of the Center-line Temperature to the Depressurized Heatup Accident for the Pebble-Bed HTGR

temperature merely decreases throughout the transient. This is consistent with GE's findings [17]. Figure 5.5 shows the radial temperature distribution at z/H = 0.2 at the time of the peak temperature.

In order to investigate the differences produced by 1-D versus 2-D calculations, SHERLOC was run at z/H = 0.2 and 0.3 with the GE thermal conductivity and heat capacity functions given by equations (4.3) and (4.4), respectively. The results are included in Table 5.2. In comparing the 1-D calculation using the GE correlations to GE's 2-D study, little difference is seen. The pebble-bed axial power profile is such that little error is introduced by considering only one dimension.

The peak temperature calculated was higher than that calculated using the Zehner-Schlünder conductivity model and the graphite specific heat of Figure 4.5. The reason for this is that the conductivity correlation used by GE (a function of temperature only) is more conservative than the combined graphite conductivity correlation of Section 2.4 and Zehner-Schlünder model. Figure 5.6 compares the thermal conductivity calculated within SHERLOC for a range of irradiation temperatures (initial fuel temperatures) at a fluence of 3.0×10^{21} n/cm^2 and the thermal conductivity produced by the GE correlation. Because the GE conductivity is somewhat lower, the temperatures calculated are higher.

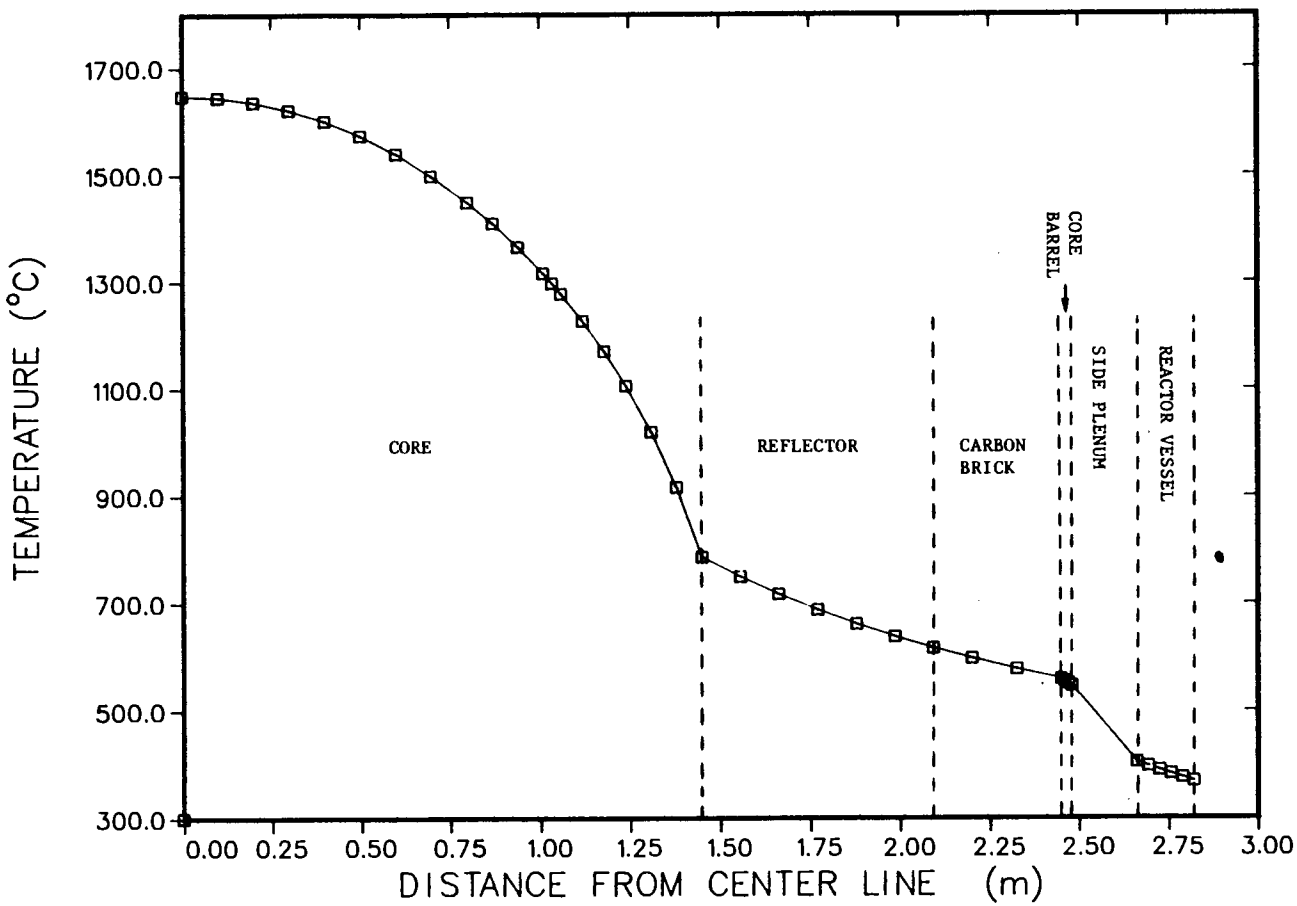

Figure 5.5 Radial Temperature Distribution at 26 Hours at z/H = 0.2 in the Pebble-Bed HTGR

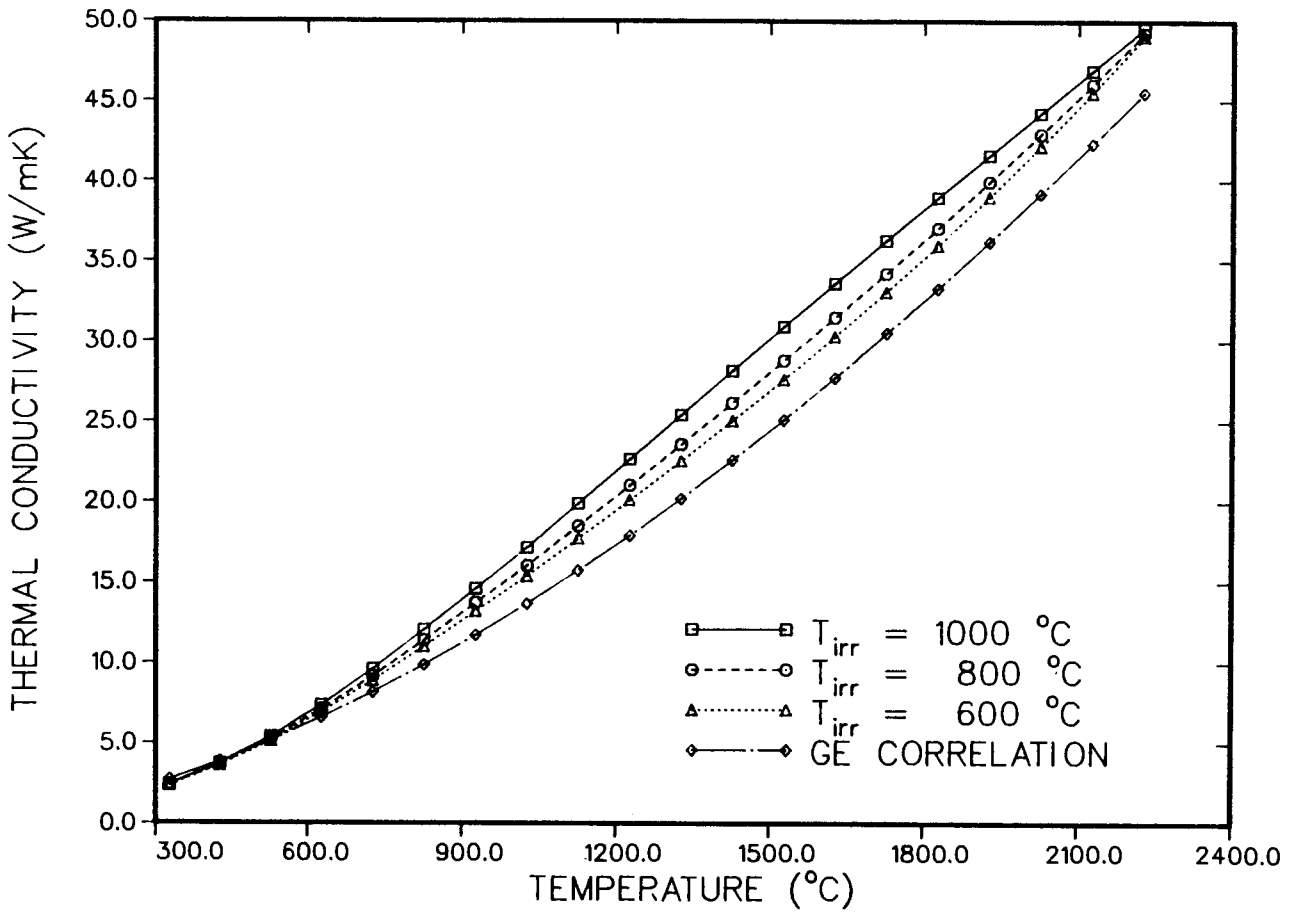

Figure 5.6 SHERLOC Pebble-Bed Conductivity Correlation (at $3x10^{21}$ n/cm^2 and Various Irradiation Temperatures) and GE Pebble-Bed Conductivity Correlation

6. SUMMARY AND RECOMMENDATIONS FOR FURTHER STUDY

6.1 Summary

The computer code SHERLOC has been developed to perform a one-dimensional evaluation of the heat removal capabilities of modular HTGR designs under depressurized loss-of-forced-convection conditions. Although developed for this specific purpose, SHERLOC may of course be used for many other types of transient or steady-state heat transfer problems. The depressurized heatup accident was analyzed for both pebble-bed and prismatic-core modular reactors; and the results compared with studies performed by GE and GA, respectively. In addition, several studies were performed to determine the effects on the behavior of the transient of initial temperatures, power density, neutron fluence; of small helium-filled gaps between prismatic fuel assemblies; and of replacing the prismatic core with a bed of graphite pebbles.

For the prismatic HTGR, a peak fuel temperature of 2152.2°C occurring 38 hours after the accident initiation was calculated using SHERLOC. The GA study indicated a peak fuel temperature of 2093°C occurring 26 hours after accident initiation - a peak temperature difference of 3%. For the pebble-bed HTGR, a peak fuel temperature of 1647.8°C occurring 26 hours after accident initiation was calculated using SHERLOC; while GE reported a peak fuel temperature of 1644°C (a difference of less than 1%) at 27 hours following the accident initiation.

The primary reason for the discrepancy between the results obtained using SHERLOC and those obtained by GA and GE is that SHERLOC performs a one-dimensional analysis, while the codes used by GA and GE perform two-dimensional calculations. In addition, small discrepancies in the problem models and the correlations used for the properties of materials contribute to differences in the results.

The power density was found to have a greater effect on the magnitude of the temperature excursion than did the initial temperature. The peak temperature was calculated using SHERLOC at the axial location of the highest power density, regardless of the location of the highest initial temperature. Including small gaps between fuel assemblies in modeling the prismatic reactor produced a 5% increase in the peak temperature.

If the effect of radiation damage on the graphite conductivity in a prismatic core is neglected, the resulting peak temperature is decreased by 10%. Thus it is concluded that the exposure to the neutron flux should be considered in determining the response of the prismatic HTGR. It was also seen that at high temperatures ($T > 1500°C$), the graphite conductivity was independent of the fluence. If one were modeling a transient in which temperatures were expected to remain lower than 1500°C, the neutron fluence would play an even more important role in predicting accurate results.

Because SHERLOC performs a one-dimensional analysis, its results are the most accurate when the axial power or temperature gradients are fairly small. The one-dimensional calculation will predict a conservative value of the peak core temperature in the depressurized

heatup accident, but it will not necessarily give the exact axial location or time until peaking.

6.2 Recommendations for Further Study

Further investigation into the thermal conductivity of graphite at high temperatures should be pursued. The data strings for the correlations given in Section 2.4 were extrapolated for temperatures above 1600 K; while reasonable results were obtained, more specific information at high temperatures is desirable. Also, in this study the core of the prismatic HTGR was assumed to be solid (except for the sensitivity study involving gaps between assemblies). The core actually contains coolant holes and other penetrations. It would be of interest to develop a more detailed model which would account for the heterogeneity of the prismatic core.

Several modifications could be made to SHERLOC to provide greater versatility in problems which may be modeled and in the accuracy of the results; these changes are as follows:

1) SHERLOC should be expanded to perform a two-dimensional analysis. The actual changes to the finite-difference equations and solution techniques would be fairly straightforward, but the coding changes involved in modifying the solution techniques and modeling a two-dimensional problem would be more complex.
2) Boundary condition options for a constant temperature or a constant heat flux should be added.

3) It would be helpful for the code to use a variable time step in order to reduce the code running time and increase the accuracy of the results. A small time step should be used when parameters are changing rapidly with time, and a larger time step when the response of the system is changing slowly.

4) The initial (steady-state) temperature distribution of the problem must be specified for a transient problem; it would be useful to have the code calculate the initial temperature distribution internally.

5) The code should be made more "user-friendly," with more versatility and ease in the input. Although the input is fairly straightforward (see Appendix C), it would be convenient to have the option of specifying all distributions (temperature, power density, properties, etc.) as either tables or analytical functions. Also, it may be useful to make the input free-format rather than formatted.

6) An option should be included to allow for heat transfer by radiation and/or conduction across gas gaps.

7) Finally, it would be of interest to adapt the code to allow coolant flow through the core. In normal, steady-state operation, heat transfer within the core is via forced convection of the helium coolant. In a pressurized, loss-of-forced-circulation transient, heat is removed from the core by natural circulation as well as conduction and radiation. Modeling coolant flow through the core would greatly expand the range of applicability of SHERLOC.

REFERENCES

1. D. C. Elrod, G. E. Giles, and W. D. Turner. "HEATING: A Multi-dimensional Heat Conduction Analysis with the Finite-Difference Formulation," SCALE: A Modular Code System for Performing Standardized Computer Analysis for Licensing Evaluation, ORNL/NUREG/CSD-2/V2, Revision 1, Union Carbide Corporation, Nuclear Division, Oak Ridge, Tennessee, October 1981.

2. C. E. Boardman and A. J. Lipps. Reduced Risk HTGR Concept for Industrial Heat Application, General Electric Company, Advanced Reactor Systems Division, Sunnyvale, California.

3. A. J. Goodjohn. "HTGR Applications Development in the U.S.," Nuclear Engineering International, 24, pp. 83-86, May 1979.

4. J. Varley. "Gas Cooled Reactors - Have They Got a Future," Nuclear Engineering International, 27, pp. 47-51, December 1982.

5. High Temperature Modular System for the Generation of Process Heat, Gesellschaft für Hochtemperaturreacktor - Technik mbH, Bergisch Gladbach 1, October 1981.

6. "Applications of the HTGR - a Russian View of Combined Systems," Nuclear Engineering International, 24, pp. 86-88, May 1979.

7. C. F. McDonald, F. S. Silady, and A. S. Shenoy. A New HTGR Plant With Inherently Safe Features Aimed at Small Energy Users Needs, General Atomic Company, San Diego, California, 1982.

8. G. Breitbach and H. Barthels. "The Radiant Heat Transfer in the HTR Core After Failure of the Afterheat Removal Systems," Nuclear Technology, 49, pp. 392-399, August 1980.

9. J. P. Holman. Heat Transfer, 2nd ed., McGraw-Hill Book Company, New York, 1968.

10. M. Necati Özişik, Heat Conduction, John Wiley and Sons, New York, 1980.

11. R. E. Nightingale, ed., Nuclear Graphite, Academic Press, New York, 1962.

12. B. T. Kelly. Physics of Graphite, Applied Science Publisher Inc., Englewood, New Jersey, 1981.

13. D. R. Vondy. PEBBLE: A Two-Dimensional Steady-State Pebble Bed Reactor Thermal Hydraulics Code, ORNL-5696, Union Carbine Corporation, Nuclear Division, Oak Ridge, Tennessee, 1981.

14. J. J. Dorgarra, C. B. Moler, J. R. Bunch, and G. W. Stewart. "LINPACK User's Guide," SIAM, Philadelphia, Pennsylvania, 1979.

15. J. F. Peterson. RECA3: A Computer Code for Thermal Analysis of HTGR Emergency Cooling Transients, Report No. GA-A14520, General Atomic Company, San Diego, California, August, 1977.

16. C. S. Kang. Core Heatup Studies for the 250 MWt VHTR Modular Reactor System, General Atomic Company, San Diego, California, January, 1982.

17. D. E. Lutz, et. al. Modular Pebble-Bed Reactor Reforming Plant Design for Process Heat, Report No. GEFR-00630, General Electric Company, Advanced Reactor Systems Division, Sunnyvale, California, September, 1982.

18. G. R. Pflasterer. "Request for GE MRS - Pebble Bed Core Data," Letter to C. F. McDonald, XL-848-830068/p2773, April 7, 1983.

19. H. Etherington, et. al. Nuclear Engineering Handbook, McGraw-Hill Book Company, New York, 1968.

20. Personal Communication with D. L. Moses, Oak Ridge National Laboratory, Oak Ridge, Tennessee, April 25, 1983.

21. A. Banerjea, et. al. Thermodynamische Stoffwerte von Helium im Bereich von 20 bis 1500°C und 1 bis 100 bar, Kernforschungsanlage Jülich, GmbH, December, 1978.

22. J. Goodman, et. al. The Thermodynamic and Transport Properties of Helium, General Atomic Company, Report No. GA-A13400, San Diego, California, October, 1975.

APPENDIX A

Derivation of the Steady-State Finite Difference Heat Transfer Equations

The one-dimensional, steady-state, finite difference heat transfer equations must be derived in rectangular and cylindrical geometries at each of the following unique types of mesh points:

1) origin (assumed to be an adiabatic boundary);
2) a point within a given material;
3) the interface of two different regions, each of which contains a material;
4) the left-hand (inner) boundary of a void region;
5) the right-hand (outer) boundary of a void region;
6) the outermost boundary

The steady-state heat balance on a control volume V is:

$$\begin{bmatrix}\text{Heat entering V through} \\ \text{the boundaries of V}\end{bmatrix} + \begin{bmatrix}\text{Heat generated} \\ \text{within V}\end{bmatrix} = 0$$

This heat balance is performed for each of the six unique types of mesh points given above. Figures A.1 through A.12 show each of the points in rectangular and cylindrical coordinates. The control volume about mesh point i, or the mesh interval, is defined as the interval enclosed by the dashed lines in Figures A.1 through A.12.

A.1 Rectangular Coordinates

The one-dimensional, steady state, conduction equation in rectangular coordinates is:

$$k(T)\,\frac{d^2T(x)}{dx^2} + g(x) = 0 \qquad \text{(A.1)}$$

The derivation of the finite difference form of equation (A.1) at each of the six unique types of mesh points in rectangular coordinates follows.

1) Origin

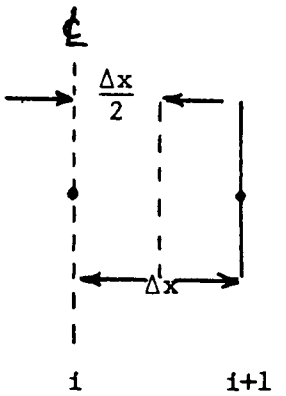

Figure A.1

Mesh Interval at the Origin - Rectangular Coordinates

Performing a heat balance on mesh point i of Figure A.1 yields the following finite difference equation:

$$ {}_iK_{i+1} \frac{(T_{i+1}-T_i)}{\Delta x} = -g_i \frac{\Delta x}{2} \qquad (A.2) $$

where

${}_iK_{i+1}$ = thermal conductivity between mesh points i and i+1

g_i = average volumetric heat generation in the mesh interval defined by i

Simplifying:

$$ -{}_iK_{i+1}\, T_i + {}_iK_{i+1} T_{i+1} = -g_i \frac{(\Delta x)^2}{2} \qquad (A.3) $$

2) Mesh Point Within a Material

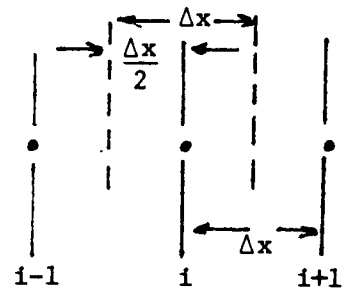

Figure A.2

Mesh Interval Within a Material - Rectangular Coordinates

The finite difference form of the heat balance on mesh point i of Figure A.2 is:

$$ {}_iK_{i-1} \frac{(T_{i-1}-T_i)}{\Delta x} + {}_iK_{i+1} \frac{(T_{i+1}-T_i)}{\Delta x} = -g_i(\Delta x) \quad (A.4) $$

where

${}_iK_{i-1}$ = thermal conductivity between mesh points i and i-1.

Manipulating equation (A.4) yields:

$$ {}_iK_{i-1}\, T_{i-1} - ({}_iK_{i-1} + {}_iK_{i+1})T_i + {}_iK_{i+1}T_{i+1} = -g_i(\Delta x)^2 \quad (A.5) $$

3) Interface of Two Materia Regions

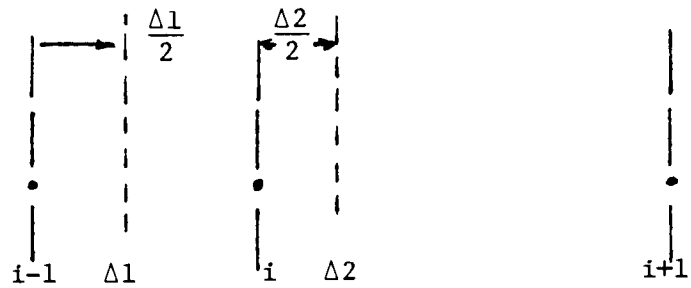

Figure A.3

Interface of Two Material Regions - Rectangular Coordinates

The finite difference form of the heat balance on mesh point i of Figure A.3 is:

$$ {}_iK_{i-1} \frac{(T_{i-1}-T_i)}{\Delta_1} + {}_iK_{i+1} \frac{(T_{i+1}-T_i)}{\Delta_2} = -g_i\left(\frac{\Delta_1}{2} + \frac{\Delta_2}{2}\right) \qquad (A.6) $$

$$ \frac{{}_iK_{i-1}}{\Delta_1} T_{i-1} - \left(\frac{{}_iK_{i-1}}{\Delta_1} + \frac{{}_iK_{i+1}}{\Delta_2}\right)T_i + \frac{{}_iK_{i+1}}{\Delta_2} T_{i+1} = \frac{-g_i}{2}(\Delta_1+\Delta_2) $$

$$ \frac{\Delta_2}{(\Delta_1+\Delta_2)} {}_iK_{i-1}T_{i-1} - ({}_iK_{i-1}\Delta_2 + {}_iK_{i+1}\Delta_1)\frac{T_i}{(\Delta_1+\Delta_2)} + \frac{\Delta_1}{(\Delta_1+\Delta_2)} {}_iK_{i+1}T_{i+1} $$

$$ = -g_i \frac{\Delta_1\Delta_2}{2} \qquad (A.7) $$

4) Inner Boundary of a Void Region

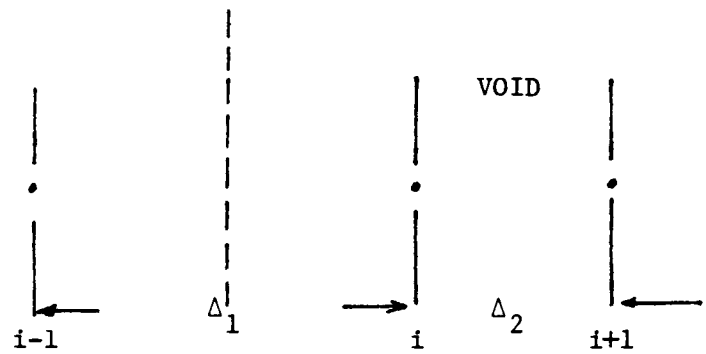

Figure A.4

Inner Boundary of a Void Region - Rectangular Coordinates

The finite difference form of the heat balance on mesh point i of Figure A.4 is:

$$ {}_iK_{i-1} \frac{T_{i-1}-T_i}{\Delta 1} + h_{r_{12}}(T_{i+1}-T_i) = -g_i \frac{\Delta 1}{2} \qquad (A.8) $$

where

$h_{r_{12}}$ = radiative heat transfer coefficient from the surface at mesh point i to the surface at i+1

$$ {}_iK_{i-1}T_{i-1} - ({}_iK_{i-1} + h_{r_{12}}\Delta_1)T_i + h_{r_{12}}\Delta_1 T_{i+1} = -g_i \frac{(\Delta_1)^2}{2} \qquad (A.9) $$

5) Outer Boundary of a Void Region

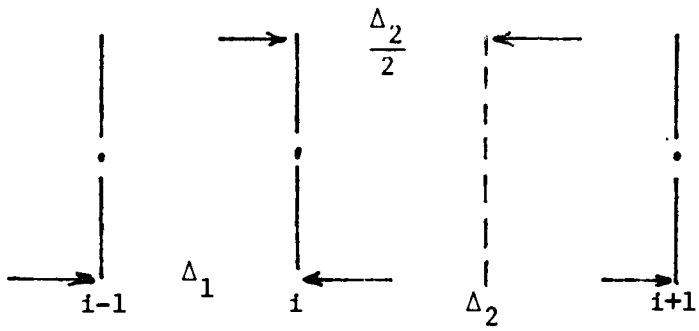

Figure A.5

Outer Boundary of a Void Region - Rectangular Coordinates

The finite difference form of the heat balance on mesh point i of Figure A.5 is:

$$h_{r_{21}}(T_{i-1}-T_i) + {}_iK_{i+1}\frac{T_{i+1}-T_i}{\Delta_2} = -g_i\frac{(\Delta_2)}{2} \qquad (A.10)$$

where

$h_{r_{21}}$ = radiative heat transfer coefficient from surface at mesh point i to surface at i-1

$$h_{r_{21}}\Delta_2\, T_{i-1} - (h_{r_{21}}\Delta_2 + {}_iK_{i+1})T_i + {}_iK_{i+1}T_{i+1} = -g_i\frac{(\Delta_2)^2}{2} \qquad (A.11)$$

6) Outermost Boundary

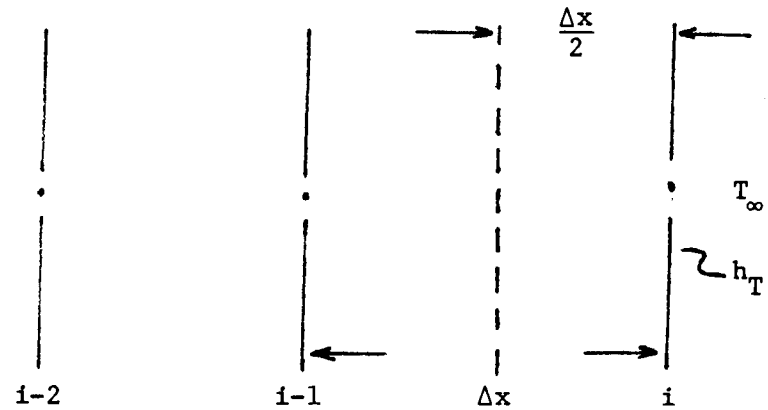

Figure A.6

Mesh Interval at the Outermost Boundary
Rectangular Coordinates

The finite difference form of the heat balance on mesh point i of Figure A.6 is:

$$ {}_iK_{i-1} \frac{T_{i-1}-T_i}{\Delta x} + h_T (T_\infty - T_1) = -g_i \frac{\Delta x}{2} \qquad (A.12) $$

where

h_T = total heat transfer coefficient (sum of radiative and convective heat transfer coefficients)

T_∞ = ambient temperature

$$ {}_iK_{i-1}T_{i-1} - ({}_iK_{i-1} + h_T \Delta x)T_i = -g_i \frac{(\Delta x)^2}{2} - h_T \Delta x \, T_\infty \qquad (A.13) $$

A.2 Cylindrical Coordinates

The one-dimensional, steady-state, conduction equation in cylindrical coordinates is:

$$k(T)\,\frac{d^2T(r)}{dr^2} + \frac{k(T)}{r}\,\frac{dT(r)}{dr} + g(r) = 0 \qquad \text{(A.14a)}$$

which may be rewritten as:

$$k(T)\,\frac{1}{r}\,\frac{d}{dr}\left(r\,\frac{dT(r)}{dr}\right) + g(r) = 0 \qquad \text{(A.14b)}$$

1) Origin

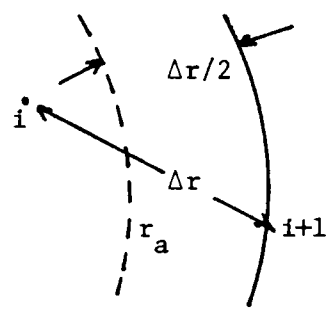

Figure A.7

Mesh Interval at the Origin
Cylindrical Coordinates

The finite difference form of the heat balance on mesh point i of Figure A.7 is:

$$2\pi r_a\,{}_iK_{i+1}\,\frac{T_{i+1}-T_i}{\Delta r} = -\pi\,r_a^{\,2}\,g_i \qquad \text{(A.15)}$$

where

$$r_a = \frac{\Delta r}{2}$$

$$-{}_iK_{i+1} + {}_iK_{i+1}\,T_{i+1} = -g_i\,\frac{(\Delta r)^2}{4} \qquad \text{(A.16)}$$

2) Mesh Point Within a Material

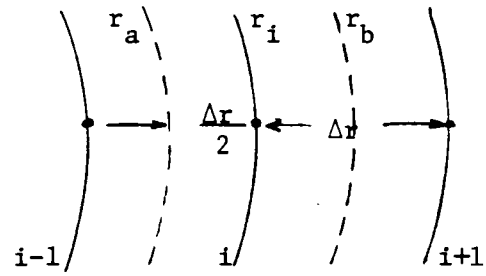

Figure A.8

Mesh Interval Within a Material - Cylindrical Coordinates

The finite difference form of the heat balance on mesh point i of Figure A.8 is

$$2\pi r_a \, {}_iK_{i-1} \frac{(T_{i-1}-T_i)}{\Delta r} + 2\pi r_b \, {}_iK_{i+1} \frac{(T_{i+1}-T_i)}{\Delta r} = g_i \, \pi(r_b^{\,2}-r_a^{\,2}) \tag{A.17}$$

where

$$r_a = r_i - \frac{\Delta r}{2}$$

$$r_b = r_i + \frac{\Delta r}{2}$$

$$r_b^{\,2}-r_a^{\,2} = 2r_i \, \Delta r$$

$$\frac{(r_i-\Delta r/2)}{\Delta r} {}_iK_{i-1}T_{i-1} - \left[\frac{(r_i-\Delta r/2)}{\Delta r} {}_iK_{i-1} + \frac{(r_i+\Delta r/2)}{\Delta r} {}_iK_{i+1}\right] T_i$$

$$+ \frac{(r_i+\Delta r/2)}{\Delta r} {}_iK_{i+1}T_{i+1} = -g_i r_i \Delta r \tag{A.18}$$

3) Interface of Two Material Regions

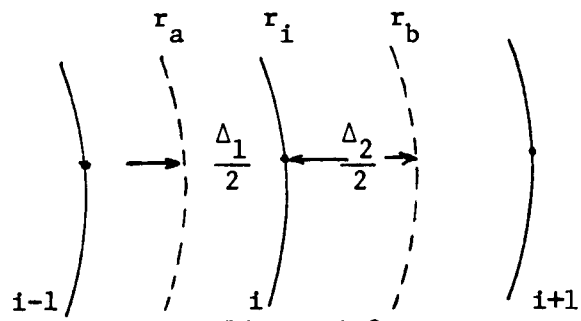

Figure A.9

Interface of Two Material Regions - Cylindrical Coordinates

The finite difference form of the heat balance on mesh point i of Figure A.9 is

$$2\pi(r_i - \frac{\Delta_1}{2})\,{}_iK_{i-1}\,\frac{(T_{i-1}-T_i)}{\Delta_1} + 2\pi(r_i + \frac{\Delta_2}{2})\,{}_iK_{i+1}\,\frac{(T_{i+1}-T_i)}{\Delta_2}$$

$$= -\,g_i\pi\left[(r_i + \frac{\Delta_2}{2})^2 - (r_i - \frac{\Delta_1}{2})^2\right] \tag{A.19}$$

$$\frac{(r_i-\Delta_1/2)}{\Delta_1}\,{}_iK_{i-1}T_{i-1} - \left[(r_i - \frac{\Delta_1}{2})\,\frac{{}_iK_{i-1}}{\Delta_1} + \frac{(r_i + \frac{\Delta_2}{2})}{\Delta_2}\,{}_iK_{i+1}\right]T_i$$

$$+\,\frac{(r_i + \Delta_2/2)}{\Delta_2}\,{}_iK_{i+1}T_{i+1} = -\,\frac{g_i}{2}\left[r_i(\Delta_1+\Delta_2) + \frac{1}{4}(\Delta_2{}^2-\Delta_1{}^2)\right] \tag{A.20}$$

4) Inner Boundary of a Void Region

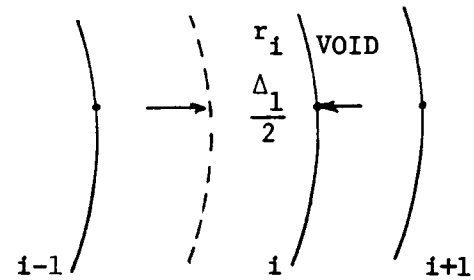

Figure A.10

Inner Boundary of a Void Region - Cylindrical Coordinates

The finite difference form of the heat balance on mesh point i of Figure A.10 is

$$2\pi(r_i - \frac{\Delta_1}{2})\,{}_iK_{i-1}\,\frac{T_{i-1}-T_i}{\Delta_1} + 2\pi r_i\, h_{r_{12}}(T_{i+1}-T_i) = g_i\pi\left[r_i^{\,2}-(r_i-\frac{\Delta_1}{2})^2\right] \tag{A.21}$$

$$\frac{(r_i-\Delta_1/2)}{\Delta_1}\,{}_iK_{i-1}T_{i-1} - \left[\frac{(r_i-\Delta_1/2)}{\Delta_1}\,{}_iK_{i-1} + r_i\, h_{r_{12}}\right]T_i + r_i\, h_{r_{12}}T_{i+1}$$

$$= -\frac{g_i}{2}\,\Delta_1(r_i - \frac{\Delta_1}{4}) \tag{A.22}$$

5) Outer Boundary of a Void Region

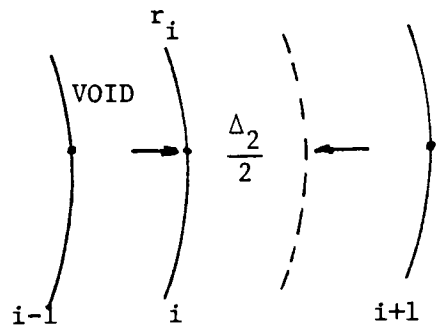

Figure A.11

Outer Boundary of a Void Region - Cylindrical Coordinates

The finite difference form of the heat balance on mesh point i of Figure A.11 is

$$2\pi r_i h_{r_{21}} (T_{i-1}-T_i) + 2\pi (r_i + \frac{\Delta 2}{2})\ {}_iK_{i+1} \frac{(T_{i+1}-T_i)}{\Delta_2} = g_i \pi \left[(r_i + \frac{\Delta_2}{2})^2 - r_i^2 \right] \tag{A.23}$$

$$r_i h_{r_{21}}\ T_{i-1} - \left[r_i h_{r_{21}} + \frac{(r_i + \Delta 2/2)}{\Delta_2}\ {}_iK_{i+1} \right] T_i + \frac{(r_i + \Delta 2/2)}{\Delta_2}\ {}_iK_{i+1} T_{i+1} =$$

$$- g_i/2\ \Delta_2 (r_i + \frac{\Delta_2}{4}) \tag{A.24}$$

6) Outermost Boundary

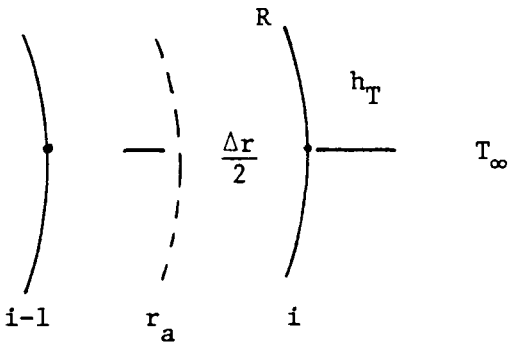

Figure A.12

Mesh Interval at the Outermost Boundary - Cylindrical Coordinates

The finite difference form of the heat balance on mesh point i of Figure A.12 is

$$2\pi r_a \, {}_iK_{i-1} \frac{(T_{r-1}-T_i)}{\Delta r} + 2\pi R \, h_T(T_\infty - T_i) = - g_i \pi (R^2 - r_a{}^2) \qquad \text{(A.25)}$$

where

R = radius of outermost surface

$r_a = R - \Delta r/2$

$R^2 - r_a{}^2 = \Delta r(R - \Delta r/4)$

$$\frac{(R-\Delta r/2)}{\Delta r} \, {}_iK_{i-1} T_{i-1} - \left[\frac{(R-\Delta r/2)}{\Delta r} + Rh_T\right] T_i = - \left[\frac{g_i \Delta r(R-\Delta r/4)}{2} + h_T R \, T_\infty\right]$$

(A.26)

APPENDIX B

Derivation of the Time-Dependent Finite Difference Heat Transfer Equations

The one-dimensional, time dependent, finite difference heat transfer equations must be derived in rectangular and cylindrical geometries at each of the following unique types of mesh points:

1) origin (assumed to be an adiabatic boundary)
2) a point within a given material
3) the interface of two difference regions, each of which contains a material
4) the left-hand (inner) boundary of a void region
5) the right-hand (outer) boundary of a void region
6) the outermost boundary

The transient heat balance on a control volume V is

$$\begin{bmatrix}\text{Rate of heat entering V} \\ \text{through the boundaries} \\ \text{of V}\end{bmatrix} + \begin{bmatrix}\text{Rate of heat} \\ \text{generated} \\ \text{in V}\end{bmatrix} = \begin{bmatrix}\text{Energy} \\ \text{stored} \\ \text{in V}\end{bmatrix}$$

The heat balance is performed for each of the six unique types of mesh points given above. Figures A.1 through A.12 of Appendix A show each of the points in rectangular and cylindrical coordinates. The control volume about mesh point i, or the mesh interval, is defined as the interval enclosed by the dashed lines in Figures A.1 through A.12.

B.1 Rectangular Coordinates

The one-dimensional, time-dependent, conduction equation in rectangular coordinates is

$$k(T)\,\frac{\partial^2 T(x,t)}{\partial x^2} + g(x,t) = (T)C_p(T)\,\frac{\partial T(x,t)}{\partial t} \qquad \text{(B.1)}$$

1) Origin

The finite difference form of the time-dependent heat balance on mesh point i of Figure A.1 is

$$(\rho_i C_{pi})\,\frac{(T_i^{n+1}-T_i^n)}{\Delta t}\,\frac{\Delta x}{2} = g_i^n\,\frac{\Delta x}{2} + {}_iK_{i+1}\,\frac{T_{i+1}^n - T_i^n}{\Delta x}$$

Applying the θ-differencing technique described in Section 2.3.1 yields

$$(\rho_i C_{pi})^{n+\theta}\,\frac{(T_i^{n+1}-T_i^n)}{\Delta t}\,\frac{(\Delta x)^2}{2} = g_i^n\,\frac{(\Delta x)^2}{2} + \theta\left[{}_iK_{i+1}^{n+\theta}(T_{i+1}^{n+1}-T_i^{n+1})\right]$$

$$+ (1-\theta)\left[{}_iK_{i+1}^{n+\theta}(T_{i+1}^n - T_i^n)\right] \qquad \text{(B.2)}$$

Rewriting equation (B.2) with all the terms evaluated at t_{n+1} on the left-hand side

$$-\theta\left[{}_iK_{i+1}^{n+\theta}\,(T_{i+1}^{n+1}-T_i^{n+1})\right] + (\rho_i C_{pi})^{n+\theta}\,\frac{T_i^{n+1}}{\Delta t}\,\frac{(\Delta x)^2}{2} = H_i \qquad \text{(B.3)}$$

where

$$H_i = (\rho_i C_{pi})^{n+\theta}\frac{T_i^n}{\Delta t}\,\frac{(\Delta x)^2}{2} + (1-\theta)\left[{}_iK_{i+1}^{n+\theta}\,(T_{i+1}^n - T_i^n)\right] \qquad \text{(B.4)}$$

Collecting the T_i^{n+1} terms in equation (B.3),

$$-\theta({}_iK_{i+1}^{n+\theta}\ T_{i+1}^{n+1}) + \left[\theta\ {}_iK_{i+1}^{n+\theta} + (\rho_i C_{pi})^{n+\theta}\ \frac{(\Delta x)^2}{2\Delta t}\right] T_i^{n+1} = H_i \qquad (8.5)$$

Let

$$D_i = \left[\theta\ {}_iK_{i+1}^{n+\theta} + (\rho_i C_{pi})^{n+\theta}\ \frac{(\Delta x)^2}{2\Delta t}\right] \qquad (B.6)$$

Substituting equation (B.6) into equation (B.5) and solving for T_i^{n+1}:

$$T_i^{n+1} = \frac{1}{D_i}\left[H_i + \theta\ {}_iK_{i+1}^{n+\theta}\ T_i^{n+1}\right] \qquad (8.7)$$

Since T_{i+1}^{n+1} is unknown, the iterative procedure described in section 2.3.1 is used. Combining the notation for the iterative procedure and the point successive overrelaxation method:

$$T_i^{\ell+1} = (1-\omega)T_i^{\ell} + \frac{\omega}{D_i}\left[H_i + \theta\ {}_iK_{i+1}^{n+\theta}\ T_{i+1}^{\ell}\right] \qquad (B.8)$$

2) Mesh Point Within a Material

The finite difference form of the time-dependent heat balance on mesh point i of Figure A.2 is

$$(\rho_i C_{pi})\ \frac{(T_i^{n+1}-T_i^n)}{\Delta t}\ \Delta x = g_i^n\ \Delta x + {}_iK_{i-1}\ \frac{(T_{i-1}^n-T_i^n)}{\Delta x} + {}_iK_{i+1}\ \frac{(T_{i+1}^n-T_i^n)}{\Delta x}$$

(B.9)

Applying the θ-differencing technique described in Section 2.3.1 yields:

$$(\rho_i C_{pi})^{n+\theta} (\Delta x)^2 \frac{(T_i^{n+1}-T_i^n)}{\Delta t} = g_i^n (\Delta x)^2 + \theta \left[{}_iK_{i-1}^{n+\theta} \ (T_{i-1}^{n+1}-T_i^{n+1}) \right.$$

$$\left. + \ {}_iK_{i+1}^{n+\theta} \ (T_{i+1}^{n+1}-T_i^{n+1}) \right] + (1-\theta) \left[{}_iK_{i-1}^{n+\theta} (T_{i-1}^n - T_i^n) + {}_iK_{i+1}^{n+\theta} \ (T_{i+1}^n - T_i^n) \right] \tag{B.10}$$

Rewriting equation (B.1) with the terms evaluated at t_{n+1} on the left-hand side:

$$- \theta \left[{}_iK_{i-1}^{n+\theta} \ (T_{i-1}^{n+1}-T_i^{n+1}) + \ {}_iK_{i+1}^{n+\theta} \ (T_{i+1}^{n+1}-T_i^{n+1}) \right] + (\rho_i C_{pi})^{n+\theta} (\Delta x)^2 \frac{T_i^{n+1}}{\Delta t} = H_i \tag{B.11}$$

where

$$H_i = (\rho_i C_{pi})^{n+\theta} (\Delta x)^2 \frac{T_i^n}{\Delta t} + g_i^n (\Delta x)^2 + (1-\theta) \left[{}_iK_{i-1}^{n+\theta} (T_{i-1}^n - T_i^n) \right.$$

$$\left. + \ {}_iK_{i+1}^{n+\theta} \ (T_{i+1}^n - T_i^n) \right] \tag{B.12}$$

Collecting the T_i^{n+1} terms in equation (B.11)

$$- \theta \left[{}_iK_{i-1}^{n+\theta} \ T_{i-1}^{n+1} + {}_iK_{i+1}^{n+\theta} T_{i+1}^{n+1} \right] + \left[\theta ({}_iK_{i-1}^{n+\theta} + {}_iK_{i+1}^{n+\theta}) + \right.$$

$$\left. (\rho_i C_{pi})^{n+\theta} \frac{(\Delta x)^2}{t} \right] T_i^{n+1} = H_i \tag{B.13}$$

Let

$$D_i = \left[\theta({}_iK_{i-1}^{n+\theta} + {}_iK_{i+1}^{n+\theta}) + (\rho_i C_{pi})^{n+\theta}\frac{(\Delta x)^2}{\Delta t}\right] \tag{B.14}$$

Substituting equation (B.14) into equation (B.13) and solving for T_i^{n+1}:

$$T_i^{n+1} = \frac{1}{D_i}\left[H_i + \theta({}_iK_{i-1}^{n+\theta}\ T_{i-1}^{n+1} + {}_iK_{i+1}^{n+\theta}\ T_{i+1}^{n+1})\right] \tag{B.15}$$

Since T_{i+1}^{n+1} is unknown, the iterative procedure described in section 2.3.1 is used. Combining the notation for the iterative procedure and the point successive overrelaxation method

$$T_i^{\ell+1} = (1-\omega)\ T_i^{\ell} + \frac{\omega}{D_i}\left[H_i + \theta({}_iK_{i-1}^{n+\theta}\ T_{i-1}^{\ell+1} + {}_iK_{i+1}^{n+\theta}T_{i+1}^{\ell})\right] \tag{B.16}$$

3) Interface of Two Material Regions

The finite difference form of the time-dependent heat balance on mesh point i of Figure A.3 is

$$(\rho_i C_{pi})\ \frac{(T_i^{n+1}-T_i^n)}{\Delta t}\ (\frac{\Delta_1}{2} + \frac{\Delta_2}{2}) = g_i^n(\frac{\Delta_1}{2} + \frac{\Delta_2}{2}) + {}_iK_{i-1}\ \frac{(T_{i-1}^n-T_i^n)}{\Delta_1}$$

$$+ {}_iK_{i+1}\ \frac{(T_{i+1}^n-T_i^n)}{\Delta_2} \tag{B.17}$$

$$(\rho_i C_{pi})\ \frac{(T_i^{n+1}-T_i^n)}{\Delta t}\ \frac{\Delta_1\Delta_2}{2} = g_i^n\ \frac{\Delta_1\Delta_2}{2} + {}_iK_{i-1}\ (T_{i-1}^n-T_i^n)\ \frac{\Delta_2}{(\Delta_1+\Delta_2)}$$

$$+ {}_iK_{i+1}(T_{i+1}^n-T_i^n)\ \frac{\Delta_1}{(\Delta_1+\Delta_2)}$$

Applying the θ-differencing technique described in Section 2.3.1:

$$(\rho_i C_{pi})^{n+\theta} \frac{(T_i^{n+1}-T_i^n)}{\Delta t} \frac{\Delta_1\Delta_2}{2} = g_i^n \frac{\Delta_1\Delta_2}{2} + \theta\left[{}_iK_{i-1}^{n+\theta} (T_{i-1}^{n+1}-T_i^{n+1}) \frac{\Delta_2}{(\Delta_1+\Delta_2)}\right.$$

$$\left. + {}_iK_{i+1}^{n+\theta} (T_{i+1}^{n+1}-T_i^{n+1}) \frac{\Delta_1}{(\Delta_1+\Delta_2)}\right] + (1-\theta)\left[{}_iK_{i-1}^{n+\theta} (T_{i-1}^{n}-T_i^{n}) \frac{\Delta_2}{(\Delta_1+\Delta_2)}\right.$$

$$\left. + {}_iK_{i+1}^{n+\theta} (T_{i+1}^{n}-T_i^{n}) \frac{\Delta_1}{(\Delta_1+\Delta_2)}\right] \tag{B.18}$$

Rewriting equation (B.8) with the terms evaluated at T_{n+1} on the left-hand side:

$$- \theta\left[{}_iK_{i-1}^{n+\theta} (T_{i-1}^{n+1}-T_i^{n+1}) \frac{\Delta_2}{(\Delta_1+\Delta_2)} + ({}_iK_{i+1}^{n+\theta}-T_i^{n+1}) \frac{\Delta_1}{(\Delta_1+\Delta_2)}\right]$$

$$+ (\rho_i C_{pi})^{n+\theta} \frac{T_i^{n+1}}{\Delta t} \frac{\Delta_1\Delta_2}{2} = H_i \tag{B.19}$$

where

$$H_i = (\rho_i C_{pi})^{n+\theta} \frac{T_i^n}{\Delta t} \frac{\Delta_1\Delta_2}{2} + g_i^n \frac{\Delta_1\Delta_2}{2} + (1-\theta)\left[{}_iK_{i-1}^{n+\theta} (T_{i-1}^{n}-T_i^{n}) \frac{\Delta_2}{(\Delta_1+\Delta_2)}\right.$$

$$\left. + {}_iK_{i+1}^{n+\theta} (T_{i+1}^{n}-T_i^{n}) \frac{\Delta_1}{(\Delta_1+\Delta_2)}\right] \tag{B.20}$$

Collecting the T_i^{n+1} terms in equation (B.19)

$$- \theta\left[{}_iK_{i-1}^{n+\theta} T_{i-1}^{n+1} \frac{\Delta_2}{(\Delta_1+\Delta_2)} + {}_iK_{i+1}^{n+\theta} T_{i+1}^{n+1} \frac{\Delta_1}{(\Delta_1+\Delta_2)}\right]$$

$$+ \left\{\theta\left[{}_iK_{i-1}^{n+\theta} \frac{\Delta_2}{(\Delta_1+\Delta_2)} + {}_iK_{i+1}^{n+\theta} \frac{\Delta_1}{(\Delta_1+\Delta_2)}\right] + (\rho_i C_{pi})^{n+\theta} \frac{\Delta_1\Delta_2}{2\Delta t}\right\} T_i^{n+1} = H_i \tag{B.21}$$

Let

$$D_i = \left\{ \theta \left[{}_iK_{i-1}^{n+\theta} \frac{\Delta_2}{(\Delta_1+\Delta_2)} + {}_iK_{i-1}^{n+\theta} \frac{\Delta_1}{(\Delta_1+\Delta_2)} \right] + (\rho_i C_{pi})^{n+\theta} \frac{\Delta_1 \Delta_2}{2\Delta t} \right\} \tag{B.22}$$

Substituting equation (B.22) into equation (B.21) and solving for T_i^{n+1}:

$$T_i^{n+1} = \frac{1}{D_i} \left\{ H_i + \theta \left[{}_iK_{i-1}^{n+\theta} \frac{\Delta_2}{(\Delta_1+\Delta_2)} T_{i-1}^{n+1} + {}_iK_{i+1}^{n+\theta} \frac{\Delta_1}{(\Delta_1+\Delta_2)} T_{i+1}^{n+1} \right] \right\} \tag{B.23}$$

Since T_{i+1}^{n+1} is unknown, the iterative procedure described in Section 2.3.1 is used. Combining the notation for the iterative procedure and the point successive overrelaxation method:

$$T_i^{\ell+1} = (1-\omega)T_i^{\ell} + \frac{\omega}{D_i} \left\{ H_i + \theta \left[{}_iK_{i-1}^{n+\theta} \frac{\Delta_2}{(\Delta_1+\Delta_2)} T_{i-1}^{\ell+1} + {}_iK_{i+1}^{n+\theta} \frac{\Delta_1}{(\Delta_1+\Delta_2)} T_{i+1}^{\ell} \right] \right\} \tag{B.24}$$

4) Inner Boundary of a Void Region

The finite difference form of the time-dependent heat balance on mesh point i of Figure A.4 is

$$(\rho_i C_{pi}) \frac{(T_i^{n+1}-T_i^n)}{\Delta t} \frac{\Delta_1}{2} = g_i^n \frac{\Delta_1}{2} + {}_iK_{i-1} \frac{(T_{i-1}^n - T_i^n)}{\Delta_1} + h_{r_{12}} (T_{i+1}^n - T_i^n) \tag{B.25}$$

Applying the θ-differencing technique described in Section 2.3.1:

$$(\rho_i C_{pi})^{n+\theta} \frac{(T_i^{n+1}-T_i^n)}{\Delta t} (\Delta_1)^2 = g_i^n (\Delta_1)^2 + 2\theta \Big[{}_iK_{i-1}^{n+\theta} (T_{i-1}^{n+1}-T_i^{n+1})$$

$$+ h_{r_{12}}^{n+\theta} \Delta_1 (T_{i+1}^{n+1}-T_i^{n+1}) \Big] + 2(1-\theta) \Big[{}_iK_{i-1}^{n+\theta} (T_{i-1}^n-T_i^n) + h_{r_{12}}^{n+\theta} \Delta_1 (T_{i+1}^n-T_i^n) \Big] \tag{B.26}$$

Rewriting equation (B.26) with the terms evaluated at t_{n+1} on the left-hand side:

$$- 2\theta \Big[{}_iK_{i-1}^{n+\theta} (T_{i-1}^{n+1}-T_i^{n+1}) + h_{r_{12}}^{n+\theta} (T_{i+1}^{n+1}-T_i^{n+1}) \Big] + (\rho_i C_{pi})^{n+\theta} \frac{(\Delta_1)^2}{\Delta t} T_i^{n+1} = H_i \tag{B.27}$$

where

$$H_i = (\rho_i C_{pi})^{n+\theta} \frac{(\Delta_1)^2}{\Delta t} T_i^n + g_i^n (\Delta_1)^2$$

$$+ 2(1-\theta) \Big[{}_iK_{i-1}^{n+\theta} (T_{i-1}^n-T_i^n) + h_{r_{12}}^{n+\theta} \Delta_1 (T_{i+1}^n-T_i^n) \Big] \tag{B.28}$$

Collecting the T_i^{n+1} terms in equation (B.27):

$$- 2\theta \Big[{}_iK_{i-1}^{n+\theta} T_{i-1}^{n+1} + h_{r_{12}}^{n+\theta} \Delta_1 T_{i+1}^{n+1} \Big] + \Big[2\theta ({}_iK_{i-1}^{n+\theta} + h_{r_{12}}^{n+\theta} \Delta_1)$$

$$+ (\rho_i C_{pi})^{n+\theta} \frac{(\Delta_1)^2}{\Delta t} \Big] T_i^{n+1} = H_i \tag{B.29}$$

Let

$$D_i = \left[2\theta \left({}_iK_{i-1}^{n+\theta} + h_{r_{12}}^{n+\theta} \right) + (\rho_i C_{pi})^{n+\theta} \frac{(\Delta_1)^2}{\Delta t} \right] \tag{B.30}$$

Substituting equation (B.30) into equation (B.29) and solving for T_i^{n+1}:

$$T_i^{n+1} = \frac{1}{D_i} \left[H_i + 2\theta \left({}_iK_{i-1}^{n+\theta} \, T_{i-1}^{n+1} + h_{r_{12}}^{n+\theta} \, \Delta_1 \, T_{i+1}^{n+1} \right) \right] \tag{B.31}$$

Since T_{i+1}^{n+1} is unknown, the iterative procedure described in Section 2.3.1 is used. Combining the notation for the iterative procedure and the point successive overrelaxation method:

$$T_i^{\ell+1} = (1-\omega) T_i^{\ell} + \frac{\omega}{D_i} \left[H_i + 2\theta \left({}_iK_{i-1}^{n+\theta} \, T_{i-1}^{\ell+1} + h_{r_{12}}^{n+\theta} \, \Delta_1 \, T_{i+1}^{\ell} \right) \right] \tag{B.32}$$

5) Outer Boundary of a Void Region

The finite difference form of the time-dependent heat balance on mesh point i of Figure A.5 is

$$(\rho_i C_{pi}) \frac{(T_i^{n+1} - T_i^n)}{\Delta t} \frac{\Delta_2}{2} = g_i^n \frac{\Delta_2}{2} + h_{r_{21}} (T_{i-1}^n - T_i^n) + {}_iK_{i+1} \frac{(T_{i+1}^n - T_i^n)}{\Delta 2} \tag{B.33}$$

Applying the θ-differencing technique described in Section 3.2.1:

$$(\rho_i C_{pi})^{n+\theta} \frac{(T_i^{n+1} - T_i^n)(\Delta_2)^2}{\Delta t} = g_i^n (\Delta_2)^2 + 2\theta \left[h_{r_{21}}^{n+\theta} \, \Delta_2 (T_{i-1}^{n+1} - T_i^{n+1}) \right.$$

$$\left. + {}_iK_{i+1}^{n+\theta} \, (T_{i+1}^{n+1} - T_i^{n+1}) \right] + 2(1-\theta) \left[h_{r_{21}}^{n+\theta} \, \Delta_2 (T_{i-1}^n - T_i^n) + {}_iK_{i+1}^{n+\theta} \, (T_{i+1}^n - T_i^n) \right] \tag{B.34}$$

Rewriting equation (B.34) with the terms evaluated at t_{n+1} on the left-hand side:

$$- 2\theta\left[h_{r_{21}}^{n+\theta}\ \Delta_2(T_{i-1}^{n+1}-T_i^{n+1}) + {}_iK_{i+1}^{n+\theta}\ (T_{i+1}^{n+1}-T_i^{n+1})\right] + (\rho_i C_{pi})^{n+\theta}\frac{(\Delta_2)^2}{t}\ T^{n+1} = H_i \tag{B.35}$$

where

$$H_i = (\rho_i C_{pi})^{n+\theta}\ \frac{(\Delta_2)^2}{\Delta t}\ T_i^n + g_i^n\ (\Delta_2)^2 + 2(1-\theta)\left[h_{r_{21}}^{n+\theta}\ \Delta_2(T_{i+1}^n-T_i^n) + {}_iK_{i+1}^{n+\theta}\ (T_{i+1}^n-T_i^n)\right] \tag{B.36}$$

Collecting the t_i^{n+1} terms in equation (B.35):

$$- 2\theta\left[h_{r_{21}}^{n+\theta}\ \Delta_2\ T_{i-1}^{n+1} + {}_iK_{i+1}^{n+\theta}\ T_{i+1}^{n+1}\right] + \left[2\theta\,(h_{r_{21}}^{n+\theta}\ \Delta_2 + {}_iK_{i+1}^{n+\theta}) + (\rho_i C_{pi})^{n+\theta}\ \frac{(\Delta_2)^2}{\Delta t}\right] T_i^{n+1} = H_i \tag{B.37}$$

Let

$$D_i = 2\theta\left[(h_{r_{21}}^{n+\theta}\ \Delta_2 + {}_iK_{i+1}^{n+\theta}) + (\rho_i C_{pi})^{n+\theta}\ \frac{(\Delta_2)^2}{\Delta t}\right] \tag{B.38}$$

Substituting equation (B.38) into equation (B.37) and solving for T_i^{n+1}:

$$T_i^{n+1} = \frac{1}{D_i}\left[H_i + 2\theta\left(h_{r_{21}}^{n+\theta}\,\Delta_2\,T_{i-1}^{n+1} + {}_iK_{i+1}^{n+\theta}\,T_{i+1}^{n+1}\right)\right] \tag{B.39}$$

Since T_{i+1}^{n+1} is unknown, the iterative procedure described in Section 2.3.1 is used. Combining the notation for the iterative procedure and the point successive overrelaxation method:

$$T_i^{\ell+1} = (1-\omega)T_i^{\ell} + \frac{\omega}{D_i}\left[H_i + 2\theta\left(h_{r_{21}}^{n+\theta}\,\Delta_2\,T_{k-1}^{\ell+1} + {}_iK_{i+1}^{n+\theta}\,T_{i+1}^{\ell}\right)\right] \tag{B.40}$$

6) Outermost Boundary

The finite difference form of the time-dependent heat balance on mesh point i of Figure A.6 is

$$(\rho_i C_{pi})\,\frac{(T_i^{n+1}-T_i^n)}{\Delta t}\,\frac{\Delta x}{2} = g_i^n\,\frac{\Delta x}{2} + {}_iK_{i-1}\,\frac{(T_{i-1}^n-T_i^n)}{\Delta x} + h_T(T_\infty-T_i^n) \tag{B.41}$$

Applying the θ-differencing technique described in Section 2.3.1:

$$(\rho_i C_{pi})^{n+\theta}\,\frac{(T_i^{n+1}-T_i^n)}{\Delta t}\,(\Delta x)^2 = g_i^n\,(\Delta x)^2 + 2\theta\Big[{}_iK_{i-1}^{n+\theta}(T_{i-1}^{n+1}-T_i^{n+1})$$

$$+ h_T^{n+\theta}\,\Delta x(T_\infty-T_i^{n+1})\Big] + 2(1-\theta)\Big[{}_iK_{i-1}^{n+\theta}\,(T_{i-1}^n-T_i^n) + h_T^{n+\theta}\Delta x(T_\infty-T_i^n)\Big] \tag{B.42}$$

Rewriting equation (B.42) with the terms evaluated at t_{n+1} on the left-hand side:

$$-\,2\theta\Big[{}_iK_{i-1}^{n+\theta}\,(T_i^{n+1}-T_i^{n+1}) + h_T^{n+\theta}\Delta x(T_\infty-T_i^{n+1})\Big] + (\rho_i C_{pi})^{n+\theta}\frac{(\Delta x)^2}{\Delta t}\,T_i^{n+1} = H_i \tag{B.43}$$

where

$$H_i = (\rho_i C_{pi})^{n+\theta} \frac{(\Delta x)^2}{\Delta t} T_i^n + g_i^n (\Delta x)^2 + 2(1-\theta)\left[{}_iK_{i-1}^{n+\theta} (T_{i-1}^n - T_i^n) + h_T^{n+\theta} \Delta x (T_\infty - T_i^n)\right] \tag{B.44}$$

Collecting the T_i^{n+1} terms in equation (B.43):

$$- 2\theta ({}_iK_{i-1}^{n+\theta} T_{i-1}^{n+1} + h_T^{n+\theta} \Delta x\ T_\infty) + \left[2\theta ({}_iK_{i-1}^{n+\theta} + h_T^{n+\theta} \Delta x) + (\rho_i C_{pi})^{n+\theta} \frac{(\Delta x)^2}{\Delta t}\right] T_i^{n+1} = H_i \tag{B.45}$$

Let

$$D_i = \left[2\theta ({}_iK_{i-1}^{n+\theta} + h_T^{n+\theta} \Delta x) + (\rho_i C_{pi})^{n+\theta} \frac{(\Delta x)^2}{\Delta t}\right] \tag{B.46}$$

Substituting equation (B.46) into equation (B.45) and solving for T_i^{n+1}:

$$T_i^{n+1} = \frac{1}{D_i}\left[H_i + 2\theta ({}_iK_{i-1}^{n+\theta} T_{i-1}^{n+1} + h_T^{n+\theta} \Delta x\ T_\infty)\right] \tag{B.47}$$

Since the iterative procedure described in Section 2.3.1 used for all of the other mesh points it must be used on the outer boundary also. Combining the notation for the iteratire procedure and the point successive overrelaxation method:

$$T_i^{\ell+1} = (1-\omega) T_i^{\ell} + \frac{\omega}{D_i}\left[H_i + 2\theta ({}_iK_{i-1}^{n+\theta} T_{i-1}^{\ell+1} + h_T^{n+\theta} \Delta x\ T_\infty)\right] \tag{B.48}$$

B.2 Cylindrical Coordinates

The one-dimensional, time-dependent, conduction equation in cylindrical coordinates is

$$K(T)\,\frac{\partial^2 T(r,t)}{\partial r^2} + k(T)\,\frac{1}{r}\,\frac{\partial T(r,t)}{\partial r} + g(r,t) = \rho(T)C_p(T)\,\frac{\partial T(r,t)}{\partial t} \qquad \text{(B.49a)}$$

which may be rewritten as

$$K(T)\,\frac{1}{r}\,\frac{\partial}{\partial r}\left(r\,\frac{\partial T(r,t)}{\partial r}\right) + g(r,t) = \rho(T)C_p(T)\,\frac{\partial T(r,t)}{\partial t} \qquad \text{(B.49b)}$$

1) Origin

The finite difference form of the time-dependent heat balance on mesh point i of Figure A.7 is

$$(\rho_i C_{pi})\,\frac{(T_i^{n+1}-T_i^n)}{\Delta t}\,\pi\left(\frac{\Delta r}{2}\right)^2 = g_i^n\,\pi\left(\frac{\Delta r}{2}\right)^2 + 2\pi\,\frac{\Delta r}{2}\;{}_iK_{i+1}\,\frac{(T_{i+1}^n-T_i^n)}{\Delta r}$$

$$(\rho_i C_{pi})\,\frac{(T_i^{n+1}-T_i^n)}{\Delta t}\,\frac{(\Delta r)^2}{2} = g_i^n\,\frac{(\Delta r)^2}{2} + 2\,{}_iK_{i+1}(T_{i+1}^n-T_i^n) \qquad \text{(B.50)}$$

Applying the θ-differencing technique described in Section 2.3.1:

$$(\rho_i C_{pi})^{n+\theta}\,\frac{(T_i^{n+1}-T_i^n)}{\Delta t}\,\frac{(\Delta r)^2}{2} = g_i^n\,\frac{(\Delta r)^2}{2} + 2\theta\left[{}_iK_{i+1}^{n+\theta}(T_{i+1}^{n+1}-T_i^{n+1})\right] + 2(1-\theta)\left[{}_iK_{i+1}^{n+\theta}\,(T_{i+1}^n-T_i^n)\right] \qquad \text{(B.51)}$$

Rewriting equation (B.51) with the terms evaluated at T_{n+1} on the left-hand side:

$$- 2\theta\left[{}_iK_{i+1}^{n+\theta}\ (T_{i+1}^{n+1}-T_i^{n+1})\right] + (\rho_i C_{pi})^{n+\theta}\ \frac{(\Delta r)^2}{2\Delta t}\ T_i^{n+1} = H_i \qquad (B.52)$$

where

$$H_i = (\rho_i C_{pi})^{n+\theta}\ \frac{(\Delta r)^2}{2\Delta t}\ T_i^n + g_i^n\ \frac{(\Delta r)^2}{2} + 2(1-\theta)\left[{}_iK_{i+1}^{n+\theta}\ (T_{i+1}^n-T_i^n)\right] \qquad (B.53)$$

Collecting the T_i^{n+1} terms in equation (B.52)

$$- 2\theta({}_iK_{i+1}^{n+\theta}T_{i+1}^{n+1}) + \left[2\theta\ {}_iK_{i+1}^{n+\theta} + (\rho_i C_{pi})^{n+\theta}\ \frac{(\Delta r)^2}{2\Delta t}\right] T_i^{n+1} = H_i \qquad (B.54)$$

Let

$$D_i = \left[2\theta\ {}_iK_{i+1}^{n+\theta} + (\rho_i C_{pi})^{n+\theta}\ \frac{(\Delta r)^2}{2\Delta t}\right] \qquad (B.55)$$

Substituting equation (B.55) into equation (B.54) and solving for T_i^{n+1}:

$$T_i^{n+1} = \frac{1}{D_i}\left[H_i + 2\theta({}_iK_{i+1}^{n+\theta}\ T_{i+1}^{n+1})\right] \qquad (B.56)$$

Since T_{i+1}^{n+1} is unknown, the iterative procedure described in Section 2.3.1 is used. Combining the notation for the iterative procedure and the point successive overrelaxation method:

$$T_i^{\ell+1} = (1-\omega)T_i^{\ell} + \frac{\omega}{D_i}\left[H_i + 2\theta({}_iK_{i+1}^{n+\theta}\ T_{i+1}^{\ell})\right] \qquad (B.57)$$

2) Mesh Point Within a Material

The finite difference form of the time-dependent heat balance on mesh point i of Figure A.8 is

$$(\rho_i C_{pi}) \frac{(T_i^{n+1}-T_i^n)}{\Delta t} \pi(r_b^2-r_a^2) = g_i^n \pi(r_b^2-r_a^2) + 2\pi r_a \, {}_iK_{i-1} \frac{(T_{i-1}^n-T_i^n)}{\Delta r}$$

$$+ 2\pi r_b \, {}_iK_{i+1} \frac{(T_{i+1}^n-T_i^n)}{\Delta r} \tag{B.58}$$

$$(\rho_i C_{pi}) \frac{(T_i^{n+1}-T_i^n)}{\Delta t} (2r_i\Delta r) = g_i^n (2r_i\Delta r) + 2(r_i - \frac{\Delta r}{2}) \, {}_iK_{i-1} \frac{(T_{i-1}^n-T_i^n)}{\Delta r}$$

$$+ 2(r_i + \frac{\Delta r}{2}) \, {}_iK_{i+1} \frac{(T_{i+1}^n-T_i^n)}{\Delta r} \tag{B.59}$$

Applying the θ-differencing technique described in Section 2.3.1:

$$(\rho_i C_{pi})^{n+\theta} \frac{(T_i^{n+1}-T_i^n)}{\Delta t}(2r_i\Delta r) = g_i^n(2r_i\Delta r) + \theta\left[\frac{(2r_i-\Delta r)}{\Delta r} \, {}_iK_{i-1}^{n+\theta} (T_{i-1}^{n+1}-T_i^{n+1})\right.$$

$$\left. + \frac{(2r_i+\Delta r)}{\Delta r} \, {}_iK_{i+1}^{n+\theta} (T_{i+1}^{n+1}-T_i^{n+1})\right] + (1-\theta)\left[\frac{(2r_i-\Delta r)}{\Delta r} \, {}_iK_{i-1}^{n+\theta} (T_{i-1}^n-T_i^n)\right.$$

$$\left. + \frac{(2r_i+\Delta r)}{\Delta r} \, {}_iK_{i+1}^{n+\theta} (T_{i+1}^n-T_i^n)\right] \tag{B.60}$$

Rewriting equation (B.60) with the terms evaluated at t_{n+1} on the left-hand side:

$$- \theta \left[\frac{(2r_i - \Delta r)}{\Delta r} \; {}_iK_{i-1}^{n+\theta} (T_{i-1}^{n+1} - T_i^{n+1}) + \frac{(2r_i + \Delta r)}{\Delta r} \; {}_iK_{i+1}^{n+\theta} \; (T_{i+1}^{n+1} - T_i^{n+1}) \right]$$

$$+ (\rho_i C_{pi})^{n+\theta} \frac{(2r_i \Delta r)}{\Delta t} T_i^{n+1} = H_i \tag{B.61}$$

where

$$H_i = (\rho_i C_{pi})^{n+\theta} \frac{(2r_i \Delta r)}{\Delta t} T_i^n + g_i^n \; (2r_i \Delta r)$$

$$+ (1-\theta) \left[\frac{(2r_i - \Delta r)}{\Delta r} \; {}_iK_{i-1}^{n+\theta} \; (T_{i-1}^n - T_i^n) + \frac{(2r_i + \Delta r)}{\Delta r} \; {}_iK_{i+1}^{n+\theta} \; (T_{i+1}^n - T_i^n) \right] \tag{B.62}$$

Collecting the T_i^{n+1} terms in equation (B.61):

$$- \theta \left[\frac{(2r_i - \Delta r)}{\Delta r} \; {}_iK_{i-1}^{n+\theta} \; T_{i-1}^{n+1} + \frac{(2r_i + \Delta r)}{\Delta r} \; {}_iK_{i+1}^{n+\theta} \; T_{i+1}^{n+1} \right]$$

$$+ \left\{ \theta \left[\frac{(2r_i - \Delta r)}{\Delta r} \; {}_iK_{i-1}^{n+\theta} + \frac{(2r_i + \Delta r)}{\Delta r} \; {}_iK_{i+1}^{n+\theta} \right] + (\rho_i C_{pi})^{n+\theta} \frac{(2r_i \Delta r)}{\Delta t} \right\} T_i^{n+1} \tag{B.63}$$

Let

$$D_i = \left\{ \theta \left[\frac{(2r_i - \Delta r)}{\Delta r} \; {}_iK_{i-1}^{n+\theta} + \frac{(2r_i + \Delta r)}{\Delta r} \; {}_iK_{i+1}^{n+\theta} \right] + (\rho_i C_{pi})^{n+\theta} \frac{(2r_i \Delta r)}{\Delta t} \right\} \tag{B.64}$$

Substituting equation (B.64) into (B.63) and solving for T_i^{n+1}:

$$T_i^{n+1} = \frac{1}{D_i} \left\{ H_i + \theta \left[\frac{(2r_i - \Delta r)}{\Delta r} \; {}_iK_{i-1}^{n+\theta} \; T_{i-1}^{n+1} + \frac{(2r_i + \Delta r)}{\Delta r} \; {}_iK_{i+1}^{n+\theta} \; T_{i+1}^{n+1} \right] \right\} \tag{B.65}$$

Since T_i^{n+1} is unknown, the iterative procedure described in Section 2.3.1 us used. Combining the notation for the iterative procedure and the point successive overrelaxation method:

$$T_i^{\ell+1} = (1-\omega)T_i^{\ell} + \frac{\omega}{D_i}\left\{H_i + \theta\left[\frac{(2r_i-\Delta r)}{\Delta r}\ {}_iK_{i-1}^{n+\theta}\ T_{i-1}^{\ell+1} + \frac{(2r_i+\Delta r)}{\Delta r}\ {}_iK_{i+1}^{n+\theta}\ T_{i+1}^{\ell}\right]\right\} \tag{B.66}$$

3) Interface of Two Material Regions

The finite difference form of the time-dependent heat balance on mesh point i of Figure A.9 is

$$(\rho_i C_{pi})\ \pi\left[(r_i+\frac{\Delta_2}{2})^2 - (r_i-\frac{\Delta_2}{2})^2\right]\frac{(T_i^{n+1}-T_i^n)}{\Delta t} = g_i^n\ \pi\left[(r_i+\frac{\Delta_2}{2})-(r_i-\frac{\Delta_1}{2})^2\right]$$

$$+\ 2\pi(r_i-\frac{\Delta_1}{2})\ {}_iK_{i-1}\ \frac{(T_{i-1}^n-T_i^n)}{\Delta_1} + 2\pi(r_i+\frac{\Delta_2}{2})\ {}_iK_{i+1}\ \frac{(T_{i+1}^n-T_i^n)}{\Delta_2} \tag{B.77}$$

$$(\rho_i C_{pi})\left[(\Delta_1+\Delta_2)(r_i + \frac{1}{4}(\Delta_2-\Delta_1))\right]\frac{(T_i^{n+1}-T_i^n)}{\Delta t} = g_i^n\left[(\Delta_1+\Delta_2)(r_i + \frac{1}{4}(\Delta_2-\Delta_1))\right]$$

$$+\ (2r_i-\Delta_1)\ {}_iK_{i-1}\ \frac{(T_{i-1}^n-T_i^n)}{\Delta_1} + \frac{(2r_i+\Delta_2)}{\Delta_2}\ {}_iK_{i+1}\ (T_{i+1}^n-T_i^n)$$

Applying the θ-differencing technique described in Section 2.3.1:

$$(\rho_i C_{pi})^{n+\theta}\left[(\Delta_1+\Delta_2)(r_i+\tfrac{1}{4}(\Delta_2-\Delta_1))\right]\frac{(T_i^{n+1}-T_i^n)}{\Delta t} = g_i^n\left[(\Delta_1+\Delta_2)(r_i+\tfrac{1}{4}(\Delta_2-\Delta_1))\right]$$

$$+\left\{\theta\ \frac{(2r_i-\Delta_1)}{\Delta_1}\ {}_iK_{i-1}^{n+\theta}\ (T_{i-1}^{n+1}-T_i^{n+1}) + \frac{(2r_i+\Delta_2)}{\Delta_2}\ {}_iK_{i+1}^{n+\theta}\ (T_{i+1}^{n+1}-T_i^{n+1})\right\}$$

$$+\ (1-\theta)\left\{\frac{(2r_i-\Delta_1)}{\Delta_1}\ {}_iK_{i+1}^{n+\theta}\ (T_{i-1}^{n}-T_i^{n}) + \frac{(2r_i+\Delta_2)}{\Delta_2}\ {}_iK_{i+1}^{n+\theta}\ (T_{i+1}^{n}-T_i^{n})\right. \tag{B.68}$$

Rewriting equation (B.68) with the terms evaluated at t_{n+1} on the left-hand side:

$$-\ \theta\left\{\frac{(2r_i-\Delta_1)}{\Delta_1}\ {}_iK_{i-1}^{n+\theta}\ (T_{i-1}^{n+1}-T_i^{n+1}) + \frac{(2r_i+\Delta_2)}{\Delta_2}\ {}_iK_{i+1}^{n+\theta}\ (T_{i+1}^{n+1}-T_i^{n+1})\right\}$$

$$+\ (\rho_i C_{pi})^{n+\theta}\left[(\Delta_1+\Delta_2)(r_i+\tfrac{1}{4}(\Delta_2-\Delta_1))\right]\frac{T_i^{n+1}}{\Delta t} = H_i \tag{B.69}$$

where

$$H_i = (\rho_i C_{pi})^{n+\theta}\left[(\Delta_1+\Delta_2)(r_i+\tfrac{1}{4}(\Delta_2-\Delta_1))\right]\frac{T_i^n}{\Delta t} + \left[g_i^n\ (\Delta_1+\Delta_2)(r_i+\tfrac{1}{4}(\Delta_2-\Delta_1))\right]$$

$$+\ (1-\theta)\left\{\frac{(2r_i-\Delta_1)}{\Delta_1}\ {}_iK_{i-1}^{n+\theta}(T_{i-1}^{n}-T_i^{n}) + \frac{(2r_i+\Delta_2)}{\Delta_2}\ {}_iK_{i+1}^{n+\theta}\ (T_{i+1}^{n}-T_i^{n})\right\} \tag{B.70}$$

Collecting the T_i^{n+1} terms in equation (B.69):

$$- \theta\left[\frac{(2r_i-\Delta_1)}{\Delta_1} {}_iK_{i-1}^{n+\theta}\, T_{i-1}^{n+1} + \frac{(2r_i+\Delta_2)}{\Delta_2} {}_iK_{i+1}^{n+\theta}\, T_{i+1}^{n+1}\right] + \left\{\theta\left[\frac{(2r_i-\Delta_1)}{\Delta_1} {}_iK_{i-1}^{n+\theta}\right.\right.$$

$$\left.\left. + \frac{(2r_i+\Delta_2)}{\Delta_2} {}_iK_{i+1}^{n+\theta}\right] + (\rho_i C_{pi})^{n+\theta}\left[(\Delta_1+\Delta_2)(r_i+\tfrac{1}{4}(\Delta_2-\Delta_1))\right]\frac{1}{\Delta t}\right\} T_i^{n+1} = H_i \tag{B.71}$$

Let

$$D_i = \left\{\theta\left[\frac{(2r_i-\Delta_1)}{\Delta_1} {}_iK_{i-1}^{n+\theta} + \frac{(2r_i+\Delta_2)}{\Delta_2} {}_iK_{i+1}^{n+\theta}\right]\right.$$

$$\left. + (\rho_i C_{pi})^{n+\theta}\left[(\Delta_1+\Delta_2)(r_i+\tfrac{1}{4}(\Delta_2-\Delta_1))\right]\right\} \tag{B.72}$$

Substituting equation (B.72) into equation (B.71) and solving for T_i^{n+1}:

$$T_i^{n+1} = \frac{1}{D_i}\left\{H_i + \left[\frac{(2r_i-\Delta_1)}{\Delta_1} {}_iK_{i-1}^{n+\theta}\, T_{i-1}^{n+1} + \frac{(2r_i+\Delta_2)}{\Delta_2} {}_iK_{i+1}^{n+\theta}\, T_{i+1}^{n+1}\right]\right\} \tag{B.73}$$

Since T_i^{n+1} is unknown, the iterative procedure described in Section 2.3.1 is used. Combining the notation for the iterative procedure and the point successive overrelaxation method:

$$T_i^{\ell+1} = (1-\omega)T_i^{\ell} + \frac{\omega}{D_i}\left\{H_i + \theta\left[\frac{(2r_i-\Delta_1)}{\Delta_1} {}_iK_{i-1}^{n+\theta}\, T_{i-1}^{\ell+1}\right.\right.$$

$$\left.\left. + \frac{(2r_i+\Delta_2)}{\Delta_2} {}_iK_{i+1}^{n+\theta}\, T_{i+1}^{\ell}\right]\right\} \tag{B.74}$$

4) Inner Boundary of a Void Region

The finite difference form of the time-dependent heat balance on mesh point i of Figure A.10 is:

$$\pi(\rho_i C_{pi})\left[r_i^2-(r_i-\frac{\Delta_1}{2})^2\right]\frac{(T_i^{n+1}-T_i^n)}{\Delta t} = g_i^n\left[r_i^2-(r_i-\frac{\Delta_1}{2})^2\right]$$

$$+ 2\pi(r_i-\frac{\Delta_2}{2})_i K_{i-1}\frac{(T_{i-1}^n-T_i^n)}{\Delta_1} + 2\pi r_i h_{r_{12}}(T_{i+1}^n-T_i^n) \qquad \text{(B.75)}$$

$$(\rho_i C_{pi})\left[\Delta_1(r_i-\frac{\Delta_1}{4})\right]\frac{(T_i^{n+1}-T_i^n)}{\Delta t} = g_i^n\left[\Delta_1(r_i-\frac{\Delta_1}{4})\right]$$

$$+ 2(r_i-\frac{\Delta_1}{2})\ {}_iK_{i-1}\frac{(T_{i-1}^n-T_i^n)}{\Delta_1} + 2\ r_i h_{r_{12}}(T_{i+1}^n-T_i^n)$$

Applying the θ-differencing technique described in Section 2.3.1:

$$(\rho_i C_{pi})^{n+\theta}\left[\Delta_1(r_i-\frac{\Delta_1}{4})\right]\frac{(T_i^{n+1}-T_i^n)}{\Delta t} = g_i^n\left[\Delta_1(r_i-\frac{\Delta_1}{4})\right]$$

$$+ 2\theta\left[\frac{(r_i-\Delta_1/2)}{\Delta_1}\ {}_iK_{i-1}^{n+}(T_{i-1}^{n+1}-T_i^{n+1}) + r_i h_{r_{12}}^{n+}\ (T_{i+1}^{n+1}-T_i^{n+1})\right.$$

$$+ 2(1-\theta)\left[\frac{(r_i-\Delta_1/2)}{\Delta_1}\ {}_iK_{i-1}^{n+\theta}\ (T_{i-1}^n-T_i^n) + r_i\ h_{r_{12}}^{n+\theta}(T_{i+1}^n-T_i^n)\right] \qquad \text{(B.76)}$$

Rewriting equation (B.76) with the terms evaluated at t_{n+1} on the left-hand side:

$$- 2\theta \left[\frac{(r_i-\Delta_1/2)}{\Delta_1} \; {}_iK_{i-1}^{n+\theta}(T_{i-1}^{n+1}-T_i^{n+1}) + r_i h_{r_{12}}^{n+\theta} \; (T_{i+1}^{n+1}-T_i^{n+1})\right]$$

$$+ (\rho_i C_{pi})^{n+\theta} \; \frac{[\Delta_1(r_i-\Delta_1/4)]}{\Delta t} \; T_i^{n+1} \; = \; H_i \qquad \text{(B.77)}$$

where

$$H_i \; = \; (\rho_i C_{pi})^{n+\theta} \frac{[\Delta_1(r_i-\Delta_1/4)]}{\Delta t} \; T_i^n \; + \; g_i^n\left[\Delta_1(r_i-\frac{\Delta_1}{4})\right]$$

$$+ 2(1-\theta) \left[\frac{(r_i-\Delta_1/2)}{\Delta_1} \; {}_iK_{i-1}^{n+\theta} \; (T_{i-1}^n-T_i^n) + r_i h_{r_{12}}^{n+\theta}(T_{i+1}^n-T_i^n)\right] \qquad \text{(B.78)}$$

Collecting the T_i^{n+1} terms in equation (B.77):

$$- 2\theta \left[\frac{(r_i-\Delta_1/2)}{\Delta_1} \; {}_iK_{i-1}^{n+\theta} \; T_{i-1}^{n+1} + r_i h_{r_{12}}^{n+\theta} \; T_{i+1}^{n+1}\right]$$

$$+ \left\{ 2\theta \left[\frac{(r_i-\Delta_1/2)}{\Delta_1} \; {}_iK_{i-1}^{n+\theta} + r_i h_{r_{12}}^{n+\theta}\right] + (\rho_i C_{pi})^{n+\theta} \; \frac{[\Delta_1(r_i-\Delta_1/4)]}{\Delta t}\right\} T_i^{n+1} = H_i$$

(B.79)

Let

$$D_i \; = \; \left\{ 2\theta\left[\frac{(r_i-\Delta_1/2)}{\Delta_1} \; {}_iK_{i-1}^{n+\theta} + r_i h_{r_{12}}^{n+\theta}\right] + (\rho_i C_{pi})^{n+\theta} \; \frac{[\Delta_1(r_i-\Delta_1/4)]}{\Delta t}\right\}$$

(B.80)

Substituting equation (B.80) into equation (B.79) and solving for T_i^{n+1}:

$$T_i^{n+1} = \left\{ \frac{1}{D_i} \quad H_i + 2\theta \left[\frac{(r_i - \Delta_1/2)}{\Delta_1} \; {}_iK_{i-1}^{n+\theta} \; T_{i-1}^{n+1} + r_i h_{r_{12}}^{n+\theta} T_{i+1}^{n+1} \right] \right\} \quad \text{(B.81)}$$

Since T_i^{n+1} is unknown, the iterative procedure described in Section 2.3.1 is used. Combining the notation for the iterative procedure and the point successive overrelaxation method:

$$T_i^{\ell+1} = (1-\omega)\, T_i^{\ell} + \frac{\omega}{D_i} \left\{ H_i + 2\theta \left[\frac{(r_i - \Delta_1/2)}{\Delta_1} \; {}_iK_{i-1}^{n+\theta} \; T_{i-1}^{\ell+1} \right.\right.$$

$$\left.\left. + \; r_i h_{r_{12}}^{n+\theta} \; T_{i+1}^{\ell} \right] \right\} \quad \text{(B.82)}$$

5) Outer Boundary of a Void Region

The finite difference form of the time-dependent heat balance on mesh point i of Figure A.11 is:

$$(\rho_i C_{pi})\pi \left[(r_i + \frac{\Delta_2}{2})^2 - r_i^2 \right] \frac{(T_i^{n+1} - T_i^n)}{\Delta t} = g_i^n \pi \left[(r_i + \frac{\Delta_2}{2})^2 - r_i^2 \right]$$

$$+ \; 2\pi r_i h_{r_{21}} (T_{i-1}^n - T_i^n) + 2\pi (r_i + \frac{\Delta_2}{2}) \; {}_iK_{i+1} \; \frac{(T_{i+1}^n - T_i^n)}{\Delta_2} \quad \text{(B.83)}$$

$$(\rho_i C_{pi}) \left[(r_i + \frac{\Delta_2}{2})^2 - r_i^2 \right] \frac{(T_i^{n+1} - T_i^n)}{\Delta t} = g_i^n \left[\Delta_2 (r_i + \frac{\Delta_2}{4}) \right]$$

$$+ \; 2 r_i h_{r_{21}} (T_{i-1}^n - T_i^n) + 2 (r_i + \frac{\Delta_2}{2}) \; {}_iK_{i+1} \; \frac{(T_{i+1}^n - T_i^n)}{\Delta_2}$$

Applying the θ-differencing technique described in Section 2.3.1:

$$(\rho_i C_{pi})^{n+\theta} \frac{[\Delta_2(r_i+\Delta_2/4)]}{\Delta t} (T_i^{n+1}-T_i^n) = g_i^n\left[\Delta_2(r_i+\frac{\Delta_2}{4})\right]$$

$$+ 2\theta \left[r_i h_{r_{21}}^{n+\theta}(T_{i-1}^{n+1}-T_i^{n+1}) + \frac{(r_i+\Delta_2/2)}{\Delta_2} {}_iK_{i+1}^{n+\theta} (T_{i+1}^{n+1}-T_i^{n+1})\right.$$

$$+ 2(1-\theta) \left[r_i h_{r_{21}}^{n+\theta} (T_{i-1}^n-T_i^n) + \frac{(r_i+\Delta_2/2)}{\Delta_2} {}_iK_{i+1}^{n+\theta} (T_{i+1}^n-T_i^n)\right] \qquad \text{(B84)}$$

Rewriting equation (B.84) with the terms evaluated at T_{n+1} on the left-hand side:

$$-2\theta \left[r_i h_{r_{21}}^{n+\theta} (T_{i-1}^{n+1}-T_i^{n+1}) + \frac{(r_i+\Delta_2/2)}{\Delta_2} {}_iK_{i+1}^{n+\theta} (T_{i+1}^{n+1}-T_i^{n+1})\right]$$

$$+ (\rho_i C_{pi})^{n+\theta} \frac{[\Delta_2(r_i+\Delta_2/4)]}{\Delta t} T_i^{n+1} = H_i \qquad \text{(B.85)}$$

where

$$H_i = (\rho_i C_{pi})^{n+\theta} \frac{[\Delta_2(r_i+\Delta_2/4)]}{\Delta t} T_i^n + g_i^n \left[\Delta_2(r_i+\frac{\Delta_2}{4})\right]$$

$$+ 2(1-\theta) \left[r_i h_{r_{21}}^{n+\theta} (T_{i-1}^n-T_i^n) + \frac{(r_i+\Delta_2/2)}{\Delta_2} {}_iK_{i+1}^{n+\theta} (T_{i+1}^n-T_i^n)\right] \qquad \text{(B.86)}$$

Collecting the T_i^{n+1} terms in Equation (B.85)

$$- 2\theta \left[r_i h_{r_{21}}^{n+\theta} T_{i-1}^{n+1} + \frac{(r_i+\Delta_2/2)}{\Delta_2} {}_iK_{i+1}^{n+\theta} T_{i+1}^{n+1} \right]$$

$$+ \left\{ 2\theta \left[r_i h_{r_{21}}^{n+\theta} + \frac{(r_i+\Delta_2/2)}{\Delta_2} {}_iK_{i+1}^{n+\theta} \right] + (\rho_i C_{pi})^{n+\theta} \frac{[\Delta_2(r_i+\Delta_2/4)]}{\Delta t} \right\} T_i^{n+1}$$

$$= H_i \tag{B.87}$$

Let

$$D_i = \left\{ 2\theta \left[r_i h_{r_{21}}^{n+\theta} + \frac{(r_i+\Delta_2/2)}{\Delta_2} {}_iK_{i+1}^{n+\theta} \right] + (\rho_i C_{pi})^{n+\theta} \frac{[\Delta_2(r_i+\Delta_2/4)]}{\Delta_t} \right\} \tag{B.88}$$

Substituting equation (B.88) into equation (B.87) and solving for T_i^{n+1}

$$T_i^{n+1} = \frac{1}{D_i} \left\{ H_i + 2\theta \left[r_i h_{r_{21}}^{n+\theta} T_{i-1}^{n+1} + \frac{(r_i+\Delta_2/2)}{\Delta_2} {}_iK^{n+\theta} T_{i+1}^{n+1} \right] \right\}$$

Since T_i^{n+1} is unknown, the iterative procedure described in Section 2.3.1 is used. Combing the notation for the iterative procedure and the point successive overrelaxation method:

$$T_i^{\ell+1} = (1-\omega)\, T_i^{\ell} + \frac{\omega}{D_i} \left\{ H_i + 2\theta \left[r_i h_{r_{21}}^{n+\theta} T_{i-1}^{\ell+1} + \frac{(r_i+\Delta_2/2)}{\Delta_2} {}_iK_{i+1}^{n+\theta} T_{i+1}^{\ell} \right] \right\} \tag{B.90}$$

6) Outermost Boundary

The finite difference form of the time-dependent heat balance on mesh point i of Figure A.12 is

$$(\rho_i C_{pi})\pi(R^2-r_a{}^2)\ \frac{(T_i^{n+1}-T_i^n)}{\Delta t} = g_i^n\ \pi(R^2-r_a{}^2) + 2\pi(R-r_a)\,{}_iK_{i-1}\ \frac{(T_{i-1}^n-T_i^n)}{\Delta r}$$

$$+\ 2\pi R\ h_T(T_\infty-T_i^n) \tag{B.91}$$

$$(\rho_i C_{pi})\Delta r(R-\frac{\Delta r}{4})\ \frac{(T_i^{n+1}-T_i^n)}{\Delta t} = g_i^n\ \Delta r(R-\frac{\Delta r}{4})$$

$$+\ 2\ \frac{(R-\Delta r/2)}{\Delta r}\ {}_iK_{i-1}\ (T_{i-1}^n-T_i^n) + 2R\ h_T(T_\infty-T_i^n)$$

Applying the θ-differencing technique described in Section 2.3.1:

$$(\rho_i C_{pi})^{n+\theta}\ \frac{\Delta r(R-\Delta r/4)}{\Delta t}(T_i^{n+1}-T_i^n) = g_i^n\ \Delta r(R-\frac{\Delta r}{4})$$

$$+\ 2\theta\left[\frac{(R-\Delta r/2)}{\Delta r}\ {}_iK_{i-1}^{n+\theta}(T_{i-1}^{n+1}-T_i^{n+1}) + R\ h_T^{n+\theta}(T_\infty-T_i^{n+1})\right]$$

$$= 2(1-\theta)\left[\frac{(R-\Delta r/2)}{\Delta r}\ {}_iK_{i-1}^{n+\theta}\ (T_{i-1}^n-T_i^n) + R\ h_T^{n+\theta}\ (T_\infty-T_i^n)\right] \tag{B.92}$$

Rewriting equation (B.92) with the terms evaluated at t_{n+1} on the left-hand side:

$$- 2\theta\left[\frac{(R-\Delta r/2)}{\Delta r}\ {}_iK_{i-1}^{n+\theta}\ (T_{i-1}^{n+1}-T_i^{n+1}) + R\ h_T^{n+\theta}(T_\infty-T_i^{n+1})\right]$$

$$+ (\rho_i C_{pi})^{n+\theta}\ \frac{\Delta r(R-\Delta r/4)}{\Delta t}\ T_i^{n+1} = H_i \tag{B.93}$$

where

$$H_i = (\rho_i C_{pi})^{n+\theta}\ \frac{\Delta r(R-\Delta r/4)}{\Delta t}\ T_i^n + g_i^n\ \Delta r(R-\frac{\Delta r}{4})$$

$$+ 2(1-\theta)\left[\frac{(R-\Delta r/2)}{\Delta r}\ {}_iK_{i-1}^{n+\theta}\ (T_{i-1}^n-T_i^n) + R\ h_T^{n+\theta}(T_\infty-T_i^n)\right] \tag{B.94}$$

Collecting the T_i^{n+1} terms in equation (B.93):

$$- 2\theta\left[\frac{(R-\Delta r/2)}{\Delta r}\ {}_iK_{i-1}^{n+\theta}\ T_{i-1}^{n+1} + R\ h_T^{n+\theta}T_\infty\right]$$

$$+ \left\{2\theta\left[\frac{(R-\Delta r/2)}{\Delta r}\ {}_iK_{i-1}^{n+\theta} + R\ h_T^{n+\theta}\right] + (\rho_i C_{pi})^{n+\theta}\ \frac{\Delta r(R-\Delta r/4)}{\Delta t}\right\} T_i^{n+1} = H_i \tag{B.95}$$

Let

$$D_i = \left\{2\theta\left[\frac{(R-\Delta r/2)}{\Delta r}\ {}_iK_{i-1}^{n+\theta} + R\ h_T^{n+\theta}\right] + (\rho_i C_{pi})^{n+\theta}\ \frac{\Delta r(R-\Delta r/4)}{\Delta t}\right\} \tag{B.96}$$

Substituting equation (B.96) into equation (B.95) and solving for T_i^{n+1}:

$$T_i^{n+1} = \frac{1}{D_i}\left\{H_i + 2\theta\left[\frac{(R-\Delta r/2)}{\Delta r}\ {}_iK_{i-1}^{n+\theta}\ T_{i-1}^{n+1} + R\ h_T^{n+\theta}T_\infty\right]\right\} \tag{B.97}$$

Since the iterative procedure described in Section 2.3.1 is used for all of the other mesh points, it must be used on the outer boundary also. Combining the notation for the iterative procedure and the point successive overrelaxation method:

$$T_i^{\ell+1} = (1-\omega)\, T_i^{\ell} + \frac{\omega}{D_i}\left[H_i + 2\theta\left[\frac{(R-\Delta r/2)}{\Delta r}\; {}_iK_{i-1}^{n+\theta}\; T_{i-1}^{\ell+1} + R\, h_T^{n+\theta} T_\infty\right]\right] \tag{B.98}$$

A summary of the time-dependent finite difference equations may be found in Section 2.3.4.

APPENDIX C

User's Guide to SHERLOC

SHERLOC is a double-precision FORTRAN computer code which solves one-dimensional, non-linear, non-homogeneous, steady-state or transient heat conduction problems in rectangular or cylindrical coordinates using finite-difference techniques. The code was developed specifically to analyze the "worst case" depressurized heatup accident for modular High Temperature Gas-Cooled Reactors (HTGRs). Because of this specific application, a correlation was incorporated into the code to calculate the temperature- and neutron fluence-dependent thermal conductivity of graphite. The modified Zehner-Schlüner model for determining the effective thermal conductivity in a pebble-bed [7] was also incorporated into SHERLOC to account for radiation through the voids in a pebble-bed as well as conduction through the pebbles.

Characteristics of problems which may be modeled using SHERLOC include the following:

1) transient or steady-state;
2) rectangular or cylindrical coordinates;
3) one-dimensional;
4) adiabatic boundary condition at the origin;
5) convective and/or radiative conditions at the outermost boundary;
6) up to 20 different regions - some of which may be void regions;
7) up to 20 different materials (the total number of materials must be less than or equal to the total number of regions);
8) void regions not containing material;

9) temperature-dependent thermal conductivity, density, and/or specific heat;

10) temperature- and neutron fluence-dependent graphite thermal conductivity;

11) time- and space-dependent internal heat generation;

12) radiation and conduction within a pebble-bed region;

13) up to a total of 200 mesh points; and

14) up to 20 ordered pairs in each tabular function (density, initial temperature, heat generation, thermal conductivity, etc.).

The input to SHERLOC is fairly straightforward. Information must be provided as to the type of problem to be solved, the number of regions and materials, the mesh point spacing, which regions are pebble beds or voids, the thermal properties of the materials, initial temperature and volumetric heat generation distributions, and problem convergence criteria. Data cards are divided into data fields at 12 columns each - no more than six values will appear on any one card, and some cards will contain fewer than six values. The user should note that integer and exponential values must be right justified in their respective data fields. Detailed input instructions for SHERLOC follow.

Card Group (CG) 1 - 1 card, 80 Alphanumeric characters

TITLE - title of problem

CG 2 1 card, 4 values, all integers

1) IGEOM - geometry indicator; 1 = rectangular, 2 = cylindrical

2) NREG - total number of regions (NREG $\leq$ 20)

3) NMAT - total number of materials (NMAT $\leq$ NREG)

4) ITYPE - problem type indicator; 0 = steady-state, 1 = transient

CG 3

NREG values - up to 6 values/card (integers)

MAT - Array containing material number for each region. NOTE: A region may contain only one material, but several regions may contain the same material.

For a void region, MAT < 0 - a void region does not contain material.

CG 4

1 card, 1 value (integer)

MGRPH - Material number which represents graphite (MGRPH = 0 if none of the materials is graphite). Temperature- and fluence-dependent thermal conductivity will be calculated for this material.

CG 5

NREG values - up to 6 values/card (integers)

PEBFLG - Array containing region type indicators.

0 = region is not pebble-bed or void
1 = region is pebble-bed
2 = region is a void (gap)

NOTE: A pebble-bed region must contain graphite

CG 6

1 card for each void region, 2 values/card (reals)

1) emittance of the material in the region to the left of the void region

2) emittance of the material in the region to the right of the void region

NOTE: Do not take shape factors into account; they are calculated by the code

CG 7 — 1 card, 3 values (reals) - may be blank if no regions contain pebble-beds, but a card must be present.

1) DIA - diameter of a pebble (m)

2) F - ϕ - porosity of pebble-bed =

$$\left(1 - \frac{\text{Volume of pebbles}}{\text{Volume of core}}\right)$$

3) EPS - ε - emittance of pebble

CG 8 — 1 card, 3 values (reals) - outermost boundary conditions

1) HC - convective heat transfer coefficient on boundary (W/m^2K)
HC = 0.0 if there is no convection

2) EMM - emissivity of outermost surface

3) TINF - T_∞ - ambient temperature (K)

CG 9 — NREG values, up to 6 values/card (reals)

WM - Array containing width of each region (m)

CG 10 — NREG values, up to 6 values/card (integers)

NM - Array containing number of mesh points in each region, including interface or boundary mesh points. (Count interface mesh points twice).

Example:

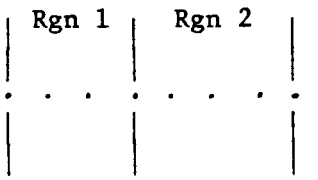

NM(1) = 4 NM(2) = 5

NOTE: A void region may have only 2 mesh points - one on each interface.

For Transient Problems (1T=1): Do not include Card Group 11

For Steady-State Problems (1T=0): Do not include Card Groups 12 through 18

CG 11

1 card, 2 values - steady-state convergence information

1) IMAX - maximum number of iterations allowed on thermal properties (integer)

2) CTD - ε_2 - convergence criterion for average relative temperature difference between iterations (real)

CG 12

1 card, 5 values - transient problem specifications

1) NTIME - total number of time steps (integer)

2) TTOT - problem time until termination of transient (sec) (real)

3) TH - θ - implicit solution type (real) $0.5 \leq \theta \leq 1.0$

$\theta = 0.5$ for Crank-Nicholson method (this method is preferred)

$\theta = 1.0$ for Classical Implicit Procedure

4) W - - relaxation factor (real) $0 < \omega < 2$

5) NEDIT - number of time steps between printing of temperature distribution (integer)

CG 13

1 card, 4 values - transient convergence information

1) ITMAX - maximum number of interations on temperature distribution (inner loop) (integer)

2) CC1 - ε_3 - convergence criterion for normalized heat residual (real)

3) IPMAX - maximum number of iterations on thermal properties (outer loop) (integer)

4) CC2 - ε_4 - convergence criterion for average relative temperature difference between property iterations (real)

CG 14 NMAT values, up to 6 values/card (integers)

IPRR - Array containing number of ordered pairs to be read for density vs. temperature function for each material. (At least 2, and no more than 20 ordered pairs are to be provided for each material.)

CG 15 NMAT sets of cards - density vs. temperature functions

NOTE: Using a temperature-dependent density will not satisfy conservation of mass. Each set must be started on a new card. Within a set, there will be up to 6 values (3 ordered pairs) per card. Each set has the number of ordered pairs indicated by the corresponding value of IPRR in CG 14. An ordered pair consists of (temperature (K), density (kg/m^3)), in that order.

CG 16 NMAT values, up to 6 values/card (integers)

IPRC - Array containing number of ordered pairs to be read for specific heat vs. temperatue function for each material. (At least 2, and no more than 20 ordered pairs are to be provided for each material.)

CG 17 NMAT sets of cards - specific heat vs. temperature functions . Each set must be started on a new card. Within a set, there will be up to 6 values (3 ordered pairs) per card. Each set has the number of ordered pairs indicated by the corresponding value of IPRC in CG 16. An ordered pair consists of (temperature (K), specific heat (J/kg K)), in that order.

CG 18 2 cards, 12 values - 6 values/car (reals)

DCY - Array containing coefficients for the analytic, time-dependent, decay heat function. (This is for the time dependence only, the space dependence will be input later.)

$$g_t(t) = A_1 + A_2 t + A_3 t^2 + A_4 \cos(A_5 t) + A_6 \exp(A_7 t) + A_8 \sin(A_9 t) + A_{10}(t + A_{11})^{A_{12}} \qquad (C.1)$$

The input values represent A. through A_{12} in the above equation.

(end of transient information)

CG 19 NREG values, up to 6 values/card (integers)

IPRG - Array containing number of ordered pairs to be read for each region for volumetric heat generation vs. position function. (At least 2, and no more than 20 ordered pairs are to be provided for each region)

CG 20 NREG sets of cards - volumetric heat generation vs. position functions. Each set must be started on a new card. Within a set, there will be up to 6 values (3 ordered pairs) per card. Each set has the number of ordered pairs indicated by the corresponding value of IPRG in CG 19. An ordered pair consists of (distance from origin (m), volumetric heat generation (W/m^3)), in that order.

CG 21 NREG values, up to 6 values/card (integers)

IPRT - Array containing number of ordered pairs to be read for each region for initial temperature vs. position function. (At lease 2, but no more than 20 ordered pairs are to be provided for each region.)

CG 22 NREG sets of cards - initial temperature vs. position functions. [NOTE: For steady-state problems, this is the initial guess at the temperature distribution, for transient problems, this is the actual initial temperature distribution.] Each set must be started on a new card. Within a set, there will be up to 6 values (3 ordered pairs) per card. Each set has the number of ordered pairs indicated by the corresponding value of IPRT in CG 21. An ordered pair consists of (distance from the origin (m), volumetric heat generation (W/m^3)), in that order.

CG 23 NMAT values, up to 6 values/card (integer)

IPRK - Array containing number of ordered pairs to be read for each material for thermal conductivity vs. temperature function. NOTE: For a material which is graphite, IPRK = 0 - no ordered pairs will be input for that material (graphite conductivity will be calculated). For each of the other materials, at least 2, but no more than 20 ordered pairs are to be provided.

CG 24 NMAT sets of cards if noe of the materials is graphite. (NMAT-1) sets of cards if graphite is one of the materials. Thermal conductivity vs. temperature functions. Each set must be started on a new card. Within a set, there will be up to 6 values (3 ordered pairs) per card. Each set has the number of ordered pairs indicated by the corresponding value of IPRK in CG 23. An ordered pair consists of (temperature (K), thermal conductivity (W/mK)), in that order.

NOTE: If no graphite is present, Card Groups 25 and 26 are omitted.

CG 25	NREG values, up to 6 values/card (integers) NFLPT - Array containing number of ordered pairs to be read for each region for neutron fluence vs. position function. (At least 2, but no more than 20 ordered pairs are to be provided for each region).
CG 26	NREG sets of cards - neutron fluence vs. position functions. Each set must be started on a new card. Within a set, there will be up to 6 values (3 ordered pairs) per card. Each set has the number of ordered pairs indicated by the corresponding value of NFLPT in CG 25. An ordered pair consists of (distance from origin (m), fluence (n/cm^2)), in that order. NOTE: The units on fluence are n/cm^2 due to the thermal conductivity correlation being used.

A sample problem to be modeled is shown in Figure C.1. While the sample problem is quite simple, it illustrates most of the qualities which might be found in a more complex problem. The sample problem consists of four regions, one of which is a pebble-bed and one of which is a void. Since the pebble-bed core and the reflector regions have different densities (the density of the carbon in the pebbles must be smeared over the volume of the entire region), they must be treated as different materials. The temperature- and fluence-dependent graphite conductivity will be calculated for the pebble-bed, and the modified Zehner-Schlünder model will be used to determine the effective pebble-bed conductivity. A temperature-dependent thermal conductivity function will be input for the reflector region. For illustrative purposes, a combined convective and radiative boundary condition will be used on the outermost surface. Figure C.2 shows the input for the sample case

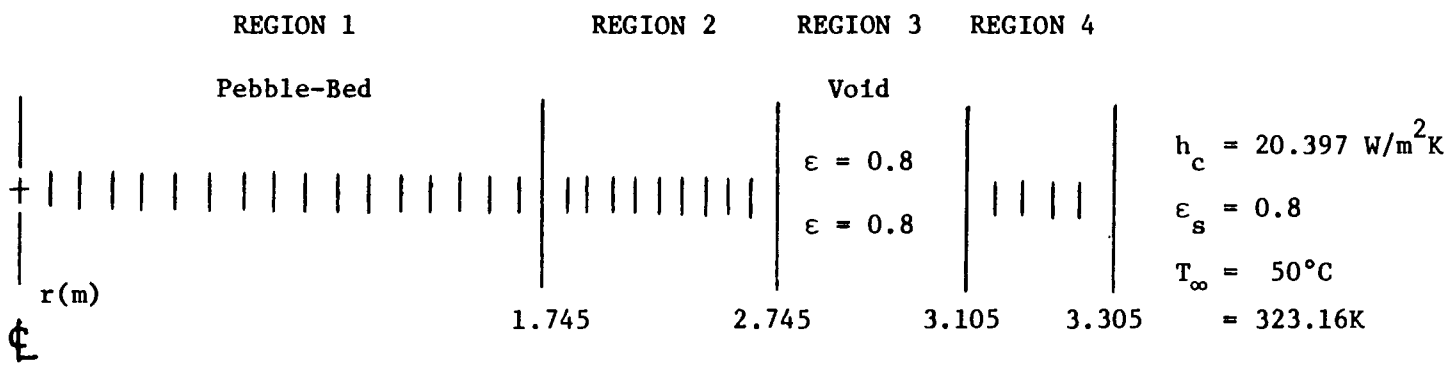

Figure C.1 Model for Sample Problem

```
 1.     SAMPLE PROBLEM - STEADY-STATE
 2.              2           4           3           0
 3.              1           2          -1           3
 4.              1
 5.              1           0           2           0
 6.            0.8         0.8
 7.           0.06        0.39         0.8
 8.        20.3970         0.8     323.160
 9.         1.7450        1.00        0.36        0.20
10.             18          11           2           6
11.             30      1.0D-06
12.              6           2           2           2
13.            0.0      6.17D3    0.780388      6.17D3     1.03635     5.590D3
14.       .351671      5.24D3    1.560775      5.03D3      1.7450     5.510D3
15.          1.745         0.0       2.745         0.0
16.          2.745         0.0       3.105         0.0
17.          3.105         0.0      3.3050         0.0
18.              6           2           2           2
19.            0.0     1378.16    0.780388     1378.16     1.03635     1282.16
20.       1.351671     1207.16    1.560775     1165.16      1.7450     1167.16
21.         1.7450     1073.16       2.745     1073.16
22.          2.745      873.16       3.105      873.16
23.          3.105      773.16       3.305      773.16
24.              0          16          12
25.          300.0      110.00       400.0      100.00       500.0        90.0
26.          600.0       84.00       700.0        78.0       800.0        72.0
27.          900.0        67.0      1000.0        62.0      1100.0        58.0
28.         1200.0        54.0      1300.0        50.0      1400.0      48.667
29.         1500.0       47.33      1600.0        46.0      1700.0      44.667
30.         1800.0       43.33
31.         323.16        36.6       400.0        37.2       450.0        37.3
32.          500.0        37.1       600.0        36.3       700.0       35.00
33.          800.0        33.4       900.0        31.6      1000.0        29.5
34.         1100.0        27.4      1200.0        25.2      1300.0        22.8
35.              6           2           2           2
36.            0.0     2.07D21    0.780388     2.07D21     1.03635     1.88D21
37.       1.351671     1.72D21    1.560775     1.55D21      1.7450     1.22D21
38.         1.7450         0.0       2.745         0.0
39.          2.745         0.0       3.105         0.0
40.          3.105         0.0       3.305         0.0
```

Figure C.2 Input for SHERLOC Sample Problem - Steady-State

as a steady-state problem, and Figure C.3 shows the output for the steady-state solution. The input for the sample case as a transient problem is shown in Figure C.5. For illustrative purposes, the transient problem is run for a short length of time.

```
SAMPLE PROBLEM - STEADY-STATE

 CASE DESCRIPTION

   PROBLEM TYPE: STEADY STATE
   GEOMETRY: CYLINDRICAL
   NUMBER OF REGIONS:  4
   NUMBER OF MATERIALS:  3
   MATERIAL # 1 IS GRAPHITE - GRAPHITE CONDUCTIVITY  WILL BE USED
   REGION # 1 IS A PEBBLE BED - GRAPHITE AND     PEBBLE BED CALCULATIONS WILL BE PERFORMED
   REGION # 3 IS A VOID REGION - RADIATION ONLY   IN THIS REGION

   REGION  MATERIAL   WIDTH (M)   NO.MESH PTS (INCL   BOUNDS)
      1       1       0.1745D 01        18
      2       2       0.1000D 01        11
      3      -1       0.3600D 00         2
      4       3       0.2000D 00         6
   MAX. ITERATIONS ON PROPERTIES: 30
   CONV. CRITERIA FOR AVG. REL. TEMP. DIFF.:  1.00000D-06
```

Figure C.3 Output of SHERLOC Sample Problem - Steady-State

INITIAL TEMPERATURE DISTRIBUTION

REGION	MATERIAL #	MESH POINT (I)	DIST. FROM ORIGIN (M)	TEMP. (DEG C)	INITIAL HEAT GEN. (W/M**3)
1	1	1	0.0	1.1050001D 03	6.1700000D 03
1	1	2	1.0264706D-01	1.1050001D 03	6.1700000D 03
1	1	3	2.0529412D-01	1.1050001D 03	6.1700000D 03
1	1	4	3.0794118D-01	1.1050001D 03	6.1700000D 03
1	1	5	4.1058824D-01	1.1050001D 03	6.1700000D 03
1	1	6	5.1323529D-01	1.1050001D 03	6.1700000D 03
1	1	7	6.1588235D-01	1.1050001D 03	6.1700000D 03
1	1	8	7.1852941D-01	1.1050001D 03	6.1700000D 03
1	1	9	8.2117647D-01	1.0897021D 03	6.0775749D 03
1	1	10	9.2382353D-01	1.0512038D 03	5.8449806D 03
1	1	11	1.0264706D 00	1.0127054D 03	5.6123864D 03
1	1	12	1.1291176D 00	9.8693504D 02	5.4870298D 03
1	1	13	1.2317647D 00	9.6252014D 02	5.3730936D 03
1	1	14	1.3344118D 00	9.3810525D 02	5.2591574D 03
1	1	15	1.4370588D 00	9.1684935D 02	5.1542463D 03
1	1	16	1.5397059D 00	8.9623197D 02	5.0511594D 03
1	1	17	1.6423529D 00	8.9288572D 02	5.2425521D 03
1	1	18	1.7450000D 00	8.4761402D 02	2.7176040D 03
2	2	19	1.8450000D 00	8.0000009D 02	0.0
2	2	20	1.9450000D 00	8.0000009D 02	0.0
2	2	21	2.0450000D 00	8.0000009D 02	0.0
2	2	22	2.1450000D 00	8.0000009D 02	0.0
2	2	23	2.2450000D 00	8.0000009D 02	0.0
2	2	24	2.3450000D 00	8.0000009D 02	0.0
2	2	25	2.4450000D 00	8.0000009D 02	0.0
2	2	26	2.5450000D 00	8.0000009D 02	0.0
2	2	27	2.6450000D 00	8.0000009D 02	0.0
2	2	28	2.7450000D 00	6.4347835D 02	0.0
3	-1	29	3.1050000D 00	5.9000009D 02	0.0
4	3	30	3.1450000D 00	5.0000009D 02	0.0
4	3	31	3.1850000D 00	5.0000009D 02	0.0
4	3	32	3.2250000D 00	5.0000009D 02	0.0
4	3	33	3.2650000D 00	5.0000009D 02	0.0
4	3	34	3.3050000D 00	5.0000009D 02	0.0

Figure C.3 (Continued)

FLUENCE DISTRIBUTION

MESH POINT	FLUENCE (N/CM**2)
1	2.07000D 21
2	2.07000D 21
3	2.07000D 21
4	2.07000D 21
5	2.07000D 21
6	2.07000D 21
7	2.07000D 21
8	2.07000D 21
9	2.03972D 21
10	1.96353D 21
11	1.88733D 21
12	1.83293D 21
13	1.78084D 21
14	1.72876D 21
15	1.65058D 21
16	1.56713D 21
17	1.40387D 21
18	6.17968D 20
19	0.0
20	0.0
21	0.0
22	0.0
23	0.0
24	0.0
25	0.0
26	0.0
27	0.0
28	0.0
29	0.0
30	0.0
31	0.0
32	0.0
33	0.0
34	0.0

Figure C.3 (Continued)

ITERATION	MAX. HT RES.	NODE	TEMP(DEG C)	AVG. REL. TEMP. DIFF.
1	1.600711D-10	33	9.923536D 01	1.112118D 00
2	3.380624D-09	3	2.271559D 03	4.917005D-01
3	3.819878D-10	28	2.431485D 02	1.125013D 00
4	1.745363D-09	4	1.632000D 03	3.138297D-01
5	5.931042D-10	5	6.571536D 02	4.237835D-01
6	1.495241D-09	3	1.138740D 03	1.478662D-01
7	1.464304D-09	2	8.155820D 02	1.169740D-01
8	2.095476D-09	26	3.152282D 02	5.192042D-02
9	9.495302D-10	2	8.850575D 02	3.064907D-02
10	1.164153D-09	31	1.451360D 02	1.489942D-02
11	1.587086D-09	2	9.072263D 02	7.849154D-03
12	6.984919D-10	31	1.451360D 02	3.910970D-03
13	4.309910D-10	34	1.367468D 02	1.989358D-03
14	1.780808D-09	2	9.163764D 02	9.969987D-04
15	6.984919D-10	30	1.480020D 02	5.022086D-04
16	5.566285D-10	2	9.155927D 02	2.520012D-04
17	5.457146D-10	2	9.151957D 02	1.266106D-04
18	1.493408D-09	2	9.153950D 02	6.354930D-05
19	1.731696D-09	2	9.152950D 02	3.190774D-05
20	1.227836D-09	2	9.153452D 02	1.601634D-05
21	1.936332D-09	2	9.153200D 02	8.038792D-06
22	4.656613D-10	25	3.170627D 02	4.033896D-06
23	4.656613D-10	26	3.130668D 02	2.023855D-06
24	3.501555D-10	34	1.367468D 02	1.014932D-06

Figure C.3 (Continued)

```
OUTERMOST BOUNDARY HEAT TRANSFER COEFFICIENT:

   EMISSIVITY:  0.800000D 00
   RADIATION HTC (W/M**2 K):    9.058079D 00
   CONVECTION HTC (W/M**2 K):   2.039700D 01
   TOTAL HTC  (W/M**2 K):       2.945508D 01
```

Figure C.3 (Continued)

TEMPERATURE DISTRIBUTION

REGION	MATERIAL #	MESH POINT (I)	DIST. FROM ORIGIN (M)	TEMP. (DEG C)
1	1	1	0.0	9.1642733D 02
1	1	2	1.0264706D-01	9.1532708D 02
1	1	3	2.0529412D-01	9.1201613D 02
1	1	4	3.0794118D-01	9.0645110D 02
1	1	5	4.1058824D-01	8.9856171D 02
1	1	6	5.1323529D-01	8.8824213D 02
1	1	7	6.1588235D-01	8.7538454D 02
1	1	8	7.1852941D-01	8.5966705D 02
1	1	9	8.2117647D-01	8.4092470D 02
1	1	10	9.2382353D-01	8.1877112D 02
1	1	11	1.0264706D 00	7.9205754D 02
1	1	12	1.1291176D 00	7.6252779D 02
1	1	13	1.2317647D 00	7.2690473D 02
1	1	14	1.3344118D 00	6.8462063D 02
1	1	15	1.4370588D 00	6.3347717D 02
1	1	16	1.5397059D 00	5.6967366D 02
1	1	17	1.6423529D 00	4.8468235D 02
1	1	18	1.7450000D 00	3.5114117D 02
2	2	19	1.8450000D 00	3.4545331D 02
2	2	20	1.9450000D 00	3.4008712D 02
2	2	21	2.0450000D 00	3.3500907D 02
2	2	22	2.1450000D 00	3.3019057D 02
2	2	23	2.2450000D 00	3.2560705D 02
2	2	24	2.3450000D 00	3.2123723D 02
2	2	25	2.4450000D 00	3.1706257D 02
2	2	26	2.5450000D 00	3.1306683D 02
2	2	27	2.6450000D 00	3.0923569D 02
2	2	28	2.7450000D 00	3.0555647D 02
3	-1	29	3.1050000D 00	1.5090416D 02
4	3	30	3.1450000D 00	1.4800198D 02
4	3	31	3.1850000D 00	1.4513604D 02
4	3	32	3.2250000D 00	1.4230543D 02
4	3	33	3.2650000D 00	1.3950929D 02
4	3	34	3.3050000D 00	1.3674679D 02

IEC002I STOP 0

Figure C.3 (Continued)

```
 1.     SAMPLE PROBLEM - TRANSIENT
 2.              2          4          3          1
 3.              1          2         -1          3
 4.              1
 5.              1          0          2          0
 6.            0.8        0.8
 7.           0.06       0.39        0.8
 8.        20.3970        0.8    323.160
 9.         1.7450       1.00       0.36       0.20
10.             18         11          2          6
11.            180    10800.0        1.0        1.0         60
12.             50     1.0D-5         50     1.0D-5
13.              2          2          2
14.            0.0      860.1      1.0D4      860.1
15.            0.0     1394.8      1.0D4     1394.8
16.            0.0     7675.0      1.0D4     7675.0
17.              9          9         10
18.          300.0     725.75      400.0     994.42      600.0     1406.1
19.          800.0     1675.4     1000.0     1793.4     1200.0     1891.1
20.         1400.0     1978.4     1700.0     2058.6     2300.0     2156.3
21.          300.0     725.75      400.0     994.42      600.0     1406.1
22.          800.0     1675.4     1000.0     1793.4     1200.0     1891.1
23.         1400.0     1978.4     1700.0     2058.6     2300.0     2156.3
24.         323.16      459.0     400.00      489.4     473.16      532.0
25.         573.16      558.9     673.16      604.2     773.16      663.5
26.         823.16      704.1     873.16      756.6     923.16      825.9
27.         973.16      918.6
28.
29.                                           0.128  -3.796D-4     -0.261
30.              6          2          2          2
31.            0.0     3.24D6   0.780388     3.24D6    1.03635    2.930D6
32.       1.351671     2.75D6   1.560775     2.64D6     1.7450    2.890D6
33.          1.745        0.0      2.745        0.0
34.          2.745        0.0      3.105        0.0
35.          3.105        0.0     3.3050        0.0
36.              6          2          2          2
37.            0.0    1378.16   0.780388    1378.16    1.03635    1282.16
38.       1.351671    1207.16   1.560775    1165.16     1.7450    1167.16
39.          1.7450    1073.16      2.745    1073.16
40.          2.745     873.16      3.105     873.16
41.          3.105     773.16      3.305     773.16
42.              0         16         12
43.          300.0     110.00      400.0     100.00      500.0       90.0
44.          600.0      84.00      700.0      78.0       800.0       72.0
45.          900.0       67.0     1000.0      62.0      1100.0       58.0
46.         1200.0       54.0     1300.0      50.0      1400.0     48.667
47.         1500.0      47.33     1600.0      46.0      1700.0     44.667
48.         1800.0      43.33
49.         323.16       36.6      400.0      37.2       450.0     37.300
50.          500.0       37.1      600.0      36.3       700.0      35.00
51.          800.0       33.4      900.0      31.6      1000.0       29.5
52.         1100.0       27.4     1200.0      25.2      1300.0       22.8
53.              6          2          2          2
54.            0.0   2.07D21   0.780388   2.07D21    1.03635    1.88D21
55.       1.351671   1.72D21   1.560775   1.55D21     1.7450    1.22D21
56.          1.7450        0.0      2.745        0.0
57.          2.745        0.0      3.105        0.0
58.          3.105        0.0      3.305        0.0
```

Figure C.4 Input for SHERLOC Sample Problem - Transient

```
SAMPLE PROBLEM - TRANSIENT

 CASE DESCRIPTION

   PROBLEM TYPE: TRANSIENT
   GEOMETRY: CYLINDRICAL
   NUMBER OF REGIONS:  4
   NUMBER OF MATERIALS:  3
   MATERIAL # 1 IS GRAPHITE - GRAPHITE CONDUCTIVITY  WILL BE USED
   REGION # 1 IS A PEBBLE BED - GRAPHITE AND     PEBBLE BED CALCULATIONS WILL BE PERFORMED
   REGION # 3 IS A VOID REGION - RADIATION ONLY   IN THIS REGION

   REGION  MATERIAL   WIDTH (M)   NO.MESH PTS (INCL   BOUNDS)
      1       1       0.1745D 01       18
      2       2       0.1000D 01       11
      3      -1       0.3600D 00        2
      4       3       0.2000D 00        6

   NORMALIZED HEAT RESIDUAL CONVERGENCE CRIT. (INNER LOOP):                    1.00000D-05
   MAX. ITERATIONS ON INNER (LINEAR)  LOOP:                                    50
   CONVERGENCE CRIT. ON PROPERTIES:                                            1.00000D-05
   MAX. ITERATIONS ON PROPERTIES:                                              50
   FINAL TIME:                                                                 1.08000D 04 SECONDS
   TIME STEP (DELTA T):                                                        6.00000D 01 SECONDS
   NO. OF TIME STEPS BETWEEN TEMPERATURE DISTRIBUTION     PRINTOUTS:           60
   THETA (0.5 FOR C-N; 1.0 FOR CIP):                                           1.00000D 00
   SOR ACCELERATION PARAMETER (OMEGA):                                         1.00000D 00

   ANALYTIC DECAY HEAT FUNCTION COEFFICIENTS:
 Y(X)=A(1) + A(2)*X + A(3)*X**2 + A(4)*DCOS(A(5)X)       + A(6)*DEXP(A(7)X)  + A(8)*DSIN(A(9)X)  + A(10)*((X+A(11))**A(12))
   A( 1) =  0.0
   A( 2) =  0.0
   A( 3) =  0.0
   A( 4) =  0.0
   A( 5) =  0.0
   A( 6) =  0.0
   A( 7) =  0.0
   A( 8) =  0.0
   A( 9) =  0.0
   A(10) =  1.2800D-01
   A(11) = -3.7960D-04
   A(12) = -2.6100D-01
```

Figure C.5 Output of SHERLOC Sample Problem - Transient

INITIAL TEMPERATURE DISTRIBUTION

REGION	MATERIAL #	MESH POINT (I)	DIST. FROM ORIGIN (M)	TEMP. (DEG C)	INITIAL HEAT GEN. (W/M**3)
1	1	1	0.0	1.1050001D 03	3.2400000D 06
1	1	2	1.0264706D-01	1.1050001D 03	3.2400000D 06
1	1	3	2.0529412D-01	1.1050001D 03	3.2400000D 06
1	1	4	3.0794118D-01	1.1050001D 03	3.2400000D 06
1	1	5	4.1058824D-01	1.1050001D 03	3.2400000D 06
1	1	6	5.1323529D-01	1.1050001D 03	3.2400000D 06
1	1	7	6.1588235D-01	1.1050001D 03	3.2400000D 06
1	1	8	7.1852941D-01	1.1050001D 03	3.2400000D 06
1	1	9	8.2117647D-01	1.0897021D 03	3.1906004D 06
1	1	10	9.2382353D-01	1.0512038D 03	3.0662828D 06
1	1	11	1.0264706D 00	1.0127054D 03	2.9419651D 06
1	1	12	1.1291176D 00	9.8693504D 02	2.8770439D 06
1	1	13	1.2317647D 00	9.6252014D 02	2.8184481D 06
1	1	14	1.3344118D 00	9.3810525D 02	2.7598524D 06
1	1	15	1.4370588D 00	9.1684935D 02	2.7050814D 06
1	1	16	1.5397059D 00	8.9623197D 02	2.6510835D 06
1	1	17	1.6423529D 00	8.9288572D 02	2.7507042D 06
1	1	18	1.7450000D 00	8.4761402D 02	1.4255082D 06
2	2	19	1.8450000D 00	8.0000009D 02	0.0
2	2	20	1.9450000D 00	8.0000009D 02	0.0
2	2	21	2.0450000D 00	8.0000009D 02	0.0
2	2	22	2.1450000D 00	8.0000009D 02	0.0
2	2	23	2.2450000D 00	8.0000009D 02	0.0
2	2	24	2.3450000D 00	8.0000009D 02	0.0
2	2	25	2.4450000D 00	8.0000009D 02	0.0
2	2	26	2.5450000D 00	8.0000009D 02	0.0
2	2	27	2.6450000D 00	8.0000009D 02	0.0
2	2	28	2.7450000D 00	6.4347835D 02	0.0
3	-1	29	3.1050000D 00	5.9000009D 02	0.0
4	3	30	3.1450000D 00	5.0000009D 02	0.0
4	3	31	3.1850000D 00	5.0000009D 02	0.0
4	3	32	3.2250000D 00	5.0000009D 02	0.0
4	3	33	3.2650000D 00	5.0000009D 02	0.0
4	3	34	3.3050000D 00	5.0000009D 02	0.0

Figure C.5 (Continued)

FLUENCE DISTRIBUTION

MESH POINT	FLUENCE (N/CM**2)
1	2.07000D 21
2	2.07000D 21
3	2.07000D 21
4	2.07000D 21
5	2.07000D 21
6	2.07000D 21
7	2.07000D 21
8	2.07000D 21
9	2.03972D 21
10	1.96353D 21
11	1.88733D 21
12	1.83293D 21
13	1.78084D 21
14	1.72876D 21
15	1.65058D 21
16	1.56713D 21
17	1.40387D 21
18	6.17968D 20
19	0.0
20	0.0
21	0.0
22	0.0
23	0.0
24	0.0
25	0.0
26	0.0
27	0.0
28	0.0
29	0.0
30	0.0
31	0.0
32	0.0
33	0.0
34	0.0

Figure C.5 (Continued)

TIME(SEC)	INNER ITER COUNT	MAX. NORM. RESID.	NODE	TEMP (DEG C)	PROP. ITER COUNT	NORM OF NODE TEMP DIFF
3600.000	1	2.934093D-04	1	1.238637D 03		
3600.000	2	3.647088D-05	29	5.378152D 02		
3600.000	3	6.938504D-06	29	5.377956D 02		
3600.000					1	6.293434D-04
3600.000	1	2.937519D-04	1	1.238636D 03		
3600.000	2	3.658972D-05	29	5.378054D 02		
3600.000	3	6.957647D-06	29	5.377857D 02		
3600.000					2	1.397509D-06

Figure C.5 (Continued)

INTERNAL HEAT GENERATION DISTRIBUTION - TIME = 3600.000 SECONDS

MESH POINT	HEAT GEN. (W/M**3)
1	4.8928290145D 04
2	4.8528290145D 04
3	4.8528290145D 04
4	4.8928290145D 04
5	4.8528290145D 04
6	4.8928290145D 04
7	4.8528290145D 04
8	4.8928290145D 04
9	4.8182290451D 04
10	4.6304929685D 04
11	4.4427568918D 04
12	4.3447172147D 04
13	4.2562298730D 04
14	4.1677425312D 04
15	4.0850310870D 04
16	4.0034871110D 04
17	4.1539276011D 04
18	2.1527061304D 04
19	0.0
20	0.0
21	0.0
22	0.0
23	0.0
24	0.0
25	0.0
26	0.0
27	0.0
28	0.0
29	0.0
30	0.0
31	0.0
32	0.0
33	0.0
34	0.0

Figure C.5 (Continued)

OUTERMOST BOUNDARY HEAT TRANSFER COEFFICIENT:

EMMISIVITY: 0.800000D 00
RADIATION HTC (W/M**2 K): 2.860527D 01
CONVECTION HTC (W/M**2 K): 2.039700D 01
TOTAL HTC (W/M**2 K): 4.900227D 01

PROPERTY DISTRIBUTIONS - TIME = 3600.000SECONDS

MESH POINT	CONDUCTIVITY (W/M K)	DENSITY (KG/M**3)	SP. HEAT (J/KG K)
1	2.39228D 01	8.60100D 02	2.00839D 03
2	2.39015D 01	8.60100D 02	2.00830D 03
3	2.38520D 01	8.60100D 02	2.00799D 03
4	2.37612D 01	8.60100D 02	2.00738D 03
5	2.36100D 01	8.60100D 02	2.00632D 03
6	2.33762D 01	8.60100D 02	2.00460D 03
7	2.30381D 01	8.60100D 02	2.00201D 03
8	2.25563D 01	8.60100D 02	1.99837D 03
9	2.18987D 01	8.60100D 02	1.99358D 03
10	2.11208D 01	8.60100D 02	1.98772D 03
11	2.01366D 01	8.60100D 02	1.98113D 03
12	1.91692D 01	8.60100D 02	1.97141D 03
13	1.81969D 01	8.60100D 02	1.95949D 03
14	1.72066D 01	8.60100D 02	1.94690D 03
15	1.62744D 01	8.60100D 02	1.93201D 03
16	1.51720D 01	8.60100D 02	1.91571D 03
17	1.38344D 01	8.60100D 02	1.89314D 03
18	5.71157D 01	1.12784D 03	1.85750D 03
19	5.77875D 01	1.39480D 03	1.84860D 03
20	5.83665D 01	1.39480D 03	1.84109D 03
21	5.88951D 01	1.39480D 03	1.83446D 03
22	5.94166D 01	1.39480D 03	1.82818D 03
23	5.99727D 01	1.39480D 03	1.82172D 03
24	6.05987D 01	1.39480D 03	1.81460D 03
25	6.13191D 01	1.39480D 03	1.80643D 03
26	6.21818D 01	1.39480D 03	1.79700D 03
27	6.33416D 01	1.39480D 03	1.78476D 03
28	0.0	1.39480D 03	1.77037D 03
29	3.33647D 01	7.67500D 03	6.94190D 02
30	3.36662D 01	7.67500D 03	6.79580D 02
31	3.39815D 01	7.67500D 03	6.63984D 02
32	3.43109D 01	7.67500D 03	6.51877D 02
33	3.46516D 01	7.67500D 03	6.39433D 02
34	0.0	7.67500D 03	6.26625D 02

Figure C.5 (Continued)

TEMPERATURE DISTRIBUTION AT TIME = 3600.000 SECONDS
NUMBER OF PROPERTY ITERATIONS = 2

REGION	MATERIAL #	MESH POINT (I)	DIST. FROM ORIGIN (M)	TEMP. (DEG C)
1	1	1	0.0	1.2390111D 03
1	1	2	1.0264706D-01	1.2386760D 03
1	1	3	2.0529412D-01	1.2375409D 03
1	1	4	3.0794118D-01	1.2352607D 03
1	1	5	4.1058824D-01	1.2312696D 03
1	1	6	5.1323529D-01	1.2248289D 03
1	1	7	6.1588235D-01	1.2151421D 03
1	1	8	7.1852941D-01	1.2015314D 03
1	1	9	8.2117647D-01	1.1836092D 03
1	1	10	9.2382353D-01	1.1617042D 03
1	1	11	1.0264706D 00	1.1370519D 03
1	1	12	1.1291176D 00	1.1108151D 03
1	1	13	1.2317647D 00	1.0835209D 03
1	1	14	1.3344118D 00	1.0546859D 03
1	1	15	1.4370588D 00	1.0224026D 03
1	1	16	1.5397059D 00	9.8321229D 02
1	1	17	1.6423529D 00	9.3150806D 02
1	1	18	1.7450000D 00	8.5805435D 02
2	2	19	1.8450000D 00	8.3984137D 02
2	2	20	1.9450000D 00	8.2446267D 02
2	2	21	2.0450000D 00	8.1089054D 02
2	2	22	2.1450000D 00	7.9803615D 02
2	2	23	2.2450000D 00	7.8481193D 02
2	2	24	2.3450000D 00	7.7023018D 02
2	2	25	2.4450000D 00	7.5351677D 02
2	2	26	2.5450000D 00	7.3420606D 02
2	2	27	2.6450000D 00	7.1220369D 02
2	2	28	2.7450000D 00	6.8782584D 02
3	-1	29	3.1050000D 00	5.3778572D 02
4	3	30	3.1450000D 00	5.1980144D 02
4	3	31	3.1850000D 00	5.0059571D 02
4	3	32	3.2250000D 00	4.8039972D 02
4	3	33	3.2650000D 00	4.5941635D 02
4	3	34	3.3050000D 00	4.3782080D 02

Figure C.5 (Continued)

TIME(SEC)	INNER ITER COUNT	MAX. NORM. RESID.	NODE	TEMP (DEG C)	PROP. ITER COUNT	NORM OF NODE TEMP DIFF
7200.000	1	2.094016D-04	1	1.317506D 03		
7200.000	2	3.784520D-05	29	5.135391D 02		
7200.000	3	7.607993D-06	29	5.135197D 02		
7200.000					1	4.809629D-04
7200.000	1	2.094996D-04	1	1.317505D 03		
7200.000	2	3.794744D-05	29	5.135322D 02		
7200.000	3	7.625410D-06	29	5.135127D 02		
7200.000					2	1.044476D-06

Figure C.5 (Continued)

INTERNAL HEAT GENERATION DISTRIBUTION - TIME = 7200.000 SECONDS

MESH POINT	HEAT GEN. (W/M**3)
1	4.0831111675D 04
2	4.0831111675D 04
3	4.0831111675D 04
4	4.0831111675D 04
5	4.0831111675D 04
6	4.0831111675D 04
7	4.0831111675D 04
8	4.0831111675D 04
9	4.0208568016D 04
10	3.8641893053D 04
11	3.7075218091D 04
12	3.6257067898D 04
13	3.5518632829D 04
14	3.4780197759D 04
15	3.4089963090D 04
16	3.3409471051D 04
17	3.4664910887D 04
18	1.7964532207D 04
19	0.0
20	0.0
21	0.0
22	0.0
23	0.0
24	0.0
25	0.0
26	0.0
27	0.0
28	0.0
29	0.0
30	0.0
31	0.0
32	0.0
33	0.0
34	0.0

Figure C.5 (Continued)

OUTERMOST BOUNDARY HEAT TRANSFER COEFFICIENT:

EMMISIVITY: 0.800000D 00
RADIATION HTC (W/M**2 K): 2.713844D 01
CONVECTION HTC (W/M**2 K): 2.039700D 01
TOTAL HTC (W/M**2 K): 4.753544D 01

PROPERTY DISTRIBUTIONS - TIME = 7200.000SECONDS

MESH POINT	CONDUCTIVITY (W/M K)	DENSITY (KG/M**3)	SP. HEAT (J/KG K)
1	2.61855D 01	8.60100D 02	2.02945D 03
2	2.61358D 01	8.60100D 02	2.02922D 03
3	2.60334D 01	8.60100D 02	2.02852D 03
4	2.58730D 01	8.60100D 02	2.02731D 03
5	2.56480D 01	8.60100D 02	2.02553D 03
6	2.53506D 01	8.60100D 02	2.02312D 03
7	2.49728D 01	8.60100D 02	2.02000D 03
8	2.44809D 01	8.60100D 02	2.01611D 03
9	2.38350D 01	8.60100D 02	2.01137D 03
10	2.30726D 01	8.60100D 02	2.00578D 03
11	2.20575D 01	8.60100D 02	1.99940D 03
12	2.10059D 01	8.60100D 02	1.99222D 03
13	1.98727D 01	8.60100D 02	1.98409D 03
14	1.86429D 01	8.60100D 02	1.97240D 03
15	1.73792D 01	8.60100D 02	1.95423D 03
16	1.59489D 01	8.60100D 02	1.93201D 03
17	1.43020D 01	8.60100D 02	1.90383D 03
18	5.67352D 01	1.12784D 03	1.86318D 03
19	5.75957D 01	1.39480D 03	1.85221D 03
20	5.83955D 01	1.39480D 03	1.84216D 03
21	5.91611D 01	1.39480D 03	1.83268D 03
22	5.99160D 01	1.39480D 03	1.82346D 03
23	6.06800D 01	1.39480D 03	1.81424D 03
24	6.14680D 01	1.39480D 03	1.80480D 03
25	6.23618D 01	1.39480D 03	1.79499D 03
26	6.34343D 01	1.39480D 03	1.78294D 03
27	6.45505D 01	1.39480D 03	1.77001D 03
28	0.0	1.39480D 03	1.75660D 03
29	3.37445D 01	7.67500D 03	6.74478D 02
30	3.40160D 01	7.67500D 03	6.61777D 02
31	3.43037D 01	7.67500D 03	6.51395D 02
32	3.46053D 01	7.67500D 03	6.40452D 02
33	3.49186D 01	7.67500D 03	6.29036D 02
34	0.0	7.67500D 03	6.17231D 02

Figure C.5 (Continued)

TEMPERATURE DISTRIBUTION AT TIME = 7200.000 SECONDS
NUMBER OF PROPERTY ITERATIONS = 2

REGION	MATERIAL #	MESH POINT (I)	DIST. FROM ORIGIN (M)	TEMP. (DEG C)
1	1	1	0.0	1.3177834D 03
1	1	2	1.0264706D-01	1.3169325D 03
1	1	3	2.0529412D-01	1.3143133D 03
1	1	4	3.0794118D-01	1.3097858D 03
1	1	5	4.1058824D-01	1.3031380D 03
1	1	6	5.1323529D-01	1.2941158D 03
1	1	7	6.1588235D-01	1.2824530D 03
1	1	8	7.1852941D-01	1.2678937D 03
1	1	9	8.2117647D-01	1.2501763D 03
1	1	10	9.2382353D-01	1.2292463D 03
1	1	11	1.0264706D 00	1.2053884D 03
1	1	12	1.1291176D 00	1.1785313D 03
1	1	13	1.2317647D 00	1.1481399D 03
1	1	14	1.3344118D 00	1.1130844D 03
1	1	15	1.4370588D 00	1.0714692D 03
1	1	16	1.5397059D 00	1.0205620D 03
1	1	17	1.6423529D 00	9.5601364D 02
1	1	18	1.7450000D 00	8.6968478D 02
2	2	19	1.8450000D 00	8.4723755D 02
2	2	20	1.9450000D 00	8.2665736D 02
2	2	21	2.0450000D 00	8.0724749D 02
2	2	22	2.1450000D 00	7.8837704D 02
2	2	23	2.2450000D 00	7.6950075D 02
2	2	24	2.3450000D 00	7.5018024D 02
2	2	25	2.4450000D 00	7.3010110D 02
2	2	26	2.5450000D 00	7.0910544D 02
2	2	27	2.6450000D 00	6.8720243D 02
2	2	28	2.7450000D 00	6.6446812D 02
3	-1	29	3.1050000D 00	5.1351271D 02
4	3	30	3.1450000D 00	4.9709257D 02
4	3	31	3.1850000D 00	4.7958666D 02
4	3	32	3.2250000D 00	4.6113394D 02
4	3	33	3.2650000D 00	4.4188319D 02
4	3	34	3.3050000D 00	4.2197964D 02

Figure C.5 (Continued)

TIME(SEC)	INNER ITER COUNT	MAX. NORM. RESID.	NODE	TEMP (DEG C)	PROP. ITER COUNT	NORM OF NODE TEMP DIFF
10800.000	1	1.682574D-04	1	1.376397D 03		
10800.000	2	3.460337D-05	29	4.931326D 02		
10800.000	3	7.188196D-06	29	4.931154D 02		
10800.000					1	3.367723D-04
10800.000	1	1.682885D-04	1	1.376397D 03		
10800.000	2	3.468379D-05	29	4.931272D 02		
10800.000	3	7.201782D-06	29	4.931100D 02		
10800.000					2	8.169973D-07

Figure C.5 (Continued)

INTERNAL HEAT GENERATION DISTRIBUTION - TIME = 10800.000 SECONDS

MESH POINT	HEAT GEN. (W/M**3)
1	3.6730884258D 04
2	3.6730884258D 04
3	3.6730884258D 04
4	3.6730884258D 04
5	3.6730884258D 04
6	3.6730884258D 04
7	3.6730884258D 04
8	3.6730884258D 04
9	3.6170855932D 04
10	3.4761505210D 04
11	3.3352154488D 04
12	3.2616162280D 04
13	3.1951880267D 04
14	3.1287598254D 04
15	3.0666676395D 04
16	3.0054518820D 04
17	3.1183888396D 04
18	1.6160548321D 04
19	0.0
20	0.0
21	0.0
22	0.0
23	0.0
24	0.0
25	0.0
26	0.0
27	0.0
28	0.0
29	0.0
30	0.0
31	0.0
32	0.0
33	0.0
34	0.0

Figure C.5 (Continued)

OUTERMOST BOUNDARY HEAT TRANSFER COEFFICIENT:

EMMISIVITY: 0.800000D 00
RADIATION HTC (W/M**2 K): 2.581495D 01
CONVECTION HTC (W/M**2 K): 2.039700D 01
TOTAL HTC (W/M**2 K): 4.621195D 01

PROPERTY DISTRIBUTIONS - TIME = 10800.000SECONDS

MESH POINT	CONDUCTIVITY (W/M K)	DENSITY (KG/M**3)	SP. HEAT (J/KG K)
1	2.78598D 01	8.60100D 02	2.04518D 03
2	2.78011D 01	8.60100D 02	2.04490D 03
3	2.76822D 01	8.60100D 02	2.04407D 03
4	2.75004D 01	8.60100D 02	2.04266D 03
5	2.72517D 01	8.60100D 02	2.04064D 03
6	2.69311D 01	8.60100D 02	2.03798D 03
7	2.65316D 01	8.60100D 02	2.03463D 03
8	2.60170D 01	8.60100D 02	2.03050D 03
9	2.53409D 01	8.60100D 02	2.02553D 03
10	2.45344D 01	8.60100D 02	2.01964D 03
11	2.34380D 01	8.60100D 02	2.01282D 03
12	2.22768D 01	8.60100D 02	2.00494D 03
13	2.09988D 01	8.60100D 02	1.99579D 03
14	1.95888D 01	8.60100D 02	1.98502D 03
15	1.81203D 01	8.60100D 02	1.96812D 03
16	1.64259D 01	8.60100D 02	1.94240D 03
17	1.45381D 01	8.60100D 02	1.91011D 03
18	5.66427D 01	1.12784D 03	1.86505D 03
19	5.76289D 01	1.39480D 03	1.85260D 03
20	5.85586D 01	1.39480D 03	1.84096D 03
21	5.94507D 01	1.39480D 03	1.82989D 03
22	6.03209D 01	1.39480D 03	1.81917D 03
23	6.11817D 01	1.39480D 03	1.80864D 03
24	6.20532D 01	1.39480D 03	1.79815D 03
25	6.31354D 01	1.39480D 03	1.78641D 03
26	6.42263D 01	1.39480D 03	1.77360D 03
27	6.53270D 01	1.39480D 03	1.76066D 03
28	0.0	1.39480D 03	1.74762D 03
29	3.40652D 01	7.67500D 03	6.59417D 02
30	3.43231D 01	7.67500D 03	6.50110D 02
31	3.45937D 01	7.67500D 03	6.40301D 02
32	3.48756D 01	7.67500D 03	6.30045D 02
33	3.51358D 01	7.67500D 03	6.19406D 02
34	0.0	7.67500D 03	6.08437D 02

Figure C.5 (Continued)

TEMPERATURE DISTRIBUTION AT TIME = 10800.000 SECONDS
NUMBER OF PROPERTY ITERATIONS = 2

REGION	MATERIAL #	MESH POINT (I)	DIST. FROM ORIGIN (B)	TEMP. (DEG C)
1	1	1	0.0	1.3766265D 03
1	1	2	1.0264706D-01	1.3756011D 03
1	1	3	2.0529412D-01	1.3724848D 03
1	1	4	3.0794118D-01	1.3672123D 03
1	1	5	4.1058824D-01	1.3596746D 03
1	1	6	5.1323529D-01	1.3497216D 03
1	1	7	6.1588235D-01	1.3371595D 03
1	1	8	7.1852941D-01	1.3217440D 03
1	1	9	8.2117647D-01	1.3031435D 03
1	1	10	9.2382353D-01	1.2811051D 03
1	1	11	1.0264706D 00	1.2555829D 03
1	1	12	1.1291176D 00	1.2261230D 03
1	1	13	1.2317647D 00	1.1919051D 03
1	1	14	1.3344118D 00	1.1516086D 03
1	1	15	1.4370588D 00	1.1032939D 03
1	1	16	1.5397059D 00	1.0443553D 03
1	1	17	1.6423529D 00	9.7039839D 02
1	1	18	1.7450000D 00	8.7351701D 02
2	2	19	1.8450000D 00	8.4802943D 02
2	2	20	1.9450000D 00	8.2420739D 02
2	2	21	2.0450000D 00	8.0154177D 02
2	2	22	2.1450000D 00	7.7960159D 02
2	2	23	2.2450000D 00	7.5803349D 02
2	2	24	2.3450000D 00	7.3656197D 02
2	2	25	2.4450000D 00	7.1499191D 02
2	2	26	2.5450000D 00	6.9327361D 02
2	2	27	2.6450000D 00	6.7135712D 02
2	2	28	2.7450000D 00	6.4924825D 02
3	-1	29	3.1050000D 00	4.9311002D 02
4	3	30	3.1450000D 00	4.7741863D 02
4	3	31	3.1850000D 00	4.6087872D 02
4	3	32	3.2250000D 00	4.4358438D 02
4	3	33	3.2650000D 00	4.2564326D 02
4	3	34	3.3050000D 00	4.0714895D 02

IBC002I STOP 0

Figure C.5 (Continued)

APPENDIX D

Listing of SHERLOC

```
C ******************************************************************
C ******************************************************************
C **                                                              **
C **     SHERLOC - A COMPUTER CODE TO DETERMINE SMALL HTGR        **
C **               THERMAL RESPONSE TO LOSS OF CIRCULATION        **
C **                                                              **
C **     WRITTEN BY: M A GIBBS              APRIL, 1983           **
C **                 THE PENNSYLVANIA STATE UNIVERSITY            **
C **                                                              **
C **     FUNDED BY: U.S. DEPARTMENT OF ENERGY NUCLEAR SCIENCE     **
C **               AND ENGINEERING AND HEALTH PHYSICS             **
C **               FELLOWSHIP                                     **
C **                                                              **
C ******************************************************************
C
C THIS CODE SOLVES ONE-DIMENSIONAL, NON-LINEAR CONDUCTION HEAT TRANSFER
C PROBLEMS USING FINITE DIFFERENCES.
C ALTHOUGH DEVELOPED SPECIFICALLY TO ANALYZE MODULAR HTGRS UNDER
C LOCA/LOFA CONDITIONS, IT MAY OF COURSE BE USED FOR OTHER APPROPRIATELY
C MODELED PROBLEMS.
C
C THE FOLLOWING CHARACTERISTICS OUTLINE THE SCOPE AND FLEXIBILITY OF
C THE CODE.
C     - TRANSIENT OR STEADY-STATE HEAT TRANSFER
C     - CYLINDRICAL OR RECTANGULAR COORDINATES (1-D)
C     - ADIABATIC BOUNDARY CONDITION AT THE ORIGIN
C     - CONVECTIVE AND/OR RADIATIVE BOUNDARY CONDITIONS
C     - AN INITIAL TEMPERATURE DISTRIBUTION MUST BE PROVIDED FOR
C       TRANSIENT PROBLEMS; AN INITIAL GUESS AT THE TEMPERATURE
C       DISTRIBUTION MUST BE PROVIDED FOR S-S PROBLEMS.
C     - UP TO 20 DIFFERENT REGIONS MAY BE SPECIFIED
C     - UP TO 20 DIFFERENT MATERIALS MAY BE SPECIFIED
C       THE TOTAL NUMBER OF MATERIALS MUST BE .LE. THE TOTAL NUMBER
C       OF REGIONS.  A REGION MAY CONTAIN ONLY ONE MATERIAL, BUT
C       SEVERAL REGIONS MAY CONTAIN THE SAME MATERIAL.
C     - IF A MATERIAL IS GRAPHITE, THE TEMPERATURE AND NEUTRON FLUENCE
C       DEPENDENT THERMAL CONDUCTIVITY WILL BE CALCULATED.
C     - IF A REGION IS A PEBBLE BED, AN EFFECTIVE CONDUCTIVITY WILL
C       BE CALCULATED TO TAKE RADIATION THROUGH THE BED INTO ACCOUNT
C       AS WELL AS CONDUCTION.
C       NOTE: THE MATERIAL IN A PEBBLE BED MUST BE SPECIFIED AS
C             GRAPHITE!
C     - VOID REGIONS MAY BE SPECIFIED (VOIDS MAY NOT CONTAIN A MATERIAL)
C     - THE THERMAL CONDUCTIVITIES, DENSITIES, AND SPECIFIC HEATS
C       OF MATERIALS MAY BE SPECIFIED IN TABULAR FORM AS FUNCTIONS
C       OF TEMPERATURE
C     - INTERNAL HEAT GENERATION MAY BE SPECIFIED IN TABULAR FORM AS
C       A FUNCTION OF TIME
C
C FOR STEADY-STATE PROBLEMS, A DIRECT SOLUTION TECHNIQUE IS USED.
C THE ROUTINES DGBFA AND DGBSL ARE USED TO SOLVE A SYSTEM OF
C SIMULTANEOUS EQUATIONS IN MATRIX FORM.
C
C TRANSIENT PROBLEMS ARE SOLVED USING AN IMPLICIT TECHNIQUE.  THE
C TRANSIENT FINITE DIFFERENCE EQUATIONS ARE SOLVED AT TIME STEP
C N+THETA, WHERE THETA IS INPUT BY THE USER.  IF THETA=0.5, THE
C TECHNIQUE BECOMES THE CRANK-NICHOLSON TECHNIQUE; IF THETA=1.0,
C THE TECHNIQUE BECOMES THE CLASSICAL IMPLICIT PROCEDURE.  THE
C SOLUTION IS STABLE FOR ALL TIME STEPS IF 0.5 .LE. THETA .LE. 1.0.
C THE OVERRELAXATION PARAMETER OMEGA IS INPUT BY THE USER:
C 0.0 .LE. OMEGA .LE. 1.0.
```

```
C
C ***********************************************************
C ***************************************************************
C
C DIMENSION ARRAYS - DECLARE VARIABLES
C
      REAL*8 A(200,200)/40000*0.0/,TEMPI(20,20,2),G(20,20,2),HC,HR,HT,
     * COND(20,2,20)/800*0.0/,TINF,EMM,P(200)/200*0.0/,TP,P1(200),
     * T(200)/200*0.0/,K(200)/200*0.0/,E(200)/200*0.0/,
     * DELI(20),NN(20),X(20),ABD(4,200),B(200),SIGMA,DEL,DIST,
     * CTD,MAX,THP,DIA,F,EPS,FLPN(20,20,2),FL(200),RTD,
     *       TL(200),TLP(200),TMEMP(200),TT(200),S1,S2,
     * B1,B2,B3,R(200),CP(200),RPN(20,2,20),CPPN(20,2,20),D(200),H(200),
     * TH,CC1,CC2,CONT(200),CONP,SGM/0.0/,TTOT,N,DT,GEN(200),DCY(12),
     * ANALPN,TIN,DUMMY,DUMMY2,A1(200),A2(200),A3,A4,HR12(20),HR21(20),
     * E1(20)/20*0.0/,E2(20)/20*0.0/,E12,E21,TTL(200),TIR(200)
      INTEGER NMAT,NM(20),IPRK(20),NL/1/,NU/1/,M,N,IPVT(200),INFO,
     * I1,I2,K1,MODE,NREG,RGN,MAT(20),MGRPH,PEBFLG(20)/20*0/,NFLPT(20),
     *       NTIME,NTI,NPI,ITMAX,IPMAX,IPRR(20),IPRC(20),IT/0/,NEDIT/1/
     * ,IEDIT,IPRG(20),IPRT(20)
      COMMON / TCDT / TDAT(13),DELTA(13),ATA(13),CN(13)
      COMMON /TKIN /CON(13)
      DIMENSION  TITLE(80)
C
C READ GENERAL PROBLEM INFORMATION
C
      READ (5,10) TITLE
10    FORMAT (80A1)
      WRITE (6,15) TITLE
15    FORMAT ('1',80A1)
      READ (5,35) IGEOM,NREG,NMAT,IT
      READ (5,35) (MAT(RGN),RGN=1,NREG)
      READ (5,35) MGRPH
      READ (5,35) (PEBFLG(I),I=1,NREG)
      DO 23 I=1,NREG
         IF (PEBFLG(I) .EQ. 2) READ(5,30) E1(I),E2(I)
         IF ((PEBFLG(I) .EQ. 1) .AND. (MAT(I) .NE. MGRPH)) GO TO 25
23    CONTINUE
      GO TO 28
25    WRITE (6,27)
27    FORMAT ('0INPUT ERROR - PEBBLE BED REGION MUST BE GRAPHITE!')
      GO TO 800
28    READ (5,30) DIA,F,EPS
30    FORMAT (6F12.7)
      READ (5,30) HC,EMM,TINF
      READ (5,30) (NN(I),I=1,NREG)
      READ (5,35) (NM(I),I=1,NREG)
35    FORMAT (6I12)
C
C WRITE GENERAL CASE DESRIPTION
C
45    WRITE (6,50)
50    FORMAT ('0 CASE DESCRIPTION')
      IF (IT .EQ. 0) WRITE (6,55)
      IF (IT .NE. 0) WRITE (6,60)
55    FORMAT ('0',T5,'PROBLEM TYPE: STEADY STATE')
60    FORMAT ('0',T5,'PROBLEM TYPE: TRANSIENT')
      IF (IGEOM .EQ. 1) WRITE (6,65)
      IF (IGEOM .EQ. 2) WRITE (6,70)
65    FORMAT (T5,'GEOMETRY: RECTANGULAR')
70    FORMAT (T5,'GEOMETRY: CYLINDRICAL')
```

```
      WRITE (6,75) NREG
75    FORMAT (T5,'NUMBER OF REGIONS: ',I2)
      WRITE (6,80) NMAT
80    FORMAT (T5,'NUMBER OF MATERIALS: ',I2)
      IF (NGRPH .NE. 0) WRITE (6,85) NGRPH
85    FORMAT (T5,'MATERIAL # ',I2,' IS GRAPHITE - GRAPHITE CONDUCTIVITY
     * WILL BE USED')
      DO 100 I=1,NREG
         IF (PEBFLG(I) .EQ. 1) WRITE (6,90) I
         IF (PEBFLG(I) .EQ. 2) WRITE (6,95) I
90       FORMAT (T5,'REGION # ',I2,' IS A PEBBLE BED - GRAPHITE AND
     *PEBBLE BED CALCULATIONS WILL BE PERFORMED')
95       FORMAT (T5,'REGION # ',I2,' IS A VOID REGION - RADIATION ONLY
     * IN THIS REGION')
100   CONTINUE
      WRITE (6,105)
105   FORMAT('0',T5,'REGION  MATERIAL   WIDTH (M)   NO.MESH PTS (INCL
     *BOUNDS)')
      DO 110 I=1,NREG
         WRITE (6,115) I,MAT(I),WM(I),NM(I)
110   CONTINUE
115   FORMAT (T7,I2,T15,I2,T24,D10.4,T40,I3)
      IF (IT .NE. 0) GO TO 140
C
C INPUT AND OUTPUT OF STEADY STATE PARAMETERS
C
      READ (5,119) IMAX,CTD
119   FORMAT (I12,F12.7)
120   FORMAT (2(I12,F12.7))
      WRITE (6,125) IMAX
125   FORMAT (T5,'MAX. ITERATIONS ON PROPERTIES: ',I2)
      WRITE (6,135) CTD
135   FORMAT (T5,'CONV. CRITERIA FOR AVG. REL. TEMP. DIFF.: ',1PD12.5)
      GO TO 220
C
C INPUT OF TRANSIENT PARAMETERS
C
140   READ (5,145) NTIME,TTOT,TH,N,NEDIT
145   FORMAT (I12,3F12.7,I12)
      READ (5,120) ITMAX,CC1,IPMAX,CC2
C
C  READ DENSITY TABLE
C
      READ (5,35) (IPRR(I),I=1,NMAT)
      DO 150 I=1,NMAT
         M1=IPRR(I)
         READ (5,30) ((RFN(I,L,M),L=1,2),M=1,M1)
150   CONTINUE
C
C  READ SPECIFIC HEAT TABLE
C
      READ (5,35) (IPRC(I),I=1,NMAT)
      DO 155 I=1,NMAT
         M1=IPRC(I)
         READ (5,30) ((CPFN(I,L,M),L=1,2),M=1,M1)
155   CONTINUE
C
C  READ DECAY HEAT FUNCTION (FUNCTION OF TIME)
C
      CALL READFN(DCY)
C
```

```
C WRITE TRANSIENT PROBLEM INFORMATION
C
      WRITE (6,160) CC1
      WRITE (6,165) ITMAX
160   FORMAT ('0',T5,'NORMALIZED HEAT RESIDUAL CONVERGENCE CRIT. (INNER
     *LOOP): ',T80,1PD12.5)
165   FORMAT (T5,'MAX. ITERATIONS ON INNER (LINEAR)  LOOP: ',T80,I3)
      WRITE (6,170) CC2
      WRITE (6,175) IPMAX
170   FORMAT (T5,'CONVERGENCE CRIT. ON PROPERTIES: ',T80,1PD12.5)
175   FORMAT (T5,'MAX. ITERATIONS ON PROPERTIES: ',T80,I3)
      WRITE (6,180) TTOT
      DT=TTOT/(DFLOAT(NTIME))
      WRITE (6,185) DT
180   FORMAT (T5,'FINAL TIME: ',T80,1PD12.5,' SECONDS')
185   FORMAT (T5,'TIME STEP (DELTA T): ',T80,1PD12.5,' SECONDS')
      WRITE (6,190) NEDIT
190   FORMAT (T5,'NO. OF TIME STEPS BETWEEN TEMPERATURE DISTRIBUTION
     * PRINTOUTS:',T80,I3)
      WRITE (6,195) TH
      WRITE (6,200) W
195   FORMAT (T5,'THETA (0.5 FOR C-N; 1.0 FOR CIP): ',T80,1PD12.5)
200   FORMAT (T5,'SOR ACCELERATION PARAMETER (OMEGA): ',T80,1PD12.5)
      WRITE (6,205)
205   FORMAT ('0',T5,'ANALYTIC DECAY HEAT FUNCTION COEFFICIENTS: ')
      WRITE (6,210)
210   FORMAT ('  Y(X)=A(1) + A(2)*X + A(3)*X**2 + A(4)*DCOS(A(5)X)
     * + A(6)*DEXP(A(7)X) + A(8)*DSIN(A(9)X) + A(10)*((X+A(11))**A(12))'
     * )
      WRITE (6,215) (I,DCY(I),I=1,12)
215   FORMAT (T5,'A(',I2,') = ',1PD11.4)
C
C END OF TRANSIENT PARAMETERS
C
C READ INTERNAL HEAT GENERATION FUNCTION - IPRG PAIRS FOR EACH REGION
220   READ (5,35) (IPRG(I),I=1,NREG)
      DO 225 I=1,NREG
         M1=IPRG(I)
         READ (5,30) ((G(I,L,M),M=1,2),L=1,M1)
225   CONTINUE
C
C READ INITIAL TEMPERATURE DISTRIBUTION ESTIMATE - IPRT PAIRS FOR
C EACH REGION
      READ (5,35) (IPRT(I),I=1,NREG)
      DO 230 I=1,NREG
         M1=IPRT(I)
         READ (5,30) ((TEMPI(I,L,M),M=1,2),L=1,M1)
230   CONTINUE
C
C READ THERMAL CONDUCTIVITY FUNCTION - IPRK PAIRS FOR EACH MAT'L
C
      READ (5,35) (IPRK(I),I=1,NMAT)
      DO 235 I=1,NMAT
      IF (I .EQ. MGRPH) GO TO 235
      M1=IPRK(I)
      READ (5,30) ((COND(I,L,M),L=1,2),M=1,M1)
235   CONTINUE
      IF (MGRPH .EQ. 0) GO TO 240
C
C READ FLUENCE DISTRIBUTION
C
```

```
            READ (5,35) (NFLPT(I),I=1,NREG)
            DO 237 I=1,NREG
               N1=NFLPT(I)
               READ (5,30) ((FLPN(I,L,M),M=1,2),L=1,N1)
237         CONTINUE
C
C PRELIMINARY INITIALIZATIONS AND CALCULATIONS
C
240      N=0
         SIGMA=5.669E-08
         DO 245 I=1,NREG
            N=N+NN(I)
            DELI(I)=WN(I)/(DFLOAT(NN(I)-1))
245      CONTINUE
         N=N-(NREG-1)
         NL=N-1
         NP=N+1
         X(1)=WN(1)
         IF (NREG .EQ. 1) GO TO 250
         DO 250 I=2,NREG
               X(I)=X(I-1)+WN(I)
250      CONTINUE
         ICOUNT=1
C
C CALCULATE INTERNAL HEAT GENERATION AND INITIAL TEMPERATURE
C ESTIMATE AT EACH MESH POINT I.
C
         CALL INTERPG (G,IPRG,P,N,DELI,X,NREG,PEBFLG,IGEOM)
         CALL INTERP (TEMPI,IPRT,T,N,DELI,X,NREG)
         IF (NGRPH .NE. 0) CALL INTERP (FLPN,NFLPT,FL,N,DELI,X,NREG)
         WRITE (6,255)
C
C PRINT INITIAL DISTRIBUTIONS (TEMP, FLUENCE, PROPS, ETC.)
C
255      FORMAT ('1     INITIAL TEMPERATURE DISTRIBUTION')
         WRITE (6,256)
256      FORMAT ('0REGION  MATERIAL #   MESH POINT (I)    DIST. FROM ORIGIN
        *(M)    TEMP. (DEG C)',T83,'INITIAL HEAT GEN. (W/M**3)')
         DIST=0.0
         RGN=1
         DO 260 I=1,N
            TP=T(I)-273.16000
            WRITE (6,445) RGN,MAT(RGN),I,DIST,TP,P(I)
            IF (DABS(X(NREG)-DIST) .LE. 1.0D-6) GO TO 260
            IF (DABS(X(RGN)-DIST) .LE. 1.0D-6) WRITE (6,450)
            IF (DABS(X(RGN)-DIST) .LE. 1.0D-6) RGN=RGN+1
            DIST=DIST+DELI(RGN)
260      CONTINUE
         IF (NGRPH .EQ. 0) GO TO 280
         WRITE (6,265)
265      FORMAT ('1 FLUENCE DISTRIBUTION')
         WRITE (6,270)
270      FORMAT (' MESH POINT',T15,'FLUENCE (N/CM**2)')
         WRITE (6,275) (I,FL(I),I=1,N)
275      FORMAT (T6,I3,T15,1PD12.5)
C
C CHECK FOR TRANSIENT OR STEADY STATE PROBLEM
C
280      IF (IT .NE. 0) GO TO 475
C
C
```

```
C ****************************************************************
C ****************************************************************
C
C
C STEADY STATE SOLUTION
C
C
C CALCULATE THERMAL CONDUCTIVITIES AT EACH MESH INTERVAL
C
      DO 282 I=1,N
         TIR(I)=(T(I)+T(I+1))/2.0
282   CONTINUE
285   CALL CONDUC (T,K,DELI,MAT,NGRPH,IGEOM,NM,X,FL,EPS,P,DIA,IPRK,
     *             COND,NREG,PEBFLG,N,TIR)
C
C CALCULATE HEAT TRANSFER COEFFICIENT ON OUTERMOST BOUNDARY
C
290   HR=EMM*SIGMA*(T(N)**2+TINF**2)*(T(N)+TINF)
      HT=HR+HC
294   FORMAT ('1OUTERMOST BOUNDARY HEAT TRANSFER COEFFICIENT:')
295   FORMAT ('0',T5,'EMMISIVITY: ',D13.6)
300   FORMAT (T5,'RADIATION HTC (W/M**2 K):  ',1PD13.6)
305   FORMAT (T5,'CONVECTION HTC (W/M**2 K): ',1PD13.6)
310   FORMAT (T5,'TOTAL HTC  (W/M**2 K):     ',1PD13.6)
C
C
315   IF (IGEOM .EQ. 2) GO TO 340
C
C SLAB GEOMETRY
C
C   SET UP FIRST AND LAST ROWS OF COEFFICIENT MATRIX
      DEL=DELI(1)
      A(1,1)=-(K(1))
      A(1,2)=K(1)
      B(1)=-((P(1)*DEL**2)/2.0)
      A(N,N-1)=K(N-1)
      A(N,N)=-(HT*DELI(NREG)+K(N-1))
      B(N)=-((P(N)*DELI(NREG)**2)/2.0+HT*DELI(NREG)*TINF)
C SET UP REMAINDER OF MATRIX
      RGN=1
      DIST=DELI(1)
      DO 335 I=2,NL
         IF (DABS(X(RGN)-DIST) .LE. 1.0E-6) GO TO 320
         A(I,I-1)=K(I-1)
         A(I,I)=-(K(I-1)+K(I))
         A(I,I+1)=K(I)
         B(I)=-(P(I)*DEL**2)
         GO TO 330
C    REGION INTERFACE
320      RGN=RGN+1
         DEL=DELI(RGN)
         IF (PEBFLG(RGN) .EQ. 2) GO TO 325
         A(I,I-1)=K(I-1)*DEL/(DELI(RGN-1)+DEL)
         A(I,I)=-(K(I)*DELI(RGN-1)+K(I-1)*DEL)/(DELI(RGN-1)+DEL)
         A(I,I+1)=K(I)*DELI(RGN-1)/(DELI(RGN-1)+DEL)
         B(I)=-(P(I)*DELI(RGN-1)*DEL)/2.00
         GO TO 330
C     VOID REGION
325      E12=(1.0)/((1.0/E1(RGN))+(1.0/E2(RGN))-1.0)
         HR12(RGN)=SIGMA*E12*(T(I)**2+T(I+1)**2)*(T(I)+T(I+1))
         A(I,I-1)=K(I-1)
```

```
367.              A(I,I)=-(HR12(RGN)*DELI(RGN-1)+K(I-1))
368.              A(I,I+1)=HR12(RGN)*DELI(RGN-1)
369.              B(I)=-(P(I)*DELI(RGN-1)**2)/2.0
370.              DIST=DIST+DEL
371.              I=I+1
372.              RGN=RGN+1
373.              DEL=DELI(RGN)
374.              A(I,I-1)=HR12(RGN-1)*DEL
375.              A(I,I)=-(HR12(RGN-1)*DEL+K(I))
376.              A(I,I+1)=K(I)
377.              B(I)=-(P(I)*DEL**2)/2.0
378.      330     DIST=DIST+DEL
379.      335   CONTINUE
380.            GO TO 365
381.      C
382.      C CYLINDRICAL GEOMETRY
383.      C
384.      C   SET UP FIRST AND LAST ROWS OF COEFFICIENT MATRIX
385.      340   DEL=DELI(1)
386.            A(1,1)=-K(1)
387.            A(1,2)=K(1)
388.            B(1)=-(P(1)*DEL**2/4.00)
389.            A(N,N-1)=K(N-1)*(X(NREG)-DELI(NREG)/2.0)/DELI(NREG)
390.            A(N,N)=-(((X(NREG)-DELI(NREG)/2.0)*K(N-1)/DELI(NREG))+
391.          *        X(NREG)*HT)
392.            B(N)=-((P(N)*(X(NREG)-DELI(NREG)/4.0)*DELI(NREG))/2.0+
393.          *          X(NREG)*HT*TINF)
394.      C SET UP REMAINDER OF MATRIX
395.            RGN=1
396.            DIST=DELI(1)
397.            DO 360 I=2,NL
398.               IF (DABS(X(RGN)-DIST) .LE. 1.0E-6) GO TO 345
399.               A(I,I-1)=((DIST-DEL/2.0)*K(I-1))/DEL
400.               A(I,I)=-((DIST+DEL/2.0)*K(I)/DEL+(DIST-DEL/2.0)*K(I-1)/DEL)
401.               A(I,I+1)=((DIST+DEL/2.0)*K(I))/DEL
402.               B(I)=-(P(I)*DIST*DEL)
403.               GO TO 355
404.      C   REGION INTERFACE
405.      345      RGN=RGN+1
406.               DEL=DELI(RGN)
407.               IF (PERFLG(RGN) .EQ. 2) GO TO 350
408.               A(I,I-1)=(DIST-DELI(RGN-1)/2.0)*K(I-1)/DELI(RGN-1)
409.               A(I,I)=-((DIST+DEL/2.0)*K(I)/DEL+(DIST-DELI(RGN-1)/2.0)*
410.          *            K(I-1)/DELI(RGN-1))
411.               A(I,I+1)=(DIST+DEL/2.0)*K(I)/DEL
412.               B(I)=-(P(I)/2.0)*(DIST*(DELI(RGN-1)+DEL)+0.25*(DEL**2-
413.          *                DELI(RGN-1)**2))
414.               GO TO 355
415.      C   VOID REGION
416.      350      E12=(1.0)/((1.0/E1(RGN))+(DIST/(DIST+DEL))*((1.0/E2(RGN))-1.0))
417.               E21=(DIST/(DIST+DEL))*E12
418.               HR12(RGN)=SIGMA*E12*(T(I)**2+T(I+1)**2)*(T(I)+T(I+1))
419.               HR21(RGN)=SIGMA*E21*(T(I)**2+T(I+1)**2)*(T(I)+T(I+1))
420.               A(I,I-1)=K(I-1)*(DIST-DELI(RGN-1)/2.0)/DELI(RGN-1)
421.               A(I,I)=-(((DIST-DELI(RGN-1)/2.0)*K(I-1)/DELI(RGN-1))+
422.          *            DIST*HR12(RGN))
423.               A(I,I+1)=DIST*HR12(RGN)
424.               B(I)=-(P(I)*DELI(RGN-1)*(DIST-DELI(RGN-1)/4.0))/2.0
425.               DIST=DIST+DEL
426.               I=I+1
427.               RGN=RGN+1
```

```
            DEL=DELI(RGN)
            A(I,I-1)=DIST*HR21(RGN-1)
            A(I,I)=-(((DIST+DEL/2.0)*K(I)/DEL)+DIST*HR21(RGN-1))
            A(I,I+1)=K(I)*(DIST+DEL/2.0)/DEL
            B(I)=-(P(I)*DEL*(DIST+DEL/4.0))/2.0
355         DIST=DIST+DEL
360      CONTINUE
C
C SET UP TRIDIAGONAL MATRIX AND TRANSFER P1 TERMS FROM B
C
365      N=NL+NU+1
         DO 375 J=1,N
            P1(J)=B(J)
            I1=MAX0(1,J-NU)
            I2=MIN0(N,J+NL)
            DO 370 I=I1,I2
               K1=I-J+M
               ABD(K1,J)=A(I,J)
370         CONTINUE
375      CONTINUE
C
C SOLVE MATRIX EQUATIONS BY ELIMINATION USING DGBFA AND DGBSL
C
         CALL DGBFA(ABD,4,N,NL,NU,IPVT,INFO)
         CALL DGBSL(ABD,4,N,NL,NU,IPVT,B,0)
         DO 380 I=1,N
C           SAVE THE PREVIOUS TEMPERATURE DISTRIBUTION IN ARRAY TL
            TL(I)=T(I)
C           TRANSFER SOLUTION FROM ARRAY B TO ARRAY T
            T(I)=B(I)
380      CONTINUE
C
C CHECK FOR CONVERGENCE
C
C CALCULATE THE HEAT RESIDUAL AT EACH NODE AND THE AVERAGE RELATIVE
C TEMPERATURE DIFFERENCE BETWEEN THE PREVIOUS AND PRESENT ITERATIONS.
C
         E(1)=(A(1,1)*T(1))+(A(1,2)*T(2))-P1(1)
         E(N)=(A(N,N-1)*T(N-1))+(A(N,N)*T(N))-P1(N)
            SUM=DABS(T(1)-TL(1))/T(1)+DABS(T(N)-TL(N))/T(N)
         DO 385 I=2,NL
           E(I)=(A(I,I-1)*T(I-1))+(A(I,I)*T(I))+(A(I,I+1)*T(I+1))-P1(I)
           SUM=SUM+DABS(T(I)-TL(I))/T(I)
385      CONTINUE
         RTD=(1.0/DFLOAT(N))*SUM
C CHECK CONVERGENCE
         IF (RTD .GT. CTD) GO TO 400
         GO TO 430
C
C PRINT CONVERGENCE INFORMATION
C
400      IF (ICOUNT .EQ. 1) WRITE (6,405)
405      FORMAT('1 ITERATION  MAX. HT RES.   NODE   TEMP(DEG C)',T52,
        * 'AVG. REL. TEMP. DIFF.')
         MAX=DABS(E(1))
         NODE=1
         TMP=T(1)-273.16000
         DO 410 I=2,N
            IF (DABS(E(I)) .LT. MAX) GO TO 410
               MAX=DABS(E(I))
               NODE=I
```

```
                TMP=T(I)-273.16000
410   CONTINUE
      WRITE (6,415) ICOUNT,MAX,MODE,TMP,RTD
415   FORMAT (T9,I2,T15,1PD13.6,T29,I3,T36,1PD13.6,T52,1PD13.6)
      IF (ICOUNT .GE. IMAX) GO TO 420
      ICOUNT=ICOUNT+1
C
C IF NOT CONVERGED, CALCULATE A NEW TEMPERATURE DISTRIBUTION
      GO TO 285
C
420   WRITE (6,425)
425   FORMAT (' ITERATIONS ON THERMAL PROPERTIES EXCEEDED')
C
C PRINT OUTERMOST BOUNDARY HTC
C
430   WRITE (6,294)
      WRITE (6,295) EMM
      WRITE (6,300) HR
      WRITE (6,305) HC
      WRITE (6,310) HT
C
C PRINT TEMPERATURE DISTRIBUTION
C
      WRITE (6,435)
435   FORMAT ('1          TEMPERATURE DISTRIBUTION')
      WRITE (6,440)
440   FORMAT ('0REGION  MATERIAL #   MESH POINT (I)   DIST. FROM ORIGIN
     *(M)   TEMP. (DEG C)')
      DIST=0.0
      RGN=1
      DO 455 I=1,N
         TP=T(I)-273.16000
         WRITE(6,445) RGN,MAT(RGN),I,DIST,TP
445      FORMAT (T4,I2,T12,I2,T26,I3,T42,1PD13.7,T63,1PD14.7,T83,
     *           1PD14.7)
         IF (DABS(X(NREG)-DIST) .LE. 1.0E-6) GO TO 455
         IF (DABS(X(RGN)-DIST) .LE. 1.0E-6) WRITE (6,450)
450      FORMAT ('        ')
         IF (DABS(X(RGN)-DIST) .LE. 1.0E-6) RGN=RGN+1
         DIST=DIST+DELX(RGN)
455   CONTINUE
C
C END OF STEADY STATE PROBLEM
      GO TO 800
C
C
C ***************************************************************
C ***************************************************************
C
C
C TRANSIENT SOLUTION
C
C INITIALIZE ARRAYS CONTAINING TEMPERATURES AT VARIOUS ITERATION LEVELS,
C TEMPERATURE AT WHICH TO CALCULATE PROPERTIES, AND IRRADIATION TEMPS.
C
475   DO 500 I=1,N
         TL(I)=T(I)
         TLP(I)=T(I)
         TNEWP(I)=T(I)
         TIR(I)=(T(I)+T(I+1))/2.0
500   CONTINUE
```

```
550.          DT=TTOT/(DFLOAT(NTIME))
551.          IEDIT=0
552.     C
553.     C BEGIN TIME STEP
554.     C
555.          DO 670 J=1,NTIME
556.             TIM=DT*DFLOAT(J)
557.             IEDIT=IEDIT+1
558.     C SAVE THE CONVERGED TEMPERATURE DISTRIBUTION FROM PREVIOUS TIME STEP
559.     C   IN ARRAY TTL.
560.             DO 502 I=1,N
561.                IF (J .EQ. 1) TTL(I)=T(I)
562.                IF (J .NE. 1) TTL(I)=TT(I)
563.     502     CONTINUE
564.     C
565.     C UPDATE HEAT GENERATION DISTRIBUTION AT TIME STEP J
566.     C
567.     501     DO 505 I=1,N
568.                GEN(I)=P(I)*ANALFN(DFLOAT(J)*DT,DCY)
569.     505     CONTINUE
570.     C
571.     C INITIALIZE INNER (NTI) AND OUTER (NPI) ITERATION COUNTERS
572.     C
573.             NPI=0
574.     C THE OUTER ITERATION LOOPS BACK TO LINE 509
575.     509     NTI=0
576.     C THE INNER ITERATION LOOPS BACK TO LINE 510
577.     510     DEL=DELI(1)
578.     C
579.     C UPDATE THERMAL PROPERTIES
580.     C
581.     C  CALCULATE BOUNDARY HEAT TRANSFER COEFFICIENT
582.          HR=EMM*SIGMA*(TNEWP(N)**2+TINF**2)*(TNEWP(N)+TINF)
583.          HT=HR+HC
584.     C  UPDATE HTC FOR VOID REGIONS
585.          L=NN(1)
586.          DO 514 RGN=2,NREG
587.             I=L+NN(RGN)-1
588.             IF (PEBFLG(RGN) .NE. 2) GO TO 514
589.             E12=(1.0)/((1.0/E1(RGN))+(X(RGN-1)/X(RGN))*((
590.        *       1.0/E2(RGN))-1.0))
591.             IF (IGEOM .EQ. 2) GO TO 512
592.     C     SLAB
593.             E21=E12
594.             GO TO 513
595.     C     CYLINDER
596.     512     E21=(X(RGN-1)/X(RGN))*E12
597.     513     HR12(RGN)=SIGMA*E12*(TNEWP(L)**2+TNEWP(L-1)**2)*(TNEWP(L)+
598.        *            TNEWP(L-1))
599.             HR21(RGN)=SIGMA*E21*(TNEWP(L)**2+TNEWP(L-1)**2)*(TNEWP(L)+
600.        *            TNEWP(L-1))
601.     514   CONTINUE
602.     C UPDATE CONDUCTIVITY, DENSITY, AND SPECIFIC HEAT
603.     515     CALL CONDUC(TNEWP,K,DELI,MAT,MGRPH,IGEOM,NN,X,FL,EPS,F,DIA,
604.        *                IPRK,COND,NREG,PEBFLG,N,TIM)
605.             CALL PROP (TNEWP,R,RFN,DELI,IPRR,MAT,N,X,NREG,IGEOM)
606.             CALL PROP (TNEWP,CP,CPFN,DELI,IPRC,MAT,N,X,NREG,IGEOM)
607.     C
608.     C SOLVE EQUATIONS FOR TEMPERATURE DISTRIBUTION
609.     C
610.     C ORIGIN
```

```
C
C     COEFFICIENTS
C
519       IF (IGEOM .EQ. 2) GO TO 520
C       RECTANGULAR GEOMETRY
            S1=1.0
            S2=(DEL**2)/2.0
            GO TO 530
C       CYLINDRICAL GEOMETRY
520         S1=2.0
            S2=(DEL**2)/2.0
C     EQUATIONS
530         D(1)=TH*S1*K(1)+R(1)*CP(1)*S2/DT
            H(1)=S2*R(1)*CP(1)*TTL(1)/DT+GEN(1)*S2+(1.0-TH)*(S1*K(1)*
     *          (TTL(2)-TTL(1)))
            TT(1)=(1.0-H)*TL(1)+H*(1.0/D(1))*(H(1)+TH*(S1*K(1)*TL(2)))
C
C INTERNAL NODES
C
C
            RGN=1
            DIST=DELI(1)
            DO 560 I=2,NL
               IF (DABS(X(RGN)-DIST) .LE. 1.0E-6) GO TO 540
C     REGION INTERNAL NODE
C
C      COEFFICIENTS
               IF (IGEOM .EQ. 2) GO TO 535
C       RECTANGULAR GEOMETRY
               A1(I)=1.0
               A2(I)=1.0
               A3=DEL**2
               GO TO 550
C       CYLINDRICAL GEOMETRY
535            A1(I)=(2.0*DIST-DEL)/DEL
               A2(I)=(2.0*DIST+DEL)/DEL
               A3=2.0*DIST*DEL
               GO TO 550
C     MATERIAL INTERFACE
540            RGN=RGN+1
               DEL=DELI(RGN)
               IF (FERFLG(RGN) .EQ. 2) GO TO 552
               IF (IGEOM .EQ. 2) GO TO 545
C       RECTANGULAR GEOMETRY
               A1(I)=DEL/(DELI(RGN-1)+DEL)
               A2(I)=DELI(RGN-1)/(DELI(RGN-1)+DEL)
               A3=DELI(RGN-1)*DEL/2.0
               GO TO 550
C       CYLIINDRICAL GEOMETRY
545            A1(I)=(2.0*DIST-DELI(RGN-1))/DELI(RGN-1)
               A2(I)=(2.0*DIST+DEL)/DEL
               A3=(DELI(RGN-1)+DEL)*(DIST+(DEL-DELI(RGN-1))/4.0)
C      EQUATIONS
550            D(I)=TH*(A1(I)*K(I-1)+A2(I)*K(I))+A3*R(I)*CP(I)/DT
               H(I)=A3*R(I)*CP(I)*TTL(I)/DT+GEN(I)*A3+(1.0-TH)*(A1(I)*
     *             K(I-1)*(TTL(I-1)-TTL(I))+A2(I)*K(I)*(TTL(I+1)-TTL(I)))
               TT(I)=(1.0-H)*TL(I)+H*(1.0/D(I))*(H(I)+TH*(A1(I)*K(I-1)*
     *                TT(I-1)+A2(I)*K(I)*TL(I+1)))
               DIST=DIST+DEL
               GO TO 560
C     VOID REGION
```

```
C     LEFT HAND POINT
C     SLAB
552         IF (IGEOM .EQ. 2) GO TO 553
            A1(I)=1.0
            A2(I)=DELI(RGN-1)
            A3=DELI(RGN-1)**2
            GO TO 554
C      CYLINDER
553         A1(I)=(DIST-DELI(RGN-1)/2.0)/DELI(RGN-1)
            A2(I)=DIST
            A3=DELI(RGN-1)*(DIST-DELI(RGN-1)/4.0)
C      EQUATIONS
554         D(I)=2.0*TH*(A1(I)*K(I-1)+A2(I)*HR12(RGN))+A3*R(I)*CP(I)/DT
            H(I)=A3*R(I)*CP(I)*TTL(I)/DT+GEN(I)*A3+2.0*(1.0-TH)*
     *            (A1(I)*K(I-1)*(TTL(I-1)-TTL(I))+A2(I)*HR12(RGN)*
     *            (TTL(I+1)-TTL(I)))
            TT(I)=(1.0-W)*TL(I)+W*(1.0/D(I))*(H(I)+2.0*TH*
     *            (A1(I)*K(I-1)*TT(I-1)+A2(I)*HR12(RGN)*TL(I+1)))
            DIST=DIST+DEL
C    RIGHT HAND POINT
            I=I+1
            RGN=RGN+1
            DEL=DELI(RGN)
            IF (IGEOM .EQ. 2) GO TO 555
C      SLAB
            A1(I)=DEL
            A2(I)=1.0
            A3=DEL**2
            GO TO 556
C      CYLINDER
555         A1(I)=DIST
            A2(I)=(DIST+DEL/2.0)/DEL
            A3=DEL*(DIST+DEL/4.0)
C      EQUATIONS
556         D(I)=2.0*TH*(A2(I)*K(I)+A1(I)*HR21(RGN-1))+A3*R(I)*CP(I)/DT
            H(I)=A3*R(I)*CP(I)*TTL(I)/DT+GEN(I)*A3+2.0*(1.0-TH)*
     *            (A2(I)*K(I)*(TTL(I+1)-TTL(I))+A1(I)*HR21(RGN-1)*
     *            (TTL(I-1)-TTL(I)))
            TT(I)=(1.0-W)*TL(I)+W*(1.0/D(I))*(H(I)+2.0*TH*
     *            (A2(I)*K(I)*TL(I+1)+A1(I)*HR21(RGN-1)*TT(I-1)))
            DIST=DIST+DEL
560       CONTINUE
C
C BOUNDARY
C
C   COEFFICIENTS
            IF (IGEOM .EQ. 2) GO TO 570
C    RECTANGULAR GEOMETRY
            B1=1.0
            B2=DELI(NREG)
            B3=(DELI(NREG)**2)
            GO TO 580
C    CYLINDRICAL GEOMETRY
570         B1=(X(NREG)-DELI(NREG)/2.0)/DELI(NREG)
            B2=X(NREG)
            B3=DELI(NREG)*(X(NREG)-DELI(NREG)/4.0)
C   EQUATIONS
580         D(N)=2.0*TH*(B1*K(N-1)+B2*HT)+B3*R(N)*CP(N)/DT
            H(N)=B3*R(N)*CP(N)*TTL(N)/DT+GEN(N)*B3+2.0*(1.0-TH)*
     *          (B1*K(N-1)*(TTL(N-1)-TTL(N))+B2*HT*(TINF-TTL(N)))
            TT(N)=(1.0-W)*TL(N)+W*(1.0/D(N))*(H(N)+TH*(2.0*B1*K(N-1)
```

```
     *          *TT(N-1)+B2*2.0*HT*TINF))
            NTI=NTI+1
C
C CHECK FOR CONVERGENCE ON ITERATIONS AT THIS PROPERTY STEP
C
C  CALCULATE HEAT RESIDUAL AT EACH NODE
            E(1)=H(1)+TH*S1*K(1)*TT(2)-D(1)*TT(1)
            E(N)=H(N)+TH*(2.0*B1*K(N-1)*TT(N-1)+B2*2.0*HT*TINF)-D(N)*TT(N)
            RGN=1
            DIST=DELI(1)
            DEL=DELI(1)
            DO 590 I=2,NL
               IF (DABS(X(RGN)-DIST) .GT. 1.0D-6) GO TO 585
               RGN=RGN+1
               DEL=DELI(RGN)
               IF (PERFLG(RGN) .NE. 2) GO TO 585
                E(I)=H(I)+2.0*TH*(A1(I)*K(I-1)*TT(I-1)+A2(I)*HR12(RGN)*
     *              TT(I+1))-D(I)*TT(I)
               DIST=DIST+DEL
               I=I+1
               RGN=RGN+1
               DEL=DELI(RGN)
                E(I)=H(I)+2.0*TH*(A2(I)*K(I)*TT(I+1)+A1(I)*HR21(RGN-1)
     *              *TT(I-1))-D(I)*TT(I)
               DIST=DIST+DEL
               GO TO 590
585            E(I)=H(I)+TH*(A1(I)*K(I-1)*TT(I-1)+A2(I)*K(I)*TT(I+1))
     *              -D(I)*TT(I)
               DIST=DIST+DEL
590         CONTINUE
            DO 600 I=1,N
               CONT(I)=DABS(E(I)/H(I))
600         CONTINUE
C
C  FIND MAXIMUM HEAT RESIDUAL AND PRINT CONVERGENCE INFO
C
            IF (((NPI .NE. 0) .OR. (NTI .NE. 1)) .OR. (IEDIT .NE. NEDIT))
     *         GO TO 592
            WRITE (6,591)
591         FORMAT ('1TIME(SEC)',T15,'INNER ITER COUNT',T35,
     *        'MAX. NORM. RESID.',T60,'NODE',T70,'TEMP (DEG C)',T85,
     *        'PROP. ITER COUNT',T110,'NORM OF NODE TEMP DIFF')
592         MAX=CONT(1)
            NODE=1
            TMP=TT(1)-273.1600
            DO 593 I=2,N
               IF (CONT(I) .LT. MAX) GO TO 593
               MAX=CONT(I)
               NODE=I
               TMP=TT(I)-273.1600
593         CONTINUE
            IF (IEDIT .NE. NEDIT) GO TO 595
            WRITE (6,594) TIM,NTI,MAX,NODE,TMP
594         FORMAT (' ',F12.3,T20,I4,T35,1PD13.6,T60,I4,T70,1PD13.6)
595         IF (MAX .LE. CC1) GO TO 610
602         IF (NTI .GE. ITMAX) GO TO 608
            DO 605 I=1,N
               TL(I)=TT(I)
605         CONTINUE
C
C IF NOT CONVERGED, ITERATE ON THIS PROPERTY STEP AGAIN
```

```
C
          GO TO 510
C
C TIMING ITERATIONS EXCEEDED
608       WRITE (6,609) NPI,NTI
609       FORMAT (' TIMING ITERATIONS EXCEEDED ON PROP ITERATION ',I3,' -
     * ',I3,' TIMING ITERATIONS PERFORMED')
C
C CHECK CONVERGENCE ON PROPERTIES
C
610       NPI=NPI+1
          SUM=DABS(TT(1)-TLP(1))/TT(1)
          DO 620 I=2,N
             SUM=SUM+DABS(TT(I)-TLP(I))/TT(I)
620       CONTINUE
          CONP=(1.0/DFLOAT(N))*SUM
          IF (IEDIT .NE. NEDIT) GO TO 622
          WRITE (6,621) TIM,NPI,CONP
621       FORMAT (' ',F12.3,T88,I4,T110,1PD12.6)
622       IF (CONP .LE. CC2) GO TO 640
          IF (NPI .GE. IPMAX) GO TO 635
C
C CALCULATE TEMPERATURES AT WHICH TO FIND NEW THERMAL PROPERTIES
C
          DO 625 I=1,N
             IF (J .EQ.1) TNEWP(I)=(1.0-TH)*T(I)+TH*TT(I)
             IF (J .NE. 1) TNEWP(I)=(1.0-TH)*TTL(I)+TH*TT(I)
623         TLP(I)=TT(I)
            IF (J .EQ. 1) TL(I)=T(I)
            IF (J .GT. 1) TL(I)=TTL(I)
625       CONTINUE
C
C GO BACK TO TIME ITERATIONS ON TIME STEP J
C
            GO TO 509
C PROPERTY ITERATIONS EXCEEDED
635         WRITE (6,638) J,NPI
638         FORMAT (' PROPERTY ITERATIONS EXCEEDED ON TIME STEP ',I3,
     *              ' - ',I3,' ITERATIONS')
C
C CONVERGED ON PROPERTIES - INCREMENT TIME STEP
C
640         DO 655 I=1,N
               TL(I)=TT(I)
               TLP(I)=TL(I)
               TNEWP(I)=TL(I)
655         CONTINUE
C
C CHECK FOR EDITS
C
      IF (J .EQ. NTIME) GO TO 657
      IF (IEDIT .NE. NEDIT) GO TO 670
657      WRITE (6,503)  TIM
503     FORMAT ('1INTERNAL HEAT GENERATION DISTRIBUTION - TIME = ',F12.3
     *          ,' SECONDS')
          WRITE (6,504)
504       FORMAT (' MESH POINT',T15,'HEAT GEN. (W/M**3)')
          WRITE (6,506) (I,GEN(I),I=1,N)
506       FORMAT (T6,I3,T15,1PD17.10)
C PRINT PROPERTY DISTRIBUTIONS, ETC.
      WRITE (6,294)
```

```
      WRITE (6,295) EHH
      WRITE (6,300) HR
      WRITE (6,305) HC
      WRITE (6,310) HT
            WRITE (6,516) TIM
516         FORMAT ('0PROPERTY DISTRIBUTIONS - TIME = ',F12.3,'SECONDS')
            WRITE (6,517)
517         FORMAT ('0MESH POINT',T15,'CONDUCTIVITY (W/M K)',T40,
     *                'DENSITY (KG/M**3)',T60,'SP. HEAT (J/KG K)')
            WRITE (6,518) (I,K(I),R(I),CP(I),I=1,N)
518         FORMAT (T6,I3,T15,1PD12.5,T40,1PD12.5,T60,1PD12.5)
      WRITE (6,660) TIM
660   FORMAT ('1  TEMPERATURE DISTRIBUTION AT TIME = ',F12.3,' SECONDS')
      WRITE (6,662) NPI
662   FORMAT (' NUMBER OF PROPERTY ITERATIONS = ',I3)
C
C PRINT CONVERGED TEMPERATURE DISTRIBUTION
C
      WRITE (6,440)
      DIST=0.0
      RGN=1
      DO 665 I=1,N
         TP=TT(I)-273.16000
         WRITE(6,445) RGN,MAT(RGN),I,DIST,TP
         IF (DABS(X(NREG)-DIST) .LE. 1.0D-6) GO TO 665
         IF (DABS(X(RGN)-DIST) .LE. 1.0D-6) WRITE (6,450)
         IF (DABS(X(RGN)-DIST) .LE. 1.0D-6) RGN=RGN+1
         DIST=DIST+DELI(RGN)
665   CONTINUE
      IEDIT=0
670   CONTINUE
800   STOP
      END
C
C*****************************************************************
C
      SUBROUTINE INTRPG (Y,L,Z,N,DELI,X,NREG,PEBFLG,IGEOM)
C
C
C THIS SUBROUTINE INTERPOLATES A TABULAR FUNCTION FOR HEAT GENERATION
C IN EACH REGION TO FIND VALUES AT EACH MESH POINT I.  THE AVERAGE HEAT
C GENERATION IS CALCULATED IN EACH INTERVAL; IT IS VOLUME AVERAGED AT
C MATERIAL REGION INTERFACES
C
      REAL*8 Y(20,20,2),Z(200),X(20),DELI(20),DIST,GR,GL,DISTI
      INTEGER RGN,PEBFLG(20),N,NREG,IFLAG,IFLAG2,L(20),IGEOM
      RGN=1
      DIST=0.0
       IFLAG2=-1
      DO 100 I=1,N
         IF (I .EQ. 1) IFLAG=1
         J2=L(RGN)
         DO 20 J=1,J2
           IF (((Y(RGN,J,1)-DIST) .LE. 1.0D-6) .AND. ((DIST-Y(RGN,J+1,1)
     *          ) .LE. 1.0D-6)) GO TO 25
20       CONTINUE
25       Z(I)=(((Y(RGN,J+1,2)-Y(RGN,J,2))*(DIST-Y(RGN,J,1)))/
     *          (Y(RGN,J+1,1)-Y(RGN,J,1)))+Y(RGN,J,2)
C CHECK FOR ADJUSTMENT TO ORIGIN OR RIGHT BOUNDARY OF VOID REGION
         IF (I .EQ. IFLAG+1) Z(I-1)=0.75*Z(I-1)+0.25*Z(I)
C CHECK FOR ADJUSTMENT TO INTERFACE
```

```
            IF (I .NE. IFLAG2+1) GO TO 30
               GR=0.75*Z(I-1)+0.25*Z(I)
               IF (IGEOM .EQ. 1) Z(I-1)=(DELI(RGN-1)*GL+DELI(RGN)*GR)/
     *            (DELI(RGN-1)+DELI(RGN))
              IF (IGEOM .EQ. 2) Z(I-1)=(DELI(RGN-1)*(4.0*DISTI-DELI(RGN-1))
     *            *GL+DELI(RGN)*(4.0*DISTI+DELI(RGN))*GR)/
     *          ((DELI(RGN)+DELI(RGN-1))*(4.0*DISTI+DELI(RGN)-DELI(RGN-1)))
C CHECK FOR BOUNDARY
30          IF (DABS(DIST-X(NREG)) .GT. 1.0D-6) GO TO 35
               Z(N)=0.75*Z(N)+0.25*Z(N-1)
               GO TO 100
C CHECK FOR INTERFACE
35          IF (DABS(DIST-X(RGN)) .GT. 1.0D-6) GO TO 95
C     REGION INTERFACE
            RGN=RGN+1
C     CHECK WHETHER VOID OR NOT
            IF (PERFLG(RGN) .NE. 2) GO TO 40
               Z(I)=0.75*Z(I)+0.25*Z(I-1)
               IFLAG=I+1
               DIST=DIST+DELI(RGN)
               RGN=RGN+1
               GO TO 100
C     NORMAL INTERFACE
40          GL=0.75*Z(I)+0.25*Z(I-1)
            IFLAG2=I
            DISTI=DIST
            I=I-1
            GO TO 100
95          DIST=DIST+DELI(RGN)
100      CONTINUE
         RETURN
         END
C
C ***********************************************************
C
         SUBROUTINE INTERP (Y,L,Z,N,DELI,X,NREG)
C
C
C THIS SUBROUTINE INTERPOLATES A TABULAR FUNCTION FOR INITIAL
C TEMPERATURE OR FLUENCE TO FIND VALUES AT EACH MESH POINT I.
C
         REAL*8 Y(20,20,2),Z(200),X(20),DELI(20),DIST,GR,GL
          INTEGER RGN,N,NREG,IFLAG2,L(20)
         RGN=1
         DIST=0.0
          IFLAG2=0
         DO 100 I=1,N
            J2=L(RGN)
            DO 20 J=1,J2
               IF (((Y(RGN,J,1)-DIST) .LE. 1.0D-6) .AND. (DIST .LE.
     *            Y(RGN,J+1,1))) GO TO 25
20          CONTINUE
25          Z(I)=(((Y(RGN,J+1,2)-Y(RGN,J,2))*(DIST-Y(RGN,J,1)))/
     *          (Y(RGN,J+1,1)-Y(RGN,J,1)))+Y(RGN,J,2)
C CHECK FOR ADJUSTMENT TO INTERFACE
            IF (I .NE. IFLAG2) GO TO 30
               GR=Z(I)
               Z(I)=(DELI(RGN-1)*GL+DELI(RGN)*GR)/(DELI(RGN-1)+DELI(RGN))
C CHECK FOR BOUNDARY
30          IF (DABS(DIST-X(NREG)) .LE. 1.0D-6) GO TO 100
C CHECK FOR INTERFACE
```

```
977.              IF (DABS(DIST-X(RGN)) .GT. 1.0D-6) GO TO 95
978.      C     REGION INTERFACE
979.              RGN=RGN+1
980.              GL=Z(I)
981.              IFLAG2=1
982.              I=I-1
983.              GO TO 100
984.      95      DIST=DIST+DELI(RGN)
985.      100   CONTINUE
986.            RETURN
987.            END
988.      C
989.      C ***********************************************************
990.      C
991.            SUBROUTINE PROP (T,P,PFN,DELI,IFR,MAT,N,X,NREG,IGEOM)
992.      C
993.      C THIS SUBROUTINE INTERPOLATES A TABULAR FUNCTION OF DENSITY OR SPECIFIC
994.      C HEAT VS. TEMPERATURE FOR EACH REGION TO OBTAIN VALUES AT EACH MESH
995.      C POINT.  VALUES ON MATERIAL INTERFACES ARE VOLUME AVERAGED.
996.      C
997.            REAL*8 T(200),P(200),PFN(20,2,20),DELI(20),X(20),DIST,PLAST
998.            INTEGER* IFR(20),MAT(20),RGN,N,JTOP,FLAG,IGEOM
999.            RGN=1
1000.           FLAG=0
1001.           DIST=0.0
1002.     135   DO 155 I=1,N
1003.              JTOP=IFR(MAT(RGN))-1
1004.              DO 140 J=1,JTOP
1005.                 IF ((T(I) .GE. PFN(MAT(RGN),1,J)) .AND. (T(I) .LE. PFN(MAT(
1006.         *          RGN),1,J+1))) GO TO 145
1007.     140      CONTINUE
1008.     145      P(I)=(((PFN(MAT(RGN),2,J+1)-PFN(MAT(RGN),2,J))*(T(I)-
1009.         *        PFN(MAT(RGN),1,J)))/(PFN(MAT(RGN),1,J+1)-PFN(MAT(RGN),
1010.         *        1,J)))+PFN(MAT(RGN),2,J)
1011.     C  CHECK FOR REGION INTERFACE - PROPERTIES MUST BE VOLUME AVERAGED
1012.              IF (FLAG .NE. 1) GO TO 149
1013.              IF (IGEOM .EQ. 1) P(I)=(DELI(RGN-1)*PLAST+DELI(RGN)*P(I))/
1014.         *        (DELI(RGN-1)+DELI(RGN))
1015.              IF (IGEOM .EQ. 2) P(I)=(DELI(RGN-1)*(4.0*DIST-DELI(RGN-1))*
1016.         *        PLAST+DELI(RGN)*(4.0*DIST+DELI(RGN))*P(I))/
1017.         *        ((DELI(RGN-1)+DELI(RGN))*(4.0*DIST+DELI(RGN)-DELI(RGN-1)))
1018.              FLAG=0
1019.     149      IF (DABS(DIST-X(NREG)) .LE. 1.0D-6) GO TO 155
1020.              IF (DABS(DIST-X(RGN)) .GT. 1.0D-6) GO TO 153
1021.               IF (MAT(RGN+1) .LT. 0) GO TO 150
1022.                 PLAST=P(I)
1023.                 RGN=RGN+1
1024.                 FLAG=1
1025.                 I=I-1
1026.                 GO TO 155
1027.     C   VOID REGION
1028.     150        DIST=DIST+DELI(RGN+1)
1029.                RGN=RGN+2
1030.                GO TO 155
1031.     153      DIST=DIST+DELI(RGN)
1032.     155   CONTINUE
1033.           RETURN
1034.           END
1035.     C
1036.     C ***********************************************************
1037.     C
```

```
      SUBROUTINE CONDUC (T,K,DELI,MAT,MGRPH,IGEOM,NM,X,FL,EPS,F,D,IPRK,
     *           COND,NREG,PEBFLG,N,TIR)
C
C THIS SUBROUTINE IS USED TO CALCULATE THE THERMAL CONDUCTIVITY OF
C EACH MESH INTERVAL (BETWEEN EACH POINT).  IF THE MATERIAL IN A REGION
C IS GRAPHITE, THIS ROUTINE CALLS THE APPROPRIATE SUBROUTINE TO
C CALCULATE GRAPHITE CONDUCTIVITY.  IF A REGION IS A PEBBLE BED REGION,
C THE ROUTINE TO CALCULATE EFFECTIVE THERMAL CONDUCTIVITY IS CALLED.
C IF THE MATERIAL IS NOT GRAPHITE, A TABULAR FUNCTION OF CONDUCTIVITY
C VS TEMPERATURE IS INTERPOLATED TO FIND THE CONDUCTIVITY OF EACH
C INTERVAL IN THAT REGION.
C
      REAL*8 T(200),K(200),DELI(20),X(20),FL(200),EPS,F,D,COND(20,2,20)
     *       ,DIST,SIGMA,TAVG,PHI,TIR(200)
      INTEGER MAT(20),MGRPH,IGEOM,NM(20),IPRK(20),NREG,RGN,PEBFLG(20)
     *       ,JTOP,N
      SIGMA=5.669D-8
      RGN=1
      DIST=DELI(1)
135   DO 155 I=2,N
C CHECK FOR GRAPHITE
         IF (MAT(RGN) .NE. MGRPH) GO TO 139
            I2=I+NM(RGN)-2
            DO 138 L=I,I2
               TAVG=(T(L-1)+T(L))/2.0
               PHI=(FL(L-1)+FL(L))/2.0
               CALL GRPHTE (TAVG,TIR(L-1),PHI,K(L-1))
               K(L-1)=100.00*K(L-1)
138         CONTINUE
            DIST=X(RGN)
C CHECK FOR PEBBLE BED
         IF (PEBFLG(RGN) .EQ. 1) CALL PEBBLE(K,T,SIGMA,EPS,F,D,I,
     *      I+NM(RGN)-2)
         IF (MAT(RGN) .EQ. MGRPH) I=I+NM(RGN)-2
         IF (MAT(RGN) .EQ. MGRPH) GO TO 150
139      IF (PEBFLG(RGN) .EQ. 2) K(I-1)=0.00
         IF (PEBFLG(RGN) .EQ. 2) GO TO 150
         TAVG=(T(I-1)+T(I))/2.0
         JTOP=IPRK(MAT(RGN))-1
         DO 140 J=1,JTOP
               IF ((TAVG .GE. COND(MAT(RGN),1,J)) .AND. (TAVG .LE.
     *            COND(MAT(RGN),1,J+1))) GO TO 145
140      CONTINUE
145      K(I-1)=(((COND(MAT(RGN),2,J+1)-COND(MAT(RGN),2,J))*(TAVG-COND
     *(MAT(RGN),1,J)))/(COND(MAT(RGN),1,J+1)-COND(MAT(RGN),1,J)))+
     *COND(MAT(RGN),2,J)
150      IF (DABS(DIST-X(NREG)) .LE. 1.0D-6) GO TO 155
         IF (DABS(DIST-X(RGN)) .LE. 1.0D-6) RGN=RGN+1
         DIST=DIST+DELI(RGN)
155   CONTINUE
      RETURN
      END
C
C*****************************************************************
C
      SUBROUTINE GRPHTE (T,TIR,PSI,CONIR)                          GRAC00
C
C THIS SUBROUTINE CALCULATED THE THERMAL CONDUCTIVITY OF GRAPHITE AS
C A FUNCTION OF FLUENCE, TEMPERATURE, AND IRRADIATION TEMPERATURE.
C
      REAL*8 T,TIR,PSI,CONIR,DELT,DELBAR,ATABAR,COUN,ALPHA,RATIO,
```

```
      * CONIR,FTIR,BETA
      COMMON / TCDT / TDAT(13),DELTA(13),ATA(13),CN(13)                 GRAC0030
      COMMON /TKIN /CON(13)                                             GRAC0040
C                                                                       GRAC0050
      DO 100 I=2,12                                                     GRAC0060
      IF (T.LT.TDAT(I)) GO TO 110                                       GRAC0070
  100 CONTINUE                                                          GRAC0080
      I=13                                                              GRAC0090
  110 CONTINUE                                                          GRAC0100
      J=I-1                                                             GRAC0110
      DELT=(T-TDAT(I))/(TDAT(J)-TDAT(I))                                GRAC0120
      DELBAR=(DELT*(DELTA(J)-DELTA(I))+DELTA(I))/DELTA(2)               GRAC0130
      ATABAR=(DELT*(ATA(J)-ATA(I))+ATA(I))/ATA(2)                       GRAC0140
      COUN=(DELT*(CON(J)-CON(I))+CON(I))/CON(2)                         GRAC0150
      IF (T.EQ.TIR) GO TO 140                                           GRAC0160
      DO 120 I=2,12                                                     GRAC0170
      IF (TIR.LT.TDAT(I)) GO TO 130                                     GRAC0180
  120 CONTINUE                                                          GRAC0190
      I=13                                                              GRAC0200
  130 CONTINUE                                                          GRAC0210
      J=I-1                                                             GRAC0220
      DELT=(TIR -TDAT(I))/(TDAT(J)-TDAT(I))                             GRAC0230
  140 C=(DELT*(CN(J)-CN(I))+CN(I))                                      GRAC0240
      ALPHA=1.055-.00057*TIR                                            GRAC0250
      IF (ALPHA.LT.0) ALPHA=0                                           GRAC0260
      H=(1.-8.45E-8*T*(420.+1.65*T))*ALPHA                              GRAC0270
      BETA=1.116-.000269*TIR                                            GRAC0280
      IF (BETA.LT.0) BETA=0                                             GRAC0290
      Y=BETA*(PSI*1.E-21)                                               GRAC0310
      IF (Y.GT.100) Y=100.                                              GRAC0320
      IF (Y.GT..001) Y=1.-EXP(-Y)                                       GRAC0330
      FTIR=8.8*H*Y                                                      GRAC0340
      RATIO=1./(1.+FTIR*COUN*(C*DELBAR+(1.-C)*ATABAR))                  GRAC0350
      CONIR=RATIO*COUN*CON(2)                                           GRAC0360
      IF (CONIR.LT.(0.1*CON(2))) CONIR=(0.1*CON(2))                     GRAC0380
      RETURN                                                            GRAC0520
      END                                                               GRAC0530
C
C*********************************************************************
C
      SUBROUTINE PEBBLE (LF,T,SIGMA,EPS,F,D,I1,I2)
C
C THIS SUBROUTINE CALCULATES THE EFFECTIVE THERMAL CONDUCTIVITY IN A
C PEBBLE BED USING THE MODIFIED ZEHNER-SCHLUENDER MODEL.
C
      REAL*8 LF(200),T(200),B,SIGMA,EPS,F,D,LAM,TAVG
      B=1.25*(((1-F)/F)**(10.0/9.0))
      DO 100 I=I1,I2
         TAVG=(T(I-1)+T(I))/2.0
         LAM=LF(I-1)/(4.0*SIGMA*TAVG**3*D)
         LF(I-1)=(4.0*SIGMA*TAVG**3*D)*((1.0-DSQRT(1.0-F))*F+(DSQRT(
     *           1.0-F)*(B+1.0)/((2.0/EPS-1.0)*B))*(1.0/(1.0+1.0/
     *           ((2.0/EPS-1.0)*LAM))))
100   CONTINUE
      RETURN
      END
C
C ***************************************************************
C
      FUNCTION ANALFN (X,CO)
C
```

ORNL/TM-9215
Distribution Category UC-77

INTERNAL DISTRIBUTION

1. L. S. Abbott
2. S. J. Ball
3. D. E. Bartine
4. J. C. Cleveland
5. H. W. Hoffman
6. R. S. Holcomb
7. F. J. Homan
8. D. T. Ingersoll
9-18. P. R. Kasten
19. F. C. Maienschein
20. D. L. Moses
21. F. R. Mynatt
22. D. J. Naus
23. J. P. Renier
24. P. L. Rittenhouse
25. C. O. Slater
26. D. B. Trauger
27. D. R. Vondy
28. C. R. Weisbin
29-30. B. A. Worley
31. A. Zucker
32. P. W. Dickson, Jr. (Consultant)
33. G. H. Golub (Consultant)
34. H. J. C. Kouts (Consultant)
35. D. Steiner (Consultant)
36. Central Research Library
37. Y-12 Document Ref. Section
38. Laboratory Records ORNL, RC
39. ORNL Patent Office

EXTERNAL DISTRIBUTION

40. Director, Division of HTR Development, DOE, NE-15, Washington, D.C. 20545.
41. Office of the Assistant Manager for Energy Research and Development, DOE-ORO, Oak Ridge, TN 37830, Attention: S. W. Ahrends.
42. Director, DOE, Office of Converter Reactor Deployment, NE-10, Washington, D.C. 20545.
43. Manager, DOE, SAN-SAN Diego, 110 West A St., Suite 460, San Diego, CA 92101
44-48. M. G. Savage, Westinghouse Electric Corp., Nuclear Fuels Div., P.O. Box 3912, Bay 307, Pittsburgh, PA 15230.

DOE, Division of HTR Development, NE-15, Washington, D.C. 20545:
49. J. E. Fox
50. I. L. Helms
51. G. A. Newby

GA Technologies, P.O. Box 81608, San Diego, CA 92138:
52. A. J. Neylan
53. R. K. Lane
54. A. M. Baxter

General Electric, P. O. Box 508, Sunnyvale, CA 94086:
55. G. R. Pflasterer
56. C. L. Cohen

57. Lt. David Ek, Air Force Weapons Laboratory, AFWL/NTYN, Kirtland AFB, NM 87117.

58-181. Given Distribution as shown in TID-4500, Distribution Category UC-77 -- Gas Cooled Reactor Technology.

☆U.S. GOVERNMENT PRINTING OFFICE: 1984-746-067/4103